The Thesis Committee for William Christopher Van Bramer
Certifies that this is the approved version of the following thesis:

Nanoparticle Dispersion Flow for Enhanced Oil Recovery Using Micromodels

APPROVED BY
SUPERVISING COMMITTEE:

Supervisor:

Matthew T. Balhoff

Chun Huh

Nanoparticle Dispersion Flow for Enhanced Oil Recovery Using Micromodels

by

William Christopher Van Bramer, B.S.

Thesis

Presented to the Faculty of the Graduate School of

The University of Texas at Austin

in Partial Fulfillment

of the Requirements

for the Degree of

Master of Science in Engineering

The University of Texas at Austin

August 2014

Dedication

To all who have helped me on this journey.

Acknowledgements

I would like to thank my supervisor, Dr. Matthew Balhoff for his support and guidance throughout my studies here at The University of Texas at Austin. His advice and insight has been invaluable. I would also like to thank Dr. Chun Huh for his guidance and wisdom throughout my research. I need to thank Dr. Bryant as well for the support and insight he has provided.

Thank you to Dr. Peixi Zhu, whose ideas and assistance has helped my research and this thesis immensely. Thank you to Shashvat Doorwar for his aid and ideas in regards to glass etching. Undergraduate research assistants Kellyn Schmitz and Lauren Pugh require acknowledgement as well for their assistance with laboratory work. Thank you to all of my colleagues in Dr. Balhoff's research group, you all made coming to the office enjoyable and challenging.

Finally I would like to thank the Nanoparticle for Subsurface Engineering consortium for funding this work.

Abstract

Nanoparticle Dispersion Flow for Enhanced Oil Recovery Using Micromodels

William Christopher Van Bramer, M.S.E

The University of Texas at Austin, 2014

Supervisor: Matthew T. Balhoff

The injection of nanoparticles is a promising and novel approach to enhancing oil recovery in depleted fields. Nanoparticles have one dimension that is smaller than 100 nm and have many unique properties that are useful when it comes to oil recovery. Their small size and the ability to manipulate particle properties are a couple of the advantageous properties. The small size of nanoparticle allows them to easily pass through porous media. Manipulating nanoparticle properties allows for wettability modifications or controlled release of chemicals at a precise location in the formation.

Injection of nanoparticle dispersions for secondary or tertiary recovery in corefloods has yielded positive results. Field tests using nanoparticles have also yielded positive results with increased oil recovery. While there has been a sizable amount of

work related to corefloods, limited investigation has been reported using micromodels. Micromodels are valuable because they allow for pore scale viewing of the oil recovery, which is not possible with corefloods. In this research both polydimethylsiloxane (PDMS) and glass microfluidic devices were fabricated to test the EOR potential of different types of nanoparticles. Much of the work described in this thesis involved the use of a dead-end pore geometry to trap oil. First the pore space was filled with oil and then waterflooded. This left some oil trapped in the dead-end pores. PDMS micromodels proved difficult to trap oil in the dead-end pores; because of this glass micromodels were tested. After trapping oil, a nanoparticle dispersion was injected into the pore space to test the potential of the dispersion to reduce the residual oil saturation in the dead-end pores. The nanoparticle dispersion was injected at different flow rates (1 μl/hr to 50 μl/hr) to test the effect of flow rate on residual oil recovery.

Table of Contents

List of Tables

List of Figures

CHAPTER 1. INTRODUCTION

Worldwide energy consumption has steadily increased and will continue to increase in the coming years. New sources or improved methods of oil extraction will be required. The U.S. Energy Information Administration has projected that worldwide energy consumption will increase by 56% between 2010 and 2040 (International Energy Outlook, 2013). While nuclear and renewable energies are the fastest growing energy sources, fossil fuels are projected to make up over 80% of the consumed energy (International Energy Outlook, 2013). Global oil consumption alone grew 1.4 million barrels per day in 2013. Non-Organization for Economic Cooperation and Development (OECD) member countries make up 51% of the consumption (BP, 2014). The year 2013 was the first time that non-OECD countries consumed more than 50% of the produced oil. A large portion of this increase in non-OECD consumption was attributed to growth in China and other non-OECD Asian countries. Non-OECD member oil consumption increases are a sign that many countries outside of North America and Europe are experiencing rapid development.

Concurrently, global oil production did not keep up with increased consumption, as production only grew by 560,000 barrels per day (BP, 2014). Shrinking production rates in many of the world's giant oil fields, such as Ghawar in Saudi Arabia and Burgan in Kuwait, are a primary reason for the low increase in worldwide production rates. As of 2007, there were 507 giant oil fields. A giant oil field is defined as a field that has over 500 million barrels of proven reserves. These oil fields are slightly greater than 1% of all

oil fields, yet they produce over 60% of the world's oil supply. Many of these large fields are over 50 years old and production rates are slowing. Of these giant oil fields, 261 have an average annual production rate decline of 6.5% (Höök, 2009). To offset these declining rates new fields must be discovered, as the need for oil is steadily increasing. Due to the declining oil production rates of fields around the world, new sources must be developed.

Lake (1989) listed four categories for adding to oil reserves:

1. Discovering new fields
2. Discovering new reservoirs
3. Extending reservoirs in known fields
4. Redefining reserves because of changes in economics of extraction technology

The expansion of technologies such as hydraulic fracturing and horizontal drilling has helped to extend reservoirs and develop known shale plays. The increase in viability of shale plays has helped the United States of America to increase oil production in 2013 by 1.1 million barrels a day (BP, 2014). While such increase in U.S. production helps meet some of the world's oil demands, more is required. Between 2000 and 2006 there were only fourteen giant oil fields discovered; and between 2007 and 2012 only seventeen giant oil fields are planned to be developed. Ten of these fields are located in deepwater environments, which are associated with high drilling and production costs (Robelius, 2007). The small amount of giant fields that have been discovered, the

increased cost of a barrel of oil, and the complex nature of most deepwater fields further precipitates the need for and value of new technologies to extend optimal, high rates of production. The increased cost of a barrel of oil allows for more capital-intensive enhanced oil recovery (EOR) techniques to be used. Another issue with many fields is primary recovery traditionally recovers 35% of the oil that is contained in an oilfield (Lake, 1989). This leaves behind 65% of the oil contained in the formation. This remaining oil is what creates value for EOR projects which, depending upon field geology and reservoir fluid characteristics can greatly increase oil recovery.

Nanoparticles are one of these new enhanced oil recovery (EOR) technologies that can be used to improve oilfield production rates. Nanoparticles are particles that have at least one dimension that is between 1 nm to 100 nm and pass through porous media with relative ease. When injected into the subsurface, they may create or break emulsions, or they may alter the porous media wettability (Kapusta, 2011). Both of these changes lead to increased oil recovery.

The objective of this thesis is to further investigate nanoparticle dispersions and their potential use in (EOR) operations. The hypothesis is that nanoparticle dispersions will decrease residual oil saturation and improve recovery. The hypothesis was tested using both polymer and glass micromodels to simulate a pore scale. The micromodels were used to trap oil and test nanoparticle potential for EOR applications.

1.1 THESIS OUTLINE

This thesis contains five chapters. The first chapter is an introduction to some of the challenges faced in the oil and gas industry and how the use of nanoparticles could potentially remedy these problems. The second chapter outlines previous research that has been done involving nanoparticles and microfluidic device fabrication and development. The next two chapters will detail the materials, procedures, results and discussion for two different types of microfluidic devices that were used. The third chapter focuses on glass and PDMS microfluidic device development. The fourth chapter discusses the results seen using glass and PDMS microfluidic devices for oil displacement. The fifth chapter states the conclusions drawn from these experiments and describes ideas for future research.

CHAPTER 2. BACKGROUND AND LITERATURE REVIEW

2.1 OIL RECOVERY METHODS

Oil production is broken down into three phases of recovery, primary, secondary and tertiary. Figure 2.1 shows a detailed breakdown of the classification of the different oil recovery methods. Primary recovery relies on the natural energy of the reservoir to displace oil to the wellbore. Natural energy sources of a reservoir are solution-gas drive, gas-cap expansion drive, natural water drive, fluid and rock expansion, and gravity drainage (Willhite, 1998). Primary recovery potential is highly dependent upon the geology, and fluid properties of the reservoir. Recovery is anywhere from 10% for solution-gas drive and up to 80% for reservoirs with a strong water-drive (Willhite, 1986). After primary depletion, there is still a significant volume of oil left behind in the reservoir. Such oil is classified as mobile oil and residual oil. Mobile oil can be extracted from the reservoir if it is contacted with enough energy (waterflooding). Residual oil cannot be removed from the reservoir unless the reservoir fluid or rock is chemically altered.

To increase recovery of uncontacted mobile oil, secondary recovery techniques are often used. Secondary recovery is often described as the addition of energy into the reservoir to increase oil displacement (Willhite, 1998). Mobile oil recovery can be increased when water or gas is injected into the reservoir to increase the energy of the reservoir. Both gas injection and water injection are used to either maintain reservoir pressure or used to immiscibly displace oil. Waterflooding can increase recovery

efficiency upwards of 50% (Willhite, 1998). After secondary recovery there is still oil that remains in the reservoir. Much of this oil is trapped and cannot be extracted without modifying the chemical makeup of the subsurface fluids. This is why tertiary recovery, which is also known as enhanced oil recovery (EOR), has become extremely common in many oil fields to further increase the economically recoverable oil (Willhite, 1998).

Tertiary recovery is broken into three main categories, gas injection, chemical injection and thermal injection. Gases (e.g. CO_2 or N_2) that are injected as part of a tertiary scheme mix with the reservoir fluid. The injected gases are either first contact miscible (FCM) or multi-contact miscible (MCM) with oil and aid in recovery. In FCM processes, the injected gas is directly miscible with oil at reservoir conditions. In MCM processes, the injected fluid is not miscible with the reservoir oil. Instead, mass transfer between phases creates miscibility. Recovery increase due to gas injection is typically between 5-15% (Lake, 1989).

The second EOR category is chemical injections. Commonly used chemicals are polymers, surfactants, and hydrocarbon solvents. Some of these injected chemicals (surfactants) can decrease the interfacial tension between the oil and the displacing fluid. Certain chemicals (polymers) may change the oil/water mobility ratio. Polymer injection can increase oil recovery up to 15% (Lake, 1989). Field trials using surfactants showed increased oil recovery up to 28%. These field tests showed that the economics of surfactants were generally unfavorable (“Chemical Methods”).

The last EOR category is thermal injection. Thermal energy, usually in the form of steam or hot water, is used to increase recovery. It is often used when recovering heavy oils. Thermal energy reduces oil viscosity and improves reservoir fluid mobility. When used in heavy oil fields, steam injection can increase recovery by upwards of 65% (Lake, 1989).

Of the three main EOR techniques thermal injection is the most popular. As of 2003, it was used in over 60% of US EOR project. Gas injection is the second most popular, making up much of the remaining EOR projects. Chemical EOR makes up a fractional amount of projects. This is likely due to higher costs of polymers and surfactants (Stosur, 2003). The average reservoir conventional oil recovery is 35%, but there is large variation from field to field. This means that EOR projects need to be reviewed on a reservoir by reservoir basis. As of 2012, EOR production is estimated to make up 4% of total oil recovery. This accounts for approximately 3 million barrels per day. There is belief that ultimately 300 billion barrels could be recovered using EOR technology (Shell, 2012).

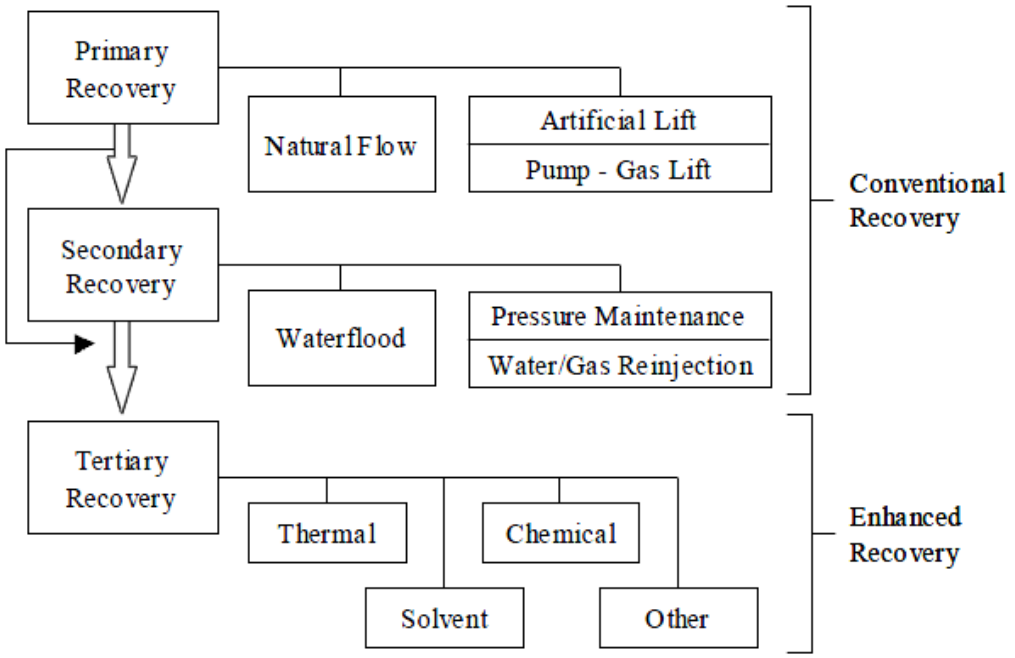

Figure 2.1 Classification of oil recovery methods (Lake, 1989).

While the three phases of production are assumed to be chronological, this is often not the case (Willhite, 1998). In certain situations, waterflooding is required from the outset of production to assist in pressure maintenance and at the outset of production; steam is needed to recover heavy oils. While immiscible gas injection is used as a secondary recovery process, Willhite (1998) notes that it is nowhere near as effective as water injections and therefore is not as common.

2.2 Residual Oil Trapping Mechanisms

Trapping of residual oil in a porous medium is due to many factors such as, pore structure, rock wettability, and interfacial tension relationships between fluids (Willhite, 1998). Reducing trapped residual oil is paramount to increasing reservoir potential. Oil trapping mechanisms are important, yet they are not well understood and can be difficult

to define mathematically. A robust understanding of how oil traps at a pore scale may help to understand the optimal method of extraction. While trapping mechanisms are complex, there are theoretical models that describe basic trapping mechanisms. Some of these models, which are described by Willhite (1998), are illustrated and explained below.

2.2.1 Pore Doublet

The pore doublet model (Figure 2.2) is a dual flow path; each flow path has a different radius. Willhite (1998), noted that a pore doublet model allows for the development of differential flow in porous media. A pore doublet model helps to understand how oil drops can be trapped and isolated. The pores are assumed to be water-wet and are filled with oil. Oil will trap if the displacement in one pore is faster than the other. Lake (1989) stated that if the length of the doublet is longer than the larger radius and the flow is slow, Poiseuille flow is applicable. In addition, the viscosity of both the wetting phase and the non-wetting phase are assumed to have the same viscosity, but this condition can be relaxed. Based on these assumptions the volumetric flow rate is given by

$$q = q_1 + q_2 = \frac{\pi}{8\mu L_t}(R_1^4 \Delta P_1 + R_2^4 \Delta P_2) \qquad \text{(Eqn. 2-1)}$$

where q_1 and q_2 are the water flow rates through each pore. The viscosities of both the wetting phase and the non-wetting phase are represented by μ. R_1 and R_2 are the radii of each pore and ΔP_1 and ΔP_2 are the pressure drops across each pore.

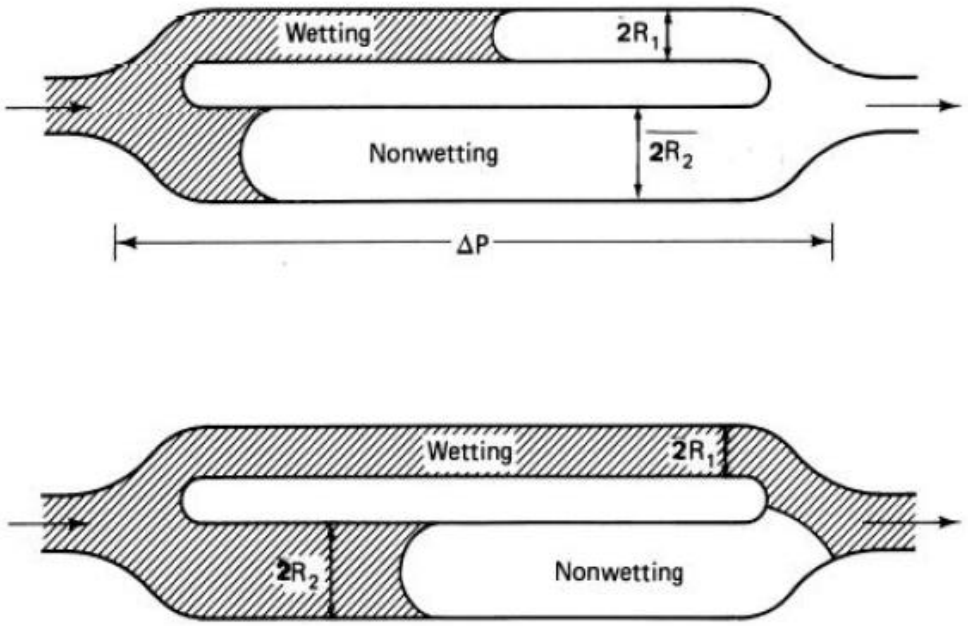

Figure 2.2 Pore doublet model example (Lake, 1989)

2.2.2 Snap-off

A snap-off model (Figure 2.3) has a single flow path with a varying cross-sectional area. The wetting phase coats the sides of the channels and the non-wetting phase flows into the pore space. The capillary pressure varies depending on the location in the pore space. At wider cross-sections, the capillary pressure is lower and at narrower cross-sections it is higher. As force is applied the non-wetting phase is pushed through the constriction until the force is insufficient to continue movement. The equation (Lake, 1989) to resume the flow of the trapped globule is

$$\Delta\Phi_w + \Delta\rho g \Delta L \sin\alpha \geq \Delta P_c \qquad \text{(Eqn. 2-2)}$$

where ΔL is the globule size, $\Delta\rho$ is the difference between the wetting phase density and the non-wetting phase density and α is the angle between the globule's major axis and the horizontal axis. $\Delta\Phi$ and ΔP_c are the wetting phase potential and the capillary pressure changes, respectively. Based upon this equation there is a competition between viscous and gravity external forces and capillary forces (Lake, 1989). The importance of a snap-off model is that 80% of trapped non-wetting phase occurs in snap-off pores and only 20% of trapped oil is found in pore doublet or other geometries (Chatzis et al., 1983). Roof (1970) did extensive work determine when snap-off will occur in converging-diverging pore space.

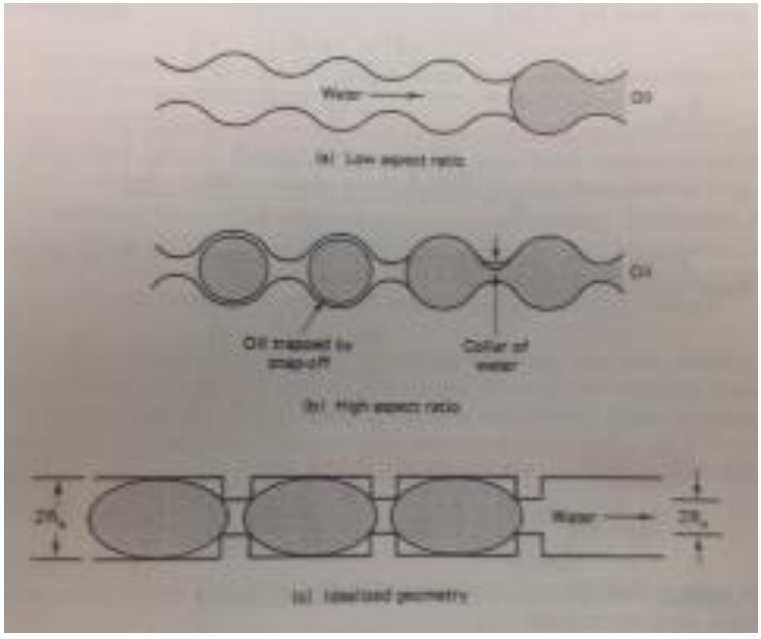

Figure 2.3 Examples of different snap-off models (Lake, 1989)

2.2.3 Dead-End Pores

Porosity is commonly broken down into absolute and effective porosity. Absolute porosity takes into account all of the rock porosity, including the unconnected pores. Effective porosity includes all of the connected pore space, which is the primary flow path of oil and gas. Dead-end pores are a part of the connected pore space, but they only have one entry to the pore system. Depending upon the system wettability, the fluid trapped in the dead-end pore becomes irreducible and cannot be removed, creating trapped oil (Tiab and Donaldson 2011).

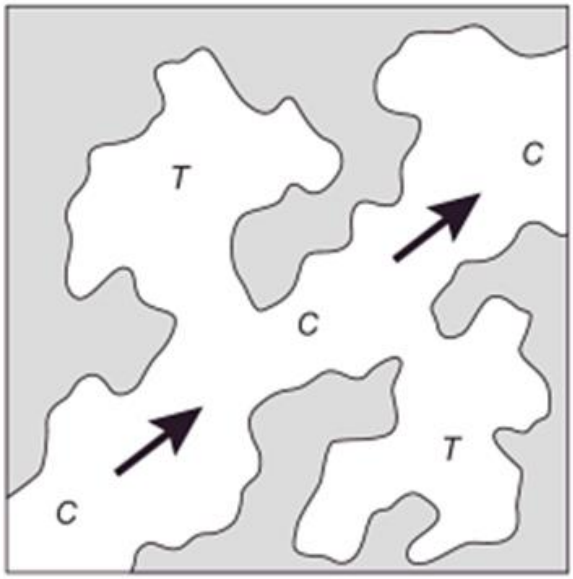

Figure 2.4 Example of two dead-end pores, fluid that flows into these pores will likely be trapped during depletion (Tiab and Donaldson 2011).

2.3 MICROFLUIDICS AND MICROMODELS

Microfluidics "is the science and technology of systems that process or manipulate small (10^{-9} to 10^{-18} liters) amounts of fluids" (Whitesides, 2006). Microfluidic

experiments may help develop an understanding of how oil traps in porous media. Microfluidic devices are valuable because they allow the experimenter the ability to see, at a pore scale, the dynamics and interactions between the fluid and solid at realistic pore scale size. The two types of micromodels that are often used are polymer based models and glass/silica based models. Table 2.1 shows a list of advantages and disadvantages of using glass and polymer micromodels in experiments.

Table 2.1 List of the potential properties of glass and polymer micromodels (adapted from Javadpour, 2008)

Polymer Micromodel	**Glass Micromodel**
Throat size ≥ 1μm	Throat size ≥ 30μm
Low cost reproduction	Costly to manufacture
Controlled wettability is possible	Controlled wettability is limited
Works best at low pressure and temperature	Operates at high pressure and temperature
Complex flow structures are easy to make	Some limitations on pattern structures
Plastic chemistry limits fluid choices	Can handle reactive fluids
Not reusable at all time	Can be cleaned for reuse
Oxygen plasma treatable	Oxygen plasma treatable

2.3.1 Glass Micromodels

In recent years, extensive work has gone into the development of fabrication techniques for glass micromodels (Grosse et al., 2001 and Chen et al., 2007). Glass

micromodels are popular because of their ability to resist mechanical stress, chemicals, and heat. Glass is also chemically well understood, inert, and it is transparent which makes it easy to view the substrate under a microscope. Much of the work with glass revolves around two distinct methods of fabrication, wet etching and dry etching. Wet etching involves the use of acids to create the desired pattern. Hydrofluoric acid tends to be the acid of choice, but the acid composition may be slightly altered depending upon needs. Dry etching initially used sand blasting of glass, but now technology has moved towards the use of gases and plasma to cut a pattern into the glass (Grosse et al., 2001).

2.3.1.1 Wet Etching

Wet etching is commonly used because is it effective for creating deep etches. It is easier and cheaper than the alternative methods. Limitations of wet etching are that it requires the use of strong and dangerous acids, such as hydrofluoric acid, to etch a pattern. It is also difficult to control the directional etching of acids which can make creating fine and intricate pattern difficult.

Wetting etching generally requires the use of photoresist film to create a pattern on the surface of the glass sample. The sample is then exposed to UV light and then developed. After development, the sample is etched in hydrofluoric acid. This is a general procedure for wetting etching glass. Figure 2.5 shows a more detailed approach.

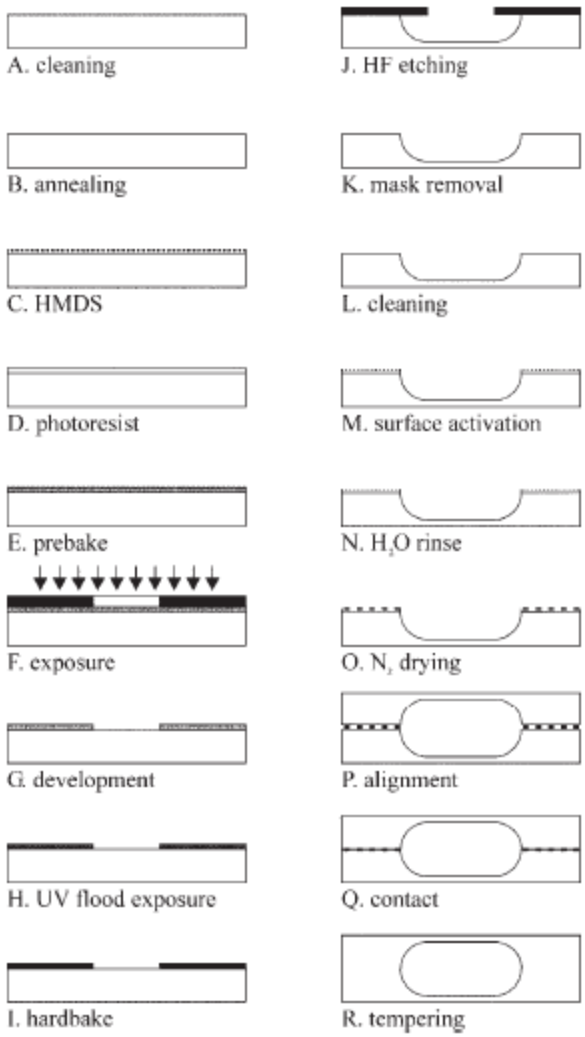

Figure 2.5 An example of a procedure for wet etching glass for the fabrication of microfluidic devices. (Grosse et al., 2001)

Many wet chemical etches of glass are accomplished using metal masks. These masks tend to be chromium layers that are used as support for metals like gold, which are etch resistant. The chromium layer is included because of its advantageous adhesive properties. Metal masks are costly, and complicated to make, as they potentially involve metal deposition. An alternative is to use soft, polymer based masks which lower

likelihood of defects, are much cheaper and easier to use. Soft masks are generally much thicker than hard masks. Although they are thicker, they are more flexible. This makes defects less likely to form during the hardening process (Grosse et al., 2001).

Iliescu et al. (2007) found that pinholes and notching are the two most common types of defects that are created when wet etching glass. According to the researchers, residual stresses in the soft mask and the hydrophilicity of the glass surface tend to cause these defects. Formation of defects is avoided by choosing the correct glass to use during fabrication. Glass which has low oxide concentrations is preferable because the oxides can react with hydrofluoric acid and create a rough surface. Annealing the glass can improve surface quality due to the redistribution of oxides and increase etch rate (Iliescu et al., 2007).

Grosse et al. (2001) showed the importance of preparing the mask in a proper manner. The mask must have good adhesion to the substrate and it must have excellent resistance to hydrofluoric acid. Without these properties the mask may dissolve and unwanted etching of the substrate can occur. To create the best etch it is important to understand the three main factors that affect the glass etch rate. The first is the etch solution, the higher the concentration of hydrofluoric acid the greater the etch rate. However, at higher concentrations, hydrofluoric acid tends to destroy photoresist film and therefore the substrate surface. The second factor is the temperature of the etch bath. Increasing the etch temperature lead to increased etching rates, but it also can increase the destruction of the soft mask. Grosse et al. (2001) found the upper limit etching

temperature to be 40°C and the best results occurred when they kept the temperature between 30 to 40°C. At a temperature of 31°C the etch rate was 120nm/min, and at 47°C the etch rate was 340 nm/min. The final factor is the level of agitation in the etch solution. When the level of agitation is too high, the soft mask may be affected and the final product may be poor. Buffered hydrofluoric acid is better to use for fused silica etching because the buffered solution is less aggressive. The buffered solution helps to protect the soft mask from being destroyed and therefore it better protects the substrate surface Grosse et al. (2001).

Another issue when etching micromodels is the quality of the etching. Soda-lime glass, which is used to make microscope slides, is commonly used to make microfluidic devices. It is chosen because it is a much cheaper alternative to expensive Pyrex or quartz glass. One of the issues that may arise in etching soda-lime glass and glass in general, is the formation of particles during the etching process. This may affect the etch rate and overall quality of the device. Because of the problems associated with soda-lime glass, many times the more expensive options must be chosen. To combat this problem, Chen et al. (2007) added hydrochloric acid to their etch solution to create a smoothly etched surface using soda-lime glass. Over the course of their two hour etch time they were able to reach depths of 110μm. They accomplished this by first soft baking a photoresist covered substrate and then after development, hard baking the substrate. This allowed for prolonged exposure to the etching solution.

2.3.1.2 Dry Etching

Dry etching techniques have been researched extensively for use in quartz and glass microfluidic devices (Li et al., 2001 and Park et al., 2005). Reactive ion etching (RIE) is a popular dry etching technique used to create deep etches in glass with a high degree of precision. RIE uses plasma to remove material from a wafer. The benefit of reactive ion etching over wet etching is that it creates an anisotropic profile because of the ability to control the directional nature of the plasma etching. Depending upon the situation, this is desirable compared to wet etching which is very isotropic. Hydrofluoric acid does not selectively etch regions of the glass, unless there is a barrier. The general procedure for dry etching is to first coat a glass plate with a thin film. The plate is then baked and lithography techniques are used. Finally, the glass is plasma etched. A more detailed procedure for a few mask techniques is shown in Figure 2.6.

The dry etch rate of CF_4 on soda lime glass is strongly affected by compounds that are created on the substrate surface. These nonvolatile halogen compounds can cause the etch rate to drop to as low as 10 nm/min. Because of the low etch rate, Li et al. (2001) attempted to use SF_6 to deep reactive ion etch Pyrex. They found that using this technique they could reach etch rates of 0.6μm/min (Li et al., 2001).

While it is possible to reach higher etch rates using the above technique; it can take large amounts of time to reach etch depths of 20μm-1mm when using plasma exposure. Fukasawa and Horiike (2003) noted that it was difficult to make a metal mask over 2μm in thickness. This was due to the internal stress in the film. One solution to

metal films was to use SU-8, which is a thick negative photoresist. The researchers were able to reach etch depths of over 100μm using CF_4 as the etching gas. Though there were two issues that they observed during etching; the development of cone defects and the variation of SU-8 etch rates over the etch time. Both problems were solved by proper cleaning of the quartz substrate followed by argon plasma cleaning.

Park et al. (2005) used SF_6 gas to create deep etches in borosilicate glass. Adjusting the gas chemistry, gas flow ratio, the top electrode power, and the dc self-bias voltage altered the etch rate and etch accuracy. Common challenges associated with dry etching are low etch rate, low glass selectivity, and the creation of high aspect ratio structures. When only SF_6 gas was used, the etch rate reached 750nm/min. Though at this etch rate microtrenching occurred in the channel because the Ni hard mask was undercut. Microtrenching creates an uneven surface at the bottom of the channel. The addition of argon gas to the etch solution solved their problem of undercutting, but the etch rate was reduced to 540 nm/min.

Baram and Naftali (2006) published results using SF_6 dry gas to etch Pyrex glass. In this work they attempted to create a better vertical profile of the channel walls. The pressure at which the etching occurs had no effect on the etching rate; so the pressure was kept low to avoid deforming the mask and to create a highly uniform etch. They used SU-8 photoresist as it would give the best etch profile. This was due to its thickness which was expected to prevent cracking of the photoresist. Using this method they could create

a notch free etch. The final channel that was developed had a depth of 47μm and a wall verticality of 85°.

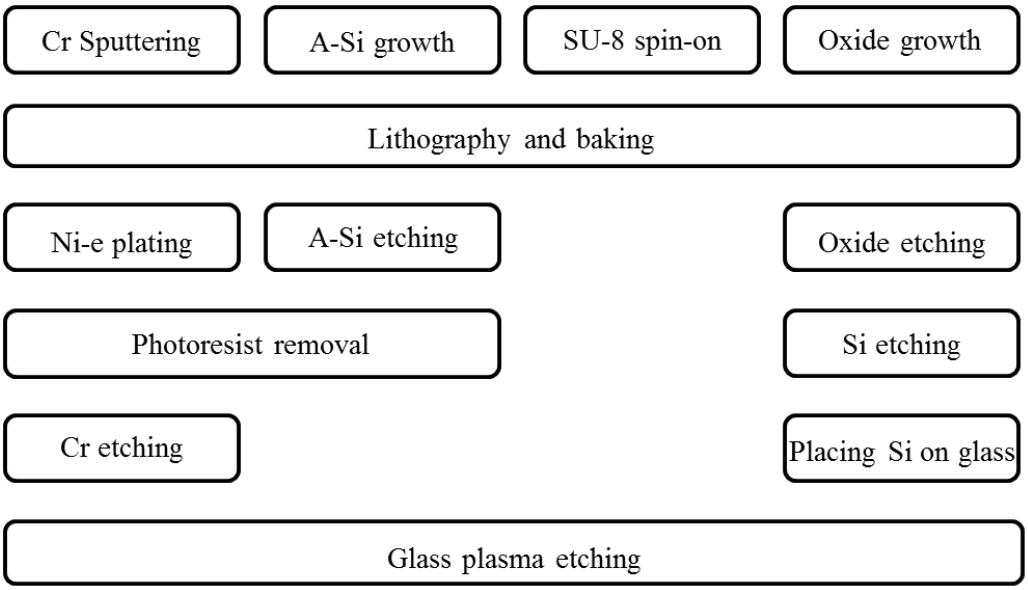

Figure 2.6 An example of different dry etching techniques (Kolari et al., 2008)

2.3.1.3 Glass Micromodel Bonding

Traditionally, glass devices are irreversibly fused together at high temperatures. This can cause problems because the surface of the glass must be thoroughly cleaned and the bonding and cooling time is usually over 10 hours. Unless one is in a clean room, it can be difficult to fully protect the device from dust. To circumvent a long fusion process Chen et al. (2007) developed a method using UV curable glue to bond glass plates together. The advantages of this method were that it did not involve dangerous chemicals and the bonding time was short. This technique only took 10 minutes to create a strong bond. If the bond needed to be adjusted or realigned, placing the chip in a sonicated acetone bath would allow for separation of the plates (Chen et al., 2007).

The high cost, complicated fabrication and long manufacturing time of glass microfluidic devices has led many researchers to look for cheap, simple and efficient alternate methods of production. Jia et al. (2004) developed a simple method to bond together two glass microscope slides at room temperature. The slide were first prewashed and then placed in a sulfuric acid bath for 8-12 hours. The sulfuric acid bath was extremely effective for removing surface contaminants, which are a major issue when bonding chips together. The plates were then cleaned under tap water and then with deionized water. To bond the slides together, they were brought into contact under deionized water and then they were air dried. During the first few hours of air drying, the bonding was extremely weak. The authors measured the strength of the bonds and found that the bond strength increased over time. The maximum bond strength for slides treated with acid was 72.2 +/- 4.1 N/cm^2. They also tested slides that were not pretreated with acid and the bond strength was slightly less than the acid cleaned plates. The likely bonding mechanism was the formation of a hydrolyzed layer between the plates. The effectiveness of the procedure was close to 95% bonding success of all the devices that were fabricated (Jia et al., 2004).

Javadpour et al. (2008) did extensive work involving high pressure and temperature micromodel development. They were able to operate their glass models up to pressures of 35MPa and temperatures up to 150°C. Much of the work done with micromodels before this study was done at low temperature and pressure, well below reservoir conditions.

2.3.2 Polymer Micromodels

Polymers are another popular material to use for microfluidic devices. Polymer micromodels are extremely common for biological applications because of their simplicity and low cost but are not yet as popular for oil and gas applications. This is mainly because many organic fluids leach from these devices. Waldbaur et al. (2011) developed a list of materials that have potential to be used in the fabrication of microfluidic devices. Table 2.2 contains the list of potential materials. As the table demonstrates, most polymers are not compatible with many hydrocarbons and many of the polymers that are compatible with hydrocarbons are more expensive. One of the most commonly used polymer materials for microfluidic device fabrication is polydimethylsiloxane (PDMS).

2.3.2.1 PDMS Micromodels

General Properties

Anderson et al. (2000) wrote about the positive and negative attributes of PDMS. PDMS is a desirable material because it cures at room temperature, it can be made extremely elastic, and it can be bonded reversibly or irreversibly depending upon the technique used. While there are many positives associated with PDMS, there are also accompanying limitations. Similar to other polymers, organic solvents are not compatible with PDMS and may cause polymer swelling. While PDMS's elasticity can be beneficial, it can also have negative consequences such as its lack of rigidity.

PDMS Device Fabrication

PDMS chips are primarily developed using photolithography and then etching silicon or glass to create a mask. First a pattern is created to make a wafer mask of the device. The mask is made using photoresist and exposing it to UV light. Then the mask is developed and pattern is now imprinted on the wafer. This mask can be used repeatedly to create a large number of PDMS chips (Duffy et al., 1998). Shown in Figure 2.7 is a set of basic steps used to create PDMS microfluidic devices.

Because PDMS swelling is such a key issue for micromodel development, understanding what fluids can and cannot be used is of the utmost importance. Koh et al. (2012) did extensive work detailing how PDMS swells when immersed in certain organic solvents. They found that the swelling of PDMS could potentially lead to delamination of bonds, which may be very detrimental to microfluidic devices. Swelling would make it impossible to keep fluid in the channel, as it would easily permeate through the walls. Of the solvents they tested hexane, toluene, ethyl acetate, n-propyl alcohol and acetone caused PDMS to swell considerably. These results were similar to the results compiled by Waldbaur et al. (2011). Another major issue with PDMS is determining the best method for sealing the microfluidic device.

2.3.2.2 Bonding and Sealing PDMS Microfluidic Devices

Bonding PDMS devices can be complicated and much work has been done to determine the best method for sealing. Duffy et al. (1998) wrote about how oxygen plasma could be used to seal PDMS microfluidic devices. Oxidized PDMS bonds to many materials, including PDMS, glass, silicon, and oxidized polystyrene.

Satyanarayana et al. (2005) described in detail the different types of bonding that are possible for all microfluidic devices. There are two main categories, direct bonding and bonding with an intermediate layer. They further categorized direct bonding into anodic bonding, fusion bonding, and activated surface bonding. Anodic bonding involves high temperatures and high voltage to form an irreversible bond between the substrates. It works well for bonding glass substrates with silicon or nitride substrates. Fusion bonding relies on attractive forces between flat surfaces in contact. Often, it is performed under vacuum to create a good contact. The substrate is then thermally cycled to strengthen the bond. Fusion bonding works well for bonding together silicon wafers. Activated surface bonding involves pretreatment with oxygen plasma, or another chemical process. These surface treatments tend to only last for a short period of time before the effects wear off and therefore bonding must be completed quickly. This process has been used frequently to bond PDMS to PDMS or PDMS to glass with high levels of success (Satyanarayana et al., 2005).

Bonding with an intermediate layer is broken down into adhesive bonding, eutectic bonding, solder bonding and thermocompression bonding. Adhesive bonding requires a thin adhesive layer on the device. Creating this thin layer is usually accomplished through the use of a spin coater. One common method is to coat glass with PDMS, and partially cure the PDMS coating. Once the PDMS is partially cured it can then be bonded to another piece of PDMS to create a sealed chip. Eutectic bonding uses a thin gold layer to bond silicon wafers together. Once in contact, the temperature is raised

to the gold-silicon eutectic point which creates an irreversible bond. Solder and thermocompression bonding are similar to eutectic bonding as they require deposition of a soft metal and use heat over pressure to create a seal (Satyanarayana et al., 2005).

Satyanarayana et al. (2005) also tested the burst pressure of a UV bonded PDMS microfluidic device and a PDMS to PDMS bonded device. The UV bonded device held to their pressure gauge limit of 700 kPa for many trials and therefore an exact burst pressure could not be determined. PDMS to PDMS bonded device held to lower burst pressures than the UV cured. The researchers also found that it was extremely difficult to peel apart PDMS to PDMS bonds and that during most of their experiments the PDMS would just tear. Another point they mentioned was that for smaller geometries ($\leq$ 20 μm) when bonding PDMS to PDMS it was necessary to partially cure the PDMS surface that the geometry was being bonded to. Otherwise the wet PDMS tended to fill the channel during bonding and destroy the device.

Samel et al. (2007) determined that PDMS, when put into contact with glass, PDMS, or silicon would form a reversible bond. This bond was formed by van der Waals attractive forces and was watertight up to 35kPa. Oxygen plasma bonding formed a much stronger, but irreversible bond due to the generation of silanol groups, and the removal of methyl groups. This, as has been previously stated, rendered the surface of the PDMS hydrophilic. One issue with oxygen plasma bonding is that the treated surfaces need to be placed into contact with one another extremely quickly. After one minute of exposure to the atmosphere, the bonding results become much weaker or the plates may not bond at

all. The bond strength varied greatly from experiment to experiment. There were many mechanisms considered to show why the surface modification lasts for such a short amount of time. Condensation of silanol groups at the surface, diffusion of low molecular mass PDMS to the surface, and the reorientation of polar groups were some of the proposed mechanisms (Samel et al., 2007).

Due to the lack of control and repeatability of oxygen plasma bonding, researchers have attempted to expand on or try new methods. These new techniques were then compared to the bond strength of traditional oxygen plasma bonding, which was used as a baseline. Eddings et al. (2008) attempted to compare different bonding techniques to determine, based upon bond strength, which one was optimal. They compared four different techniques to oxygen plasma bonding. The four techniques tried were corona discharge, partial curing, cross-linker variation and uncured adhesive. The average bond strength of a device created using oxygen plasma had an average strength of 300kPa. Though there was a large bond strength range from 180kPa to 715kPa. This agreed with earlier work which stated that oxygen plasma bonding had a large range of variation. The high fees potentially associated with using the technique may prohibit or limit use. The average bond strength of corona discharge was similar to oxygen plasma bonding. A benefit of using the corona discharge technique was the fact that a clean room facility was not required. The cross-linker variation method average bond strength was 474kPa, which was much higher than the two previous options. The method was inexpensive, and easy to use. However, increasing the base elastomer to curing agent

ratio created a much stickier and softer surface which may not be ideal for many applications. Partial curing of the PDMS layer, which was similar to the previous option, had an average bond strength of 651kPa. The benefits of this method were similar to varying the cross-linker ratio, plus it had an added benefit of keeping the elastomer base to curing agent ratio the same. A problem with partially curing the PDMS layer was that the curing time must be optimized to get optimal results. The final technique tested was the stamp-and-stick method. It had the highest average bond strength at 671 kPa. Benefits of this method were its flexibility with respect to temperature of fabrication and the cleanliness of the surface. One potential issue with the method was that the channels of the microfluidic device could be filled with PDMS if care was not taken during the stamp and glue process.

While many researchers have attempted completely new bonding techniques, some have worked to improve oxygen plasma bonding. Tan et al. (2010) attempted to extend the hydrophilic life of the oxygen plasma coated PDMS chips. They treated their chips for up to five minutes to see if that may help to prolong hydrophilicity. Increasing treatment time may lead to surface cracks in the PDMS. A longer treatment time resulted in a smaller contact angle between the PDMS surface and the flowing water. At longer exposure times the PDMS plate was also able to stay hydrophilic for up to six hours. They were able to store their devices in deionized water under vacuum conditions and the hydrophilicity lasted for over 7 days. They reasoned that this was due to the high surface energy of water, which prevented the reorganization of the silanol groups. Koh et al.

(2012) developed a method using piranha solution to bond PDMS to PDMS. Piranha solution, which is a strong oxidizer, is a mixture of sulfuric acid and hydrogen peroxide. It is commonly used to clean organic surface residue. PDMS surfaces treated with Piranha solution became noticeably more hydrophilic. This was due to the piranha solution being a strong oxidizer. It changes the surface properties of many polymers, including PDMS. When the surface of PDMS was oxidized, silanol groups form on the surface. When two layers of oxidized PDMS were brought into contact intermolecular forces created a Si-O-Si bond between the surfaces. The bonds created could withstand up to 210kPa-350kPa of air pressure. Researchers also tested different acids in an attempt to reduce the risk associated with using a sulfuric acid based piranha solution. Compared to sulfuric acid, nitric acid was not as effective. This was due to the fact that there are less hydrogen ions in nitric acid than sulfuric acid. During tensile testing the strength of the nitric acid treated chips was 25% less than that of the sulfuric acid treated chips. They concluded that a higher number of hydrogen ions mean that it would take less time to oxidize PDMS. They saw similar, lower bond strength, results when testing phosphoric acid and hydrochloric acid. Also, if PDMS was treated for too long with piranha solution a silica layer will form on the PDMS surface.

Table 2.2 List of potential micromodel materials and their swellability with different chemical groups (Waldbaur et al., 2011).

Material	Hydrocarbons, aliphatic[a]	Hydrocarbons, aromatic[b]	Halogenated hydrocarbons, aliphatic[g]	Mineral acids[c]	Organic acids[d]	Bases[e]	Organic solvents[f]	Plasma, UV irradiation	Swelling in water (mass %), long term exposure	Price
Classical materials										
Glass	+	+	+	+[i]	+	+	+	+	0	Medium
Silicon	+	+	+	+	+	–	~/+	–	0	Medium
Silicon dioxide[h]	+	+	+	+[i]	+	+	+	+	0	Medium
Duroplastic polymers (thermosets)										
Epoxy resins (SU-8)	+	+	~/–	+	~	+	+	–	High	High
TE	n/a	n/a	+	n/a	+	–	+	–	Medium	High
PU	~/+	~/+	–	~/+	–	~/+	–	–	0	Low
Parylene C[j]	+	+	+	+	+	+	+	~	0	High
Thermoplastic materials (thermoplasts)										
PMMA	+	–	–	~/+	~/+	–	–	+	2	Low
PC	~/–	~/–	–	~/+	~/–	–	–	–	0.4	Low
POM	+	+	~/–	~/+	~/+	+	+	–	0.2	Low
PS	–	–	–	~/+	+	+	–	–	0	Low
PSU	+	–	–	+	+	+	–	–	0.6	High
PEEK	+	+	–	~/+	~	+	+	~/+	0.5	High
PE[k]	+	~	~/+	+	+	+	+	–	0.1	Low
PVC	+	–	–	+	+	+	–	–	1.6	Low
PET	~	–	~	~	–	–	–	–	0.5	Low
COC	–	–	–	–	+	+	+	–	<0.1	Low
PP	+	~	–	+	+	+	+	+	0	Low
PTFE	+	+	+	+	+	+	+	+	0	High
Elastomers										
PDMS	–	–	–	~/+	~/+	~/–	–	–	Medium	Medium
PFPE	+	+	+	+	+	+	+	+	Low	High
FFKM	+	+	+	+	+	+	+	+	Small	High
FKM/FPM	+	+	+	+	+	~/+	–	+	Small	High
FEPM	+	+	–	+	+	+	~/+	+	Small	High

[a] *E.g.*, tetradecane. [b] *E.g.*, toluene, ethylbenzene, xylene. [c] Sulfuric acid, hydrochloric acid, nitric acid. [d] *E.g.* lactic acid, acetic acid, formic acid. [e] *E.g.*, potassium hydroxide, sodium hydroxide, calcium hydroxide. [f] *E.g.*, acetone, methyl acetate, ethyl acetate. [g] *E.g.*, trichloroethylene, perchloroethylene. [h] Usually as coating only. [i] Very high solubility in hydrofluoric acid (HF). [j] Details about other types of parylene can be found in the literature.[40] [k] High density (PEHD).

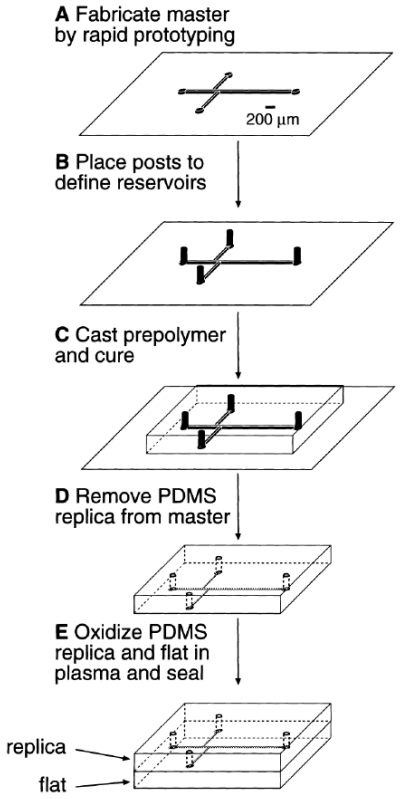

Figure 2.7 Example procedure for PDMS micromodel fabrication (Duffy et al., 1998)

2.3.3 Micromodels in Experimental Work of Hydrocarbon Recovery

Xia et al. (2008) did extensive work with polymer flooding. Their work related to both computational and experimental investigation of micromodel scale dead-end geometries. In their computational simulations, they determined that streamlines and velocities changed depending on the elasticity of the polymer injected. They found that micro-forces increased with increasing elasticity. The researchers used Hydrolyzed Polyacrylamide (HPAM), which is a viscoelastic polymer, in their experimental work. Using a dead-end geometry they ran simulations comparing different Weissenberg number (*We*) fluids at a constant Reynolds number. A Weissenberg number is the ratio of

the shear rate of a fluid multiplied by its relaxation time. A *We* of zero represents a fluid with no elastic nature (an example fluid would be water). A *We* greater than zero means that the fluid has some elasticity.

Xia et al. (2008) revealed that the velocity in their dead-end geometry simulation of HPAM was greater than the velocity in the water case. They also found that it was easier for HPAM to enter the dead-end pores and it was more difficult to remove it from the dead-end. This was a benefit of HPAM and other viscoelastic polymers, because viscoelastic polymers spend more time in the dead-end. Because HPAM remains in the dead-end for a longer period of time, there was more potential for increased oil recovery.

In conjunction with the computational modeling of a dead-end pore, Xia et al. (2008) also developed an experiment using microfluidic devices with the same dead-end pore geometry. An oil-wet microfluidic device was used to experimentally determine the benefits of viscoelastic polymers in dead-end pores. They compared the viscoelastic polymer results to those of glucose, which is completely inelastic. To ensure an equal pressure gradient between trials researchers kept the viscosities of both solutions similar. Comparing to a base case of water, the researchers showed that dead-end oil recovery increases slightly due to increased viscosity (glucose), but viscoelasticity was much more important for increasing oil recovery and reducing residual oil saturation. Figure 2.8 shows the experimental results obtained by Xia et al. (2008). It shows that oil recovery was much higher and the residual saturation was much lower in the viscoelastic polymer trial (c) than the other two cases. This was an extremely interesting result and the dead-

end geometry seems to be an idea that would be easier to execute than other geometries such as the pore doublet and the snap-off model.

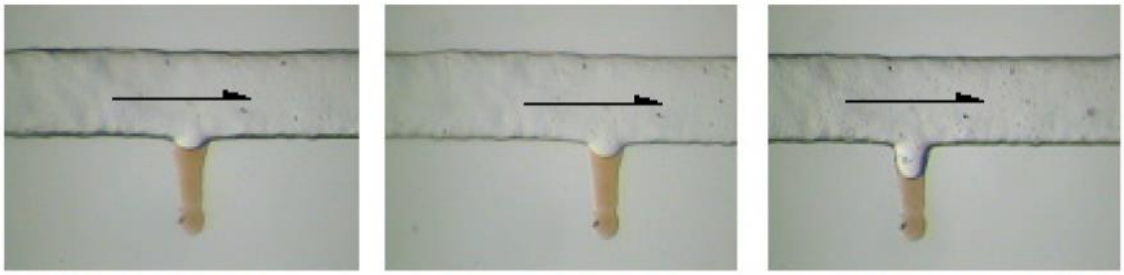

Figure 2.8 Microfluidic device experiments using water (base case), glucose, and polymer to recover oil (Xia et al., 2008).

2.4 NANOPARTICLES FOR EOR

Nanoparticle use for EOR is a relatively new concept that is still in development. This section will give a basic introduction to potential nanoparticle applications and it will describe different types of nanoparticles that may be of use in EOR applications. Next, potential nanoparticle mechanisms that aid in oil recovery will be described. Finally, previously accomplished nanoparticles in micromodel work will be described.

2.4.1 Introduction to Nanoparticles

Nanoparticles with potential for oil applications are any particles that have dimension between 1 to 100nm. These particles have potential applications in upstream oil exploration and production (Kapusta, 2011). Investigators, (Mcelfresh, Hendraningrat) have provided anecdotal and experimental evidence of improved oil recovery in porous media using nanoparticle solutions.

The characteristics of nanoparticles that make them potentially beneficial to oil and gas production are their size, and the ability to manipulate properties. Particles that are smaller than one micrometer can travel through a reservoir pore space with relative ease. Manipulation of nanoparticles can modify particle wetting properties, or fluid surface tension among other properties. Nanoparticles may also have the potential to release surfactants, breakers, and other chemicals downhole at a precise location. The release may be related to time, pH, or temperature and may help to further increase field productivity (Kapusta, 2011). This would help to reduce chemical loss to the rock matrix during injection. An example nanoparticle application was to control waterfloods using swellable particles. During a waterflood there may be a preferential flow path that reduces sweep efficiency. These nanoparticles could swell and plug large water channels, and help to improve reservoir sweep efficiency. Swelling may be caused by changes in pH or temperature (Kapusta, 2011). Another potential use of nanoparticles (studied in this thesis) was to directly enhance oil recovery through the use of nanoparticle dispersions. Nanoparticle dispersions have a higher viscosity than water, without a large increase in density. These dispersions may also alter rock wettability and interfacial tension. These surface modifications may help to increase recovery in both developed and undeveloped fields (Kapusta, 2011).

There are many different nanoparticles with potential for use in EOR. To better understand the positive and negative aspects of certain nanoparticles Ogolo et al. (2012) populated a list of particles types that would potentially be effective for enhancing

recovery. The researchers experimented with aluminum, zinc, magnesium, iron, zirconium, tin, and silicon oxide particles. In their experiments they used brine, distilled water, ethanol, and diesel as the dispersing agent. They tried to displace oil with a nanoparticle dispersion and they also left nanoparticles in sand for sixty days and then injected oil and displaced oil with brine. The authors found that displacing oil with nanofluids was more effective for recovering oil than coating sand with nanoparticles.

Based upon their research, aluminum oxide and silicon oxide particles were the best options for enhanced oil recovery. The aluminum nanoparticles reduced oil viscosity and the silicon particles altered rock wettability. They also stated that using ethanol as a dispersing agent in their experiments could alter the outcome. This was because ethanol reduces the oil-water interfacial tension, which would help to recover more oil. Out of the four base dispersants (ethanol, brine, distilled water, and diesel), distilled water was the worst with regards to recovering oil. They also noted high recovery when using silica nanoparticles in brine. Success using particles in brine was extremely important because when these particles are injected into the subsurface they will be interacting and mixing with reservoir brine.

There are many benefits to silica nanoparticles compared to other potential options. Some of those benefits are ease and control of production, and the properties and interactions of silica-based materials are extremely well known. Also, silica particles are easily functionalized with different groups to make them more hydrophobic or hydrophilic (Miranda et al., 2012). However a reoccurring problem with silica

nanoparticles was that at higher salt concentrations, the stability of nanoparticle dispersion could wane and agglomeration might occur (Miranda et al., 2012).

Iron nanoparticles have also been experimented with in porous media. Iron nanoparticles have potential benefits for environmental cleanup because of their ability to treat chlorinated compounds. A major issue with iron nanoparticles in glass micromodels was that they tend towards agglomeration due to high surface energies and magnetic interactions (Wang et al., 2011). While this does not seem ideal for enhanced oil recovery, the magnetic nature of the particles makes them an interesting concept.

Two other interesting nanomaterials are titanium dioxide (TiO_2) and aluminum trioxide (Al_2O_3) nanoparticles. Researchers found that TiO_2 particles show a higher degree of wettability alteration of a quartz plate than silica particles and Al_2O_3. TiO_2 particles reduced the brine-quartz contact angle from 54° to 21°. This wettability alteration has the potential to be extremely beneficial for enhancing oil recovery as the dispersant can more easily spread and displace oil. One negative aspect of metal oxide particles was that when untreated, and left in a brine solution, they tended to aggregate more quickly than silica particles. Aggregation of nanoparticles may cause pore blockage. This was not unexpected as the silica nanofluid has a higher particle charge potential. To create a more stable metal oxide solution, researchers Hendraningrat et al. (2014) used polyvinylpyrrolidone (PVP) as a dispersant. PVP is a polymer and may be an effective due to its emulsifying properties or it may coat the particles. Using PVP, they

increased metal oxide nanofluid aggregation time from a few hours to over 48 days (Hendraningrat et al., 2014).

2.4.2 Other Nanoparticle EOR Experiments/Oil Field Uses

Significant work has been performed using a variety of EOR techniques in corefloods and micromodels. Much of the work in corefloods and micromodels has involved polymers, such as Hydrolyzed Polyacrylamide (HPAM). Recently, researchers have experimented with nanoparticles in corefloods and experimental success has led researchers to attempt to use nanoparticles in field tests. These field tests tended to deal with formation damage removal rather than EOR. While there has been little reported field work involving EOR, the success related to formation damage removal may lend itself to nanoparticle potential for EOR.

2.4.2.1 Filter Cake Cleaning

Mcelfresh et al. (2012) performed work determining the potential oil field applications of nanoparticles and have observed success using nanoparticles in both experimental and field tests. In field studies they used nanoparticles to remove near wellbore paraffin damage and polymer blockage. Paraffin damage was alleviated by injecting solvents into a well. Polymer blockage of the near wellbore region was due to increased use and development of hydraulic fracturing. Flow-back after a frac job is between 30-50% of the injected fluid and much of the substance left behind is the associated polymer or the proppant pack. When polymer material is left behind it can cause serious well performance problems. Typical methods of remediation involve doing

of a workover, and dissolving and displacing the damage. For both types of damage stated above, these methods tend to be temporary fixes as they only push the damage further into the formation. This can negatively impact reservoir performance and precipitates the need for another intervention.

The use of nanoparticle dispersions may potentially alleviate the problem. Instead of pushing damage into the formation, nanoparticles may be able to help effectively pump the damage out of the well. The author's stated that the mechanism of damage removal must be similar to, if not the same as, the spreading mechanisms postulated by Wasan et al. (2003). Once the nanofluid removes the damage from the surface of the rock, a solvent is used to dissolve the damage, and to make transportation to the surface much easier.

The authors also completed experimental studies using polymer-coated filter cakes. Their goal was to determine the most effective method for removing the polymer from the surface of the filter cake. They tested three different solutions including a base solution, one with unmodified silica particles solution, and a surface modified silica particles solution. In the last solution, the silica particles were modified using silane. It led to particles which were hydrophobic on one side and hydrophilic on the other. Each solution contained a small amount of ammonium persulfate breaker. However, the amount of breaker in the solution was not enough to remove the damage by itself. A filter cake was left in each solution overnight. When reviewing the results they noted that both nanoparticle trials performed better than the base case, which left behind over half of the

polymer filter cake. The silica particle trials removed over 90% of the polymer from the filter cake. The modified particles demonstrated the best performance, removing 100% of the polymer from the filter cake.

They also discussed the positive results that they observed using nanoparticles in the field. One example given was associated with an underperforming well in the Sprayberry formation. Using a nanoparticle dispersion mixed with a paraffin solvent, a 100% increase in daily production was recorded. This was similar to what was normally seen with standard oil hot treatment for paraffin remediation. The difference was that the production levels remained high for 90 days before retreatment was needed. This was three times longer than the operator had seen using only hot oil. They have tested nanoparticle dispersions in a few other situations, such as a salt water disposal well in Colorado, and they saw similar levels of success. They reported that after treatment of the injection well with a nanoparticle dispersion and acid, injection pressure had dropped by 350 psig with the same amount of water injected per day. These anecdotal success stories show nanoparticle potential in subsurface operations.

2.4.2.2 Coreflood Experiments

There are three board categories that nanoparticles for improved oil recovery (IOR) can fit into. These three categories are stabilized emulsions and foams, delivery vehicles for chemicals and sensors, image-enhancement for improved formation evaluation. The nanoparticles required for these categories must show long term stability and the must be able to travel long distances. Nanoparticles should show minimal

reservoir retention (Zhang et al., 2011). To better understand nanoparticle EOR utility at a large field-size scale, rigorous experimental work must be completed. Much of the recent work has revolved around coreflood experiments. Yu et al. (2012) tested the adsorption of silica nanoparticles in sandstone, limestone, and dolomite cores. Particle adsorption was 1.272 mg/g in sandstone, 5.501 mg/g in limestone, and 0 mg/g in dolomite. They postulated that the cause of the low adsorption of silica particles in sandstone was because both sandstones and silica particles were comprised of SiO_2. Therefore it was due to particle to particle repulsion. Clay minerals in the sandstone core may have caused the low adsorption. The higher adsorption that was seen in the limestone core was likely due to the electrostatic forces between the silica nanoparticles and limestone. Though the sandstone and the limestone cores had some adsorption, the researchers stated the permeability of both cores was not affected by this adsorption. However, the dolomite core, which had no adsorption likely, had some permeability reduction. This was a possibility, because there was an increasing pressure drop across the dolomite core over time, indicating that core plugging and a permeability reduction was occurring. This work demonstrated that, nanoparticle adsorption was a likely outcome and if used improperly, there was potential for nanoparticles to plug formations and impede production.

Caldelas et al. (2011) tested nanoparticle retention in unconsolidated rock. Boise sandstone and Texas Cream limestone were crushed and pack into columns. Clays were added to some of the sandstone cores. The researchers hoped to better understand the

mechanisms for nanoparticle retention in porous rock. Coated and uncoated silica nanoparticle dispersions were in injected into the columns. Experiments were performed varying different parameters such as nanoparticle surface area, salinity, velocity among others. They found that nanoparticle retention was low and averaged about 8% for all experiments. The factors that had the most profound effect on particle retention were particle surface area and to a lesser extent increased salinity. An interesting finding was that grain lithology had a modest impact on nanoparticle retention.

While the above study only reviewed adsorption of nanoparticles in different rock media, many other studies have examined nanoparticle potential to increase oil recovery. One such study involved the use high permeability Berea sandstone cores. Torsater et al. (2012) showed that nanoparticles were effective when used as part of an EOR scheme. In their work, they used hydrophilic silica nanofluids in two injection schemes, both as a secondary and a tertiary process. Using nanofluids of 0.01%-0.05% silica particles, they saw an 8% higher recovery of oil using nanoparticles as a secondary recovery process over a standard brine flood. Using nanoparticles as a tertiary process they saw an additional recovery of 2%. The probable cause of this increase in oil recovery for both secondary and tertiary recovery was due to a decrease in interfacial tension. While there was an increase in the amount of oil recovered, there were permeability and porosity alterations to the core. There was high permeability and porosity impairment in the core. Core impairment was likely the result of nanoparticle adsorption at the rock surface.

To complement their work with high permeability Berea sandstone cores, Torsater et al. (2013) completed work with low and medium permeability Berea sandstones. They found that using nanoparticles did not always lead to the positive results that they saw with high permeability Berea cores. When a 0.1 wt.% silica nanoparticle solution was used there was very little additional oil recovered. They stated that this was likely due to the fact that the nanoparticles had blocked pore throats and reduced permeability. Using a 0.05 wt.% silica nanoparticle solution increased oil recovery up to 6%. They concluded that there likely was some critical weight percentage of nanoparticles over which enhanced recovery would be negatively impacted. Due to the heterogeneous nature of most reservoirs, finding this critical weight percentage could prove difficult.

Mcelfresh et al. (2012) completed work using both sandstone and limestone cores to test the enhanced oil recovery potential of nanoparticles. They used Berea sandstone and Indiana limestone cores for their testing. The concentration of their nanoparticle dispersion was 10 wt.% silica nanoparticles, 2 wt.% KCl and the rest was deionized water. They had to slightly modify the nanoparticle dispersion for the limestone core due to the rock's positive surface charge. The cores were first saturated with oil and then they flooded the cores with brine to reach residual oil saturation. The nanoparticle dispersion was then injected. After 10 pore volumes of the nanoparticle dispersion were injected the cores were shut in overnight. The next day, the cores were injected with brine and oil recovery was monitored. They were able to recover over 40% of the remaining oil in the

limestone core after injecting with nanoparticles. From the sandstone core they were able to recover over 60% of the oil that was left behind after the initial brine flood.

Gabel (2014) recently completed coreflood work using nanoparticles to enhance oil recovery. The cores were initially at residual water saturation, with the remaining pore space filled with mineral oil. IPA-ST nanoparticle dispersions were injected into the core. The flow rate was incrementally increased from 3 mL/min to 24 mL/min. At 3 mL/min the oil bank was displaced, but no emulsion was produced. When the flow rate was increased to 6 mL/min, a small amount of additional oil was recovered, but no emulsion formed. The flow rate was increased to 12 mL/min and the shear rate was 1784 s^{-1} and additional oil was recovered as a stable emulsion. At 24 mL/min the shear rate was 3568 s^{-1} and more oil was recovered. Gabel noted that an increase in the capillary number at higher flow rates allowed for some additional oil recovery. The amount of oil that was recovered using the nanoparticle dispersion was more than just using a brine flood at the same flow rates.

Hendraningrat et al. (2014) used metal oxide nanoparticles in corefloods and have found some success. Using Berea sandstone cores they were able to increase oil recovery 7-11% using TiO_2 and Al_2O_3 nanoparticles in a tertiary flood. Following up a nanoparticle flood with an additional brine flood resulted in an increase in the amount of oil recovered from the core. They proposed that this increased recovery was due to wettability alterations of the rock caused by the addition of metal oxide particles. They

also stated that a lower pH due to the metal oxide nanoparticles may have affected recovery, but they believe that the effect is not the major part of displacement.

2.4.3 Potential Nanoparticle Recovery Mechanisms

Recent work related to the use of nanoparticles for EOR has involved studying fundamental mechanisms through which nanoparticles modify the contact line between phases. The methods described below are wedge spreading theory, IFT reduction and wettability alterations. Alterations to the contact line change the rock surface wettability, which may increase oil recovery. An understanding of this behavior will help realize nanoparticle potential for enhanced oil recovery.

2.4.3.1 Wedge Spreading

Wasan et al. (2003) have completed extensive work studying nanofluids and their potential application. The spreading and adhesive properties of nanoparticles can create a desirable, an effective circumstance in a multitude of oil and gas related processes. These include soil remediation after potential environmental disasters, and enhancing oil recovery. De gennes (1985) stated that the displacement of one fluid by another spreading fluid is caused by the need to minimize free energy of the system. As noted by Chengara et al. (2004), nanofluids do not follow spreading or adhesive concepts of simple liquids. Instead, Wasan et al. (2003) stated that nanofluids will "self-assemble" at a three-phase contact. This region-specific assembling of nanoparticles was a result of an increase in entropy, which was due to the nanoparticles in the bulk fluid phase having more freedom to move.

Monte Carlo simulation work and experimental work were conducted and demonstrated that this order and assembly would enhance the spreading behavior of a nanofluid (Tata et al., 2000 and Wasan et al., 2003). The nanoparticle spreading and wedging behavior is shown in Figure 2.9. Wasan et al. (2003) found that as the film thickness decreased, the spreading coefficient *S* increased. The spreading coefficient is described by the equation

$$S = \sigma_{S/O} - \sigma_{S/L} - \sigma_{O/L} \qquad \text{(Eqn. 2-3)}$$

where each σ term describes the interfacial tension between each part of the system, water-oil (O/L), water-solid(S/L), and oil-solid(S/O). Liu et al. (2012) determined that when the spreading coefficient was positive, spontaneous spreading would occur. In Figure 2.10 the wedging and organization of latex nanoparticles can be seen around an aqueous layer.

The nanofluid spreading behavior seen in Figure 2.10 was caused by structural disjoining pressure (Chengara et al., 2004). Structural disjoining pressure, as defined by the authors, was created by the confinement of nanoparticles in the aqueous spreading wedge film. Through simulation work, they found structural disjoining pressure to be a strong enough force to move the nanofluid wedge. The spreading of the nanofluid wedge helped to peel the oil from the rock surface. The structural disjoining pressure was normal to solid-liquid interface. There was an increase in the structural disjoining pressure increases the spreading coefficient of the aqueous film. The authors suggested that the driving force for aqueous film spreading was excess film energy, which took the

form of structural disjoining pressure. De gennes (1985) developed a relationship between disjoining pressure of the wetting phase and the spreading coefficient.

$$S = \Pi(h)h + \int_h \Pi(h)dh \qquad \text{(Eqn. 2-4)}$$

The spreading coefficient is described by *S,* Π(h) is the value of the disjoining pressure of the wetting phase and h is the thickness of the wetting phase film.

Kondiparty et al. (2011) used Monte Carlo simulations to show that nanoparticles displayed more order and structure near the vertex of the three phase contact. The pressure exerted on the wedge was highest at this point. Based upon simulation results, the tip pressure could be as high as 50 kPa. The authors also determined that the concentration of nanoparticles, particle size and contact angle greatly affect the spreading quality of the nanofluid. Using silica nanoparticles in their nanofluid simulations the authors found that displacement of the contact line was greater with a smaller particle diameter, a higher particle concentration and the solid-water contact angle less than 5°. A major conclusion of their work was that they were able to obtain complete wetting, and therefore spreading at contact angles greater than 0°. The authors also determined that when a sodium chloride (NaCl) solution was added to their simulation, the result was a reduction in structural disjoining pressure. They concluded that this was likely caused by the fact that the driving force for spreading was removed or decreased, due to the addition of the an ionic salt. A decrease in the driving force of spreading due to salt concentrations was something that may negatively impact nanoparticle performance in a reservoir due to the presence of brine in the formation.

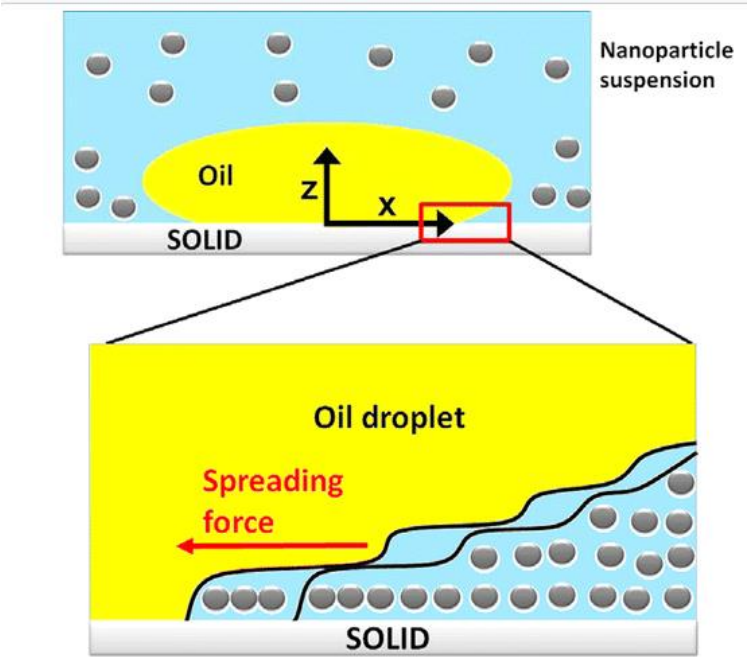

Figure 2.9 An example schematic of nanoparticle wedging and spreading at the three phase contact. (Kondiparty et al. 2011)

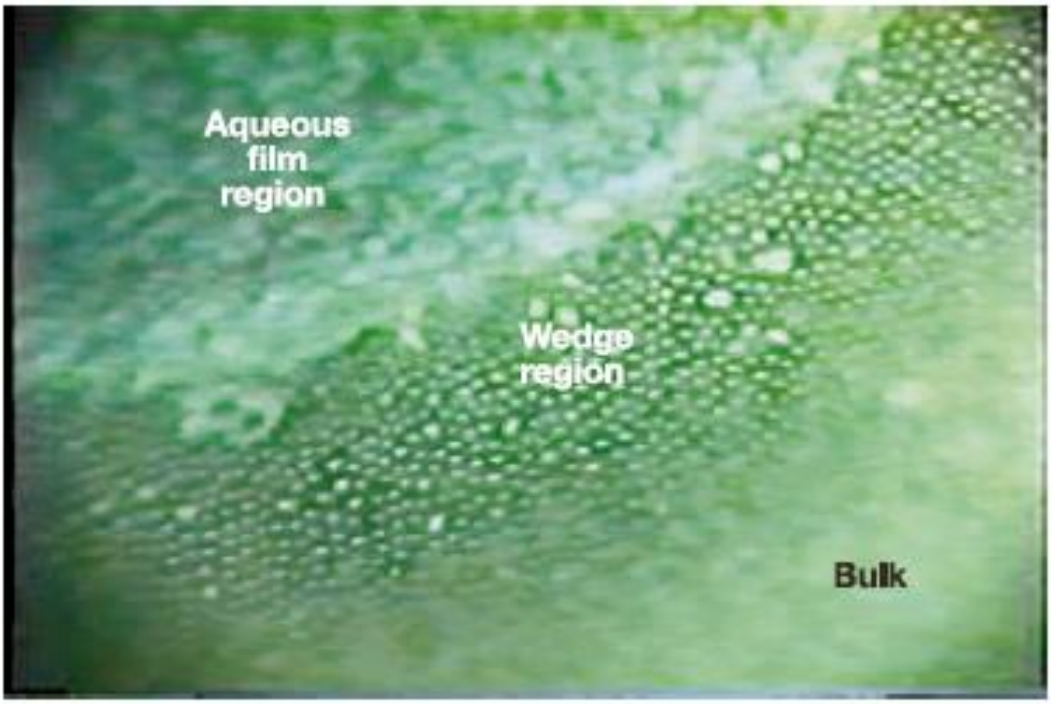

Figure 2.10 Latex particles forming a wedge region around an aqueous film, showing that particle arrangement occurs. (Wasan et al. 2003)

2.4.3.2 Interfacial Tension (IFT) Reduction

Research has also been completed which analyzed the potential impact of interfacial tension (IFT) on enhancing oil recovery using nanoparticles. IFT reduction was seen when a nanoparticle dispersion, which was delivered in a brine solution, contacted oil. Hendraningrat et al. (2012) used a spinning drop and observed a decrease in the interfacial tension between synthetic oil and a brine/nanofluid. A 0.01% wt. silica nanoparticle solution in brine will decrease the interfacial tension from 14.7mN/m to 9.3mN/m. Increasing the percent by weight to .05% resulted in a reduction of the interfacial tension to 5.2mN/m. Lower IFT was one of the potential mechanisms by

which nanoparticles may aid in enhanced oil recovery. This was because less energy will be required to mobilize and remove oil trapped in the formation.

2.4.3.3 Wettability

Wettability is another factor that is extremely important when attempting to understand and improve oil recovery. Willhite (1998) defined wettability as the tendency of one fluid to spread or adhere to a solid surface in the presence of a second fluid. Wettability is extremely important to understanding reservoir behavior. Sandstone and clastic reservoirs are traditionally water-wet and carbonate reservoirs tend to be oil-wet. Water-wet means that water will cover the surface of the rock and oil-wet means that an oil phase will coat the rock. Figure 2.11 shows a comparison of water-wet and oil-wet rock. While this has been traditionally held as the standard, Willhite (1998) wrote that this is not always the case. Many reservoirs are considered to be intermediate wet or mixed wet. Intermediate-wetting occurs when both of the fluids (oil and water) are able to wet the rock surface; but one phase may have a slight wetting preference. Figure 2.12 shows an example of a mixed-wetting rock. Mixed-wetting is the result of heterogeneous variations in the fluid contacted rock surface. Increasing reservoir rock heterogeneity leads to a higher degree of difficulty when attempting to optimize oil recovery (Willhite 1998). This difficultly is due to the contrasting and inconsistent nature of the fluid-rock interaction.

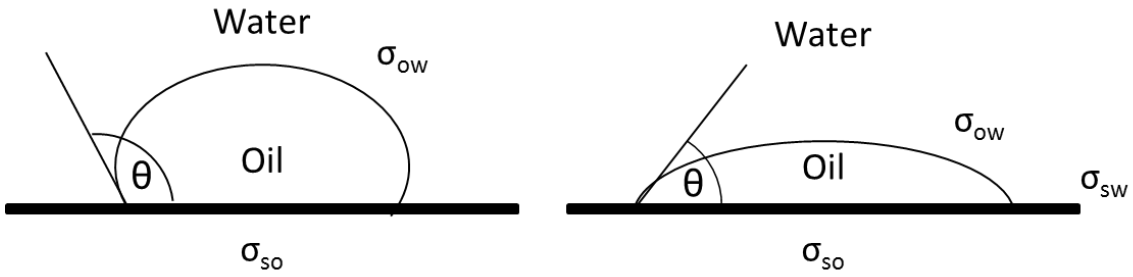

Figure 2.11 A comparison of a water-wet (R) surface and an oil-wet surface (L).

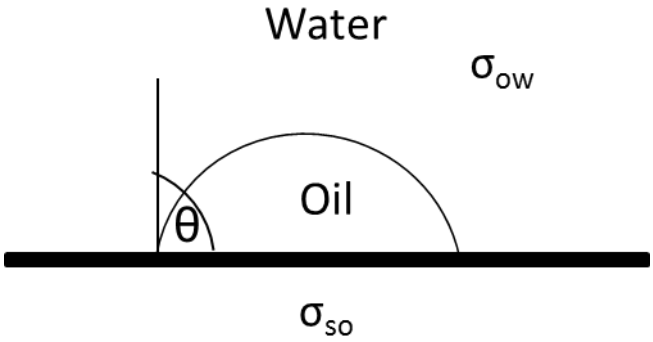

Figure 2.12 Intermediate-wet rock, the oil-water contact angle is approximately 90°

Rock wettability alteration can occur during many phases of oil production. The alteration of water-wet rock to oil-wet rock due to interactions with oil-based drilling fluids and asphaltene adsorption onto the rock surface are a few of the potential reason for the change in wettability changes (Karimi, 2012) These changes can greatly affect the productive life of an oil field. An example of how wettability affects reservoirs would be oil-wet carbonate reservoirs. Due to their oil-wet nature, more oil is left behind in carbonate reservoirs than in sandstone reservoirs, because the trapped oil is difficult and even potentially impossible to move, especially during a waterflood. Modifying the

wettability of the rock to create a more water-wet surface could help to increase the oil recovery of a carbonate reservoir. Wettability alterations can be made using chemical agents such as surfactants, or solvents. There are two proposed mechanisms to explain how surfactants alter rock surface wettability. The first is surfactant adsorption onto the surface of the oil-wet rock. The second is that the surfactant cleans the rock surface, which alters the surface wettability. Nanoparticles are believed to have a similar potential for altering the wettability of a rock. This is due to their high surface energy, which allows them to easily adsorb onto the rock surface. If the nanoparticles used are hydrophilic in nature, their adsorption onto the rock creates a more water-wet surface (Giraldo, 2013). Karimi et al. (2012) tested a surfactant and nanoparticle mixture by using ZrO_2 particles, to determine the potential of their wettability modification on carbonate rocks. They found that this mixture changed the carbonate wettability from oil-wet to water-wet. Such change creates an effective means for increasing oil recovery, although the wettability alteration was a slow process which took 2 days to occur. When operating at a field scale, this may require wells to be shut-in to allow for nanoparticle adsorption. This may lead to well downtime and loss of profits due to well shut-in.

The wettability alteration of sandstone cores due to nanoparticles has also been tested. Giraldo et al. (2013) used Al_2O_3 particles in an attempt to understand the wettability alteration potential of oil-wet sandstone cores. From their study they determined that Al_2O_3 nanoparticles have the ability to modify the rock surface of a sandstone core from oil-wet to water-wet. The wettability alteration effectiveness of

anionic surfactants was improved when using concentrations of 100 ppm Al_2O_3 nanoparticles. Even without the presence of surfactant, adding Al_2O_3 nanoparticles alone to a waterflood can improve total oil recovery, indicating that nanoparticles alone had the ability to enhance oil recovery.

2.4.4 Nanoparticles in Micromodels

Corefloods provide excellent insight into how nanoparticles respond to flow through actual rock; but they are somewhat of a black box because visualization at the pore scale is difficult. There has been a limited amount of work performed involving the use of micromodels to study nanoparticles and their effect on enhanced oil recovery. One such study was done by Hendraningrat et al. (2012). In this study they ran experiments using glass micromodels to determine the effect of nanoparticles on oil recovery in the glass model. They used two different types of silica nanoparticles, HNP-A which had a diameter range from 15nm-40nm and HNP-B which had a size range of 20nm-50nm. The other properties of both particles were very similar. The initial permeability of the glass micromodel was 25 D. The permeability impairment using HNP-A of their model was between 41%-72%. The impairment using HNP-B was between 17%-21%. The specific surface area of the HNP-B particles was less than that of HNP-A at similar weight concentrations. They could not confirm a relationship between nanoparticle concentrations, permeability and injection rate of the particles.

Li et al. (2013) used multi-pore glass micromodels to test the EOR potential of hydrophilic silica nanoparticles. They found that at lower nanoparticle concentrations

(0.01 wt.% and 0.05 wt.%) oil recovery was controlled by increasing flow rate. At higher nanoparticle injection concentration (0.1 wt.%) model oil saturation decreased. The researchers noted that at higher injection rates, some of the oil droplets would break into smaller drop emulsions and help push oil through pore throats. Similar to Hendraningrat et al. (2012), there was potential for micromodel permeability reduction due to nanoparticle injection.

CHAPTER 3: MATERIALS AND METHODS

Methods used to produce PDMS and glass microfluidic devices are described in Chapter 2. PDMS microfluidic devices are quick, easy, and cheap to produce. Glass, while it is more time consuming to fabricate, has more robust properties that make it well suited for oil recovery testing. The pore geometry initially tested was a dead-end geometry. The dead-end geometry was tested because it was assumed that fabrication would be easy and repeatable. Other models were such as a converging-diverging pore space and a pore doublet model were also fabricated. This chapter will describe the methods and procedures used to produce PDMS micromodels as well as the experimental procedure. Finally, the results that were obtained and a discussion of key findings will be summarized this chapter.

3.1 PDMS MICROMODELS

In this section, the materials required and methods used to fabricate and manufacture PDMS microfluidic devices are described. These fabricated devices will be used to test the EOR potential of nanoparticles. Many experiments were run using PDMS devices and the procedure describing how to flow fluid through the device is described in section 3.2.

3.1.1 PDMS Device Fabrication

The methods used to fabricate PDMS microfluidic devices are standardized in the field and there is little differentiation in common practice. Duffy et al. (1999) or

Anderson et al. (2000) are good sources for standard methods of PDMS micromodel fabrication.

3.1.1.1 Materials

PDMS microfluidic devices were created using a silicone elastomer kit. Sylgard® 184, manufactured by Dow Corning, is the most common kit used to make PDMS microfluidic devices. The kit contains an elastomer base and a curing agent. From the Dow Corning website, PDMS has a clear color; it cures after 20 minutes when left at 125°C. It is a self-leveling, hydrophobic material, with an operating temperature range of -45°C to 200°C. It is compatible with ceramics, plastics, and polyesters. Some other general properties of PDMS are that it has a low odor, it resists oxidation reasonably well, and after curing it is a thermoset polymer.

3.1.1.2 Steps to Produce PDMS Micromodels

1. Photolithography

A pattern was required to create a mask to develop a PDMS mold. The mask was created using CAD software. If available, a high resolution printer can be used to print the mask out. Otherwise the CAD drawing needs to be sent out for printing. CAD/Art Services, Inc. (Bandon, Oregon) was used to print out masks. Shown below in Figure 3.1 is a pattern that was received from CAD/Art Services, Inc.

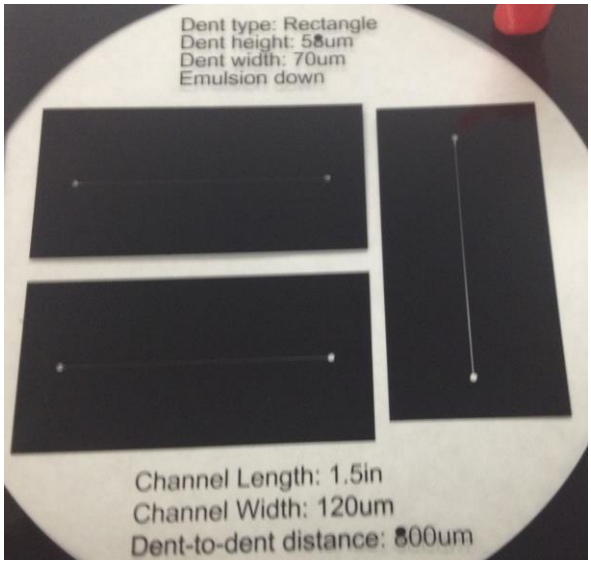

Figure 3.1 Example of a pattern that was received from CAD/Art Services, Inc. The pattern was used as a mask to develop a PDMS mold.

To create the mold, cleanroom facilities were required. The mold was created using a circular silicon wafer. Next, the surface of the silicon wafer was coated with a thin film of photoresist (SU-8 3025, MicroChem). One item to note when using photoresist is to determine whether a positive or a negative resist is required. SU-8 is a negative photoresist which means that when it is exposed to UV light, the photoresist is polymerized and hardened. Positive photoresist works opposite to negative photoresist. It is important to choose the correct photoresist for the material and method that is implemented. Figure 3.2 shows diagram of the difference between positive and negative photoresist.

After coating the wafer, it was placed on a spin coater (Laurell Technologies). The wafer was spin coated to create an even uniform layer of photoresist. Figure 3.3 is an

image of the spin coater. The spin rate was 500 rpm for 5 to 10 seconds and then it was increased to 3000 rpm for 30 seconds.

The wafer was then baked for 10 to 15 minutes at 95°C to ensure solvent was evaporated and the photoresist was hardened. After baking, the photoresist layer should be hard and no imprint should be left behind. After the photoresist hardens, the wafer was ready to be imprinted. To imprint the artwork pattern onto the wafer, the Suss Mask Aligner located in the UT Nanocenter was used. Figure 3.3 contains an image of the mask aligner. The mask aligner exposes the silicon wafer to UV light, which baked and crosslinked the area on the wafer that was not covered by the mask. The exposure time should be 20 seconds. After exposure the wafer was baked again for 1 minute at 65°C and then another 3 minutes at 95°C. Once baking was complete, the wafer needed to be developed using the SU-8 developer solution. The wafer should be left in the developer solution for about 6 minutes. Once the wafer was developed, the final mold has been created. Figure 3.4 shows what the silicon wafer looks like after it has been developed.

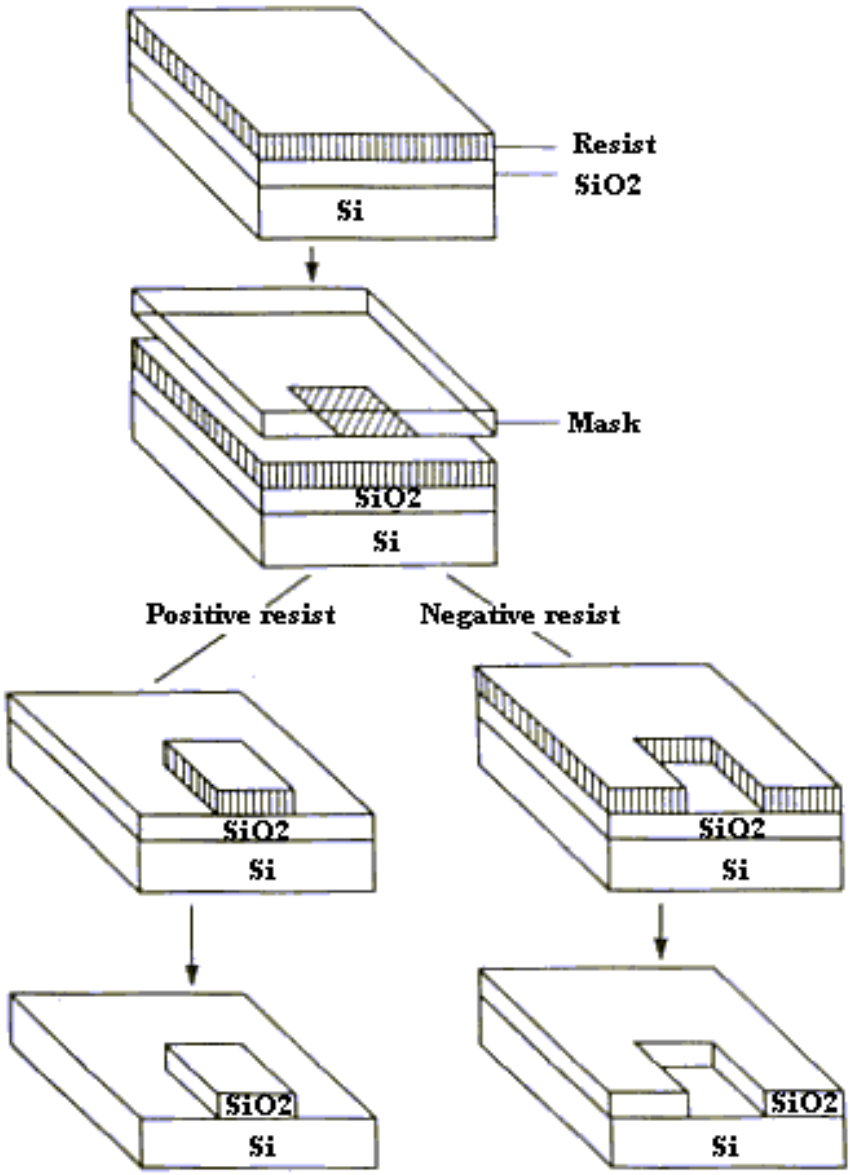

Figure 3.2 Diagram which visually describes positive and negative photoresists when used on a silicon wafer.
(http://www.ece.gatech.edu/research/labs/vc/theory/PosNegRes.html)

Figure 3.3 The Laurel Technologies Spin Coater (Left) and the Suss Mask Aligner (Right). Both pieces of equipment are found in the UT Nanocenter Clean Room.

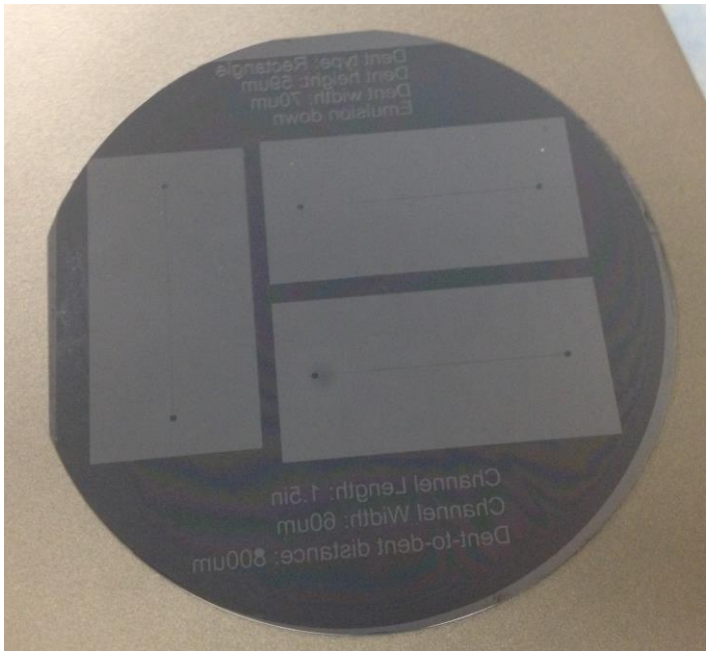

Figure 3.4 Final PDMS mold that was created using the above technique.

2. PDMS Chip Molding

Once the mold has been created, PDMS device fabrication can commence. The first step of fabrication was to mix together a 10:1 ratio of Sylgard® 184 base elastomer to curing agent. This is the manufacturer's recommended ratio. After mixing the elastomer and the curing agent, there was a tendency for air bubbles to trap in the mix. To remove bubbles, degas the mix with desiccator attached to a vacuum pump. Once the pockets of air were removed from the PDMS mix, it was poured onto the silicon wafer mold. The wafer was placed into the oven at 110°C for 20 minutes to cure the PDMS.

Once fully hardened, take the PDMS out of the oven. Care must be taken, when removing the PDMS from the wafer. An X-Acto® knife or a utility blade was helpful to peel the PDMS from the wafer. Now that the PDMS chip has been peeled, 0.5" diameter holes were be punched into the inlet and outlet ports of the channel.

3. Sealing

The next step was to create the glass backing for the chip. A glass microscope slide was coated with a layer of PDMS. This layer of PDMS was used as a bonding surface for the chip. To create a thin, even layer for bonding a spin coater was used. A hot plate was used to partially cure the PDMS on the glass slide. Partial curing was deemed the best option to use when bonding. The small size of the pore space would make using uncured PDMS difficult. The chip was partially cured on the hot plate at 70°C for 17 minutes. The slide should be checked after 15 minutes to see if partial curing was complete. Partial curing was complete when marks were no longer left behind on the PDMS layer.

The partially cured PDMS was brought into contact with the channel side of the chip. The newly constructed microfluidic device was placed into the oven at 100ºC for 15 minutes to complete the bonding between the plates. Once the bonding was complete, tubing was attached to the inlet and outlet ports of the chip. Tubing stability was increased by placing a cap around it and then filling with PDMS. The device was then put back into the oven at 100ºC for 10 minutes to bake the PDMS which provided support to the tubing.

Once the tubing was sufficiently stabilized, slide a screw onto the tubing. This screw was used to attach the tubing to a valve, which allowed for fluid flow into the device. Once the screw has been placed on the tubing, the end of the tubing needed to be flanged. This ensured the tubing would not be easy to pull from the valve. Flanging was done with a Hamilton flanging kit. Flanging was done slowly to ensure that the tubing did not tear. When the tubing was fully flanged, place the flanged end of the tubing into water to cool it. Figure 3.5 shows an example of a completed PDMS microfluidic device. Figure 3.6 shows a microscope view of the pore space tested in many of the experiments. The geometry tested had five dead-end pores.

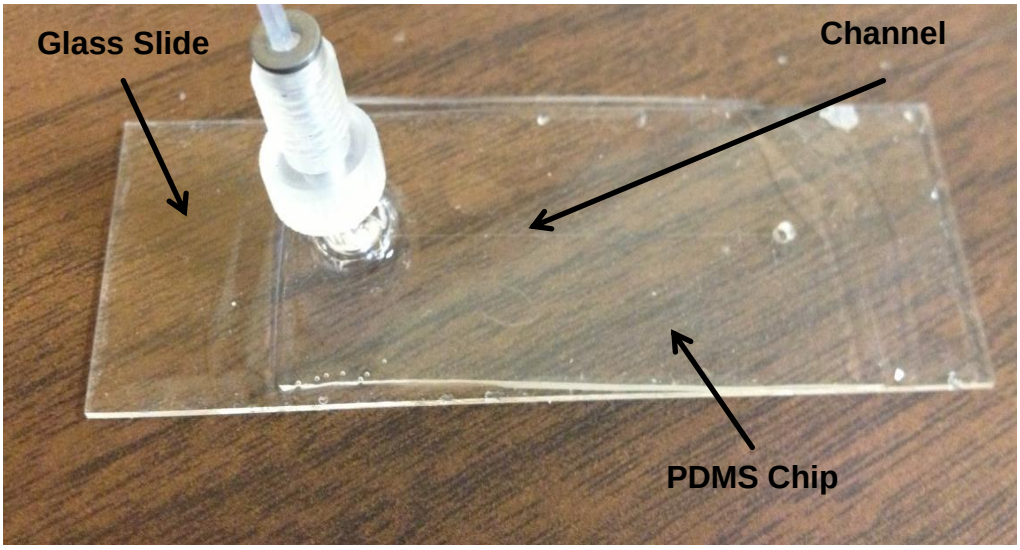

Figure 3.5 A PDMS microfluidic device. The labels on the figure point to the "Glass Slide" that provides the rigid support for the device. The "PDMS Chip" and the "Channel" through which fluid flows are also labelled. Other items contained in this image are the tubing through with the fluid flows to the chip and the screw used to attach the tubing to a valve.

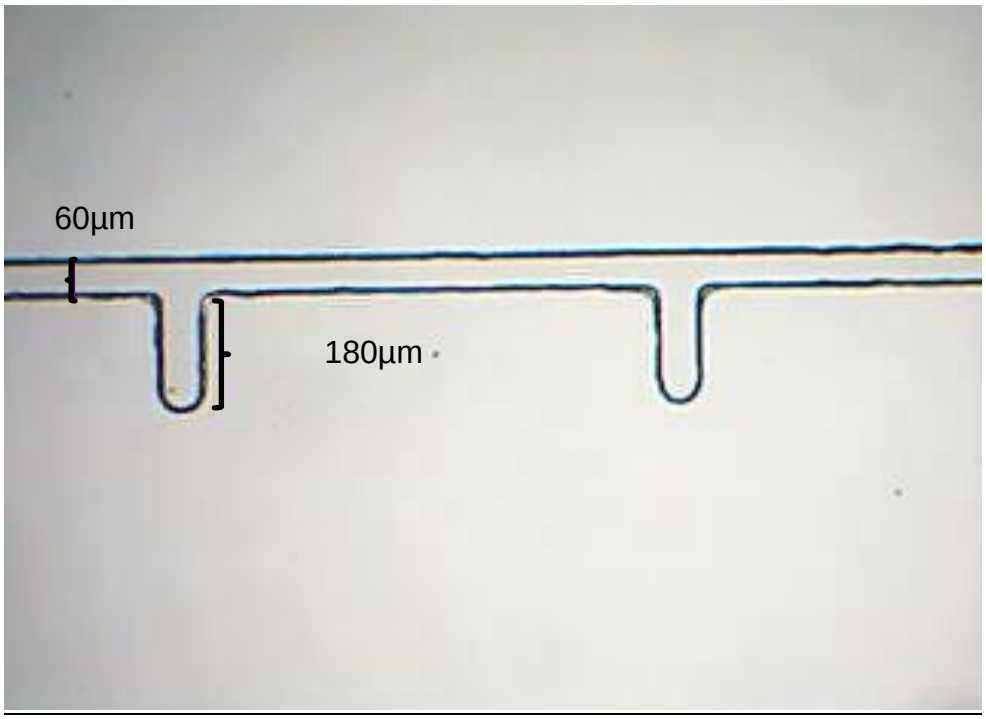

Figure 3.6 Image of a dead-end pore space, with labeled dimensions, of the above microfluidic device.

3.2 Flow Through PDMS Devices

The materials required to test the enhanced oil recovery potential of nanoparticles were a nanoparticle dispersion, oil, and deionized water. As stated, in Chapter 2, many oils easily diffuse into PDMS, so for these experiments mineral oil was used as it should not permeate as easily.

3.2.1 Materials Used

Pumps

There was only one pump required for the system. Figure 3.7 shows the experimental setup. At the left side of the figure is an image of the Chemyx Fusion 200 syringe pump. The pump is used to inject water, and oil into the microfluidic device.

Microscope and Camera

An OMAX light microscope was used to observe the flow inside the channel, and the phenomena were recorded by a digital camera attached to the microscope. A picture of the OMAX microscope is at the center of Figure 3.7.

3.2.2 PDMS Flow Procedure

1. Attach the mineral oil filled syringe to the Hamilton HVD4-5 valve (Figure 3.8)
2. Attach waste line to the Hamilton HVD4-5 valve
3. Attach microfluidic device to the Hamilton HVD4-5 valve
4. Place microfluidic device on the microscope platform and find the geometry
5. Turn on the Dell Latitude laptop and open the camera program "amcap.exe"
6. Once the pore space is on is clear on the video screen; turn on the syringe pump and begin flowing fluid, if there are pockets of air in the tubing, make sure the valve is turned to flow towards the waste to remove the air pockets
7. Once the pockets of air are removed; begin flowing fluid into the channel
8. Once the channel is filled with mineral oil, switch to deionized water; flow the deionized water through the waste line to remove any air pockets
9. After the air pockets are removed, begin flowing water towards to the microfluidic device
10. Once the fluid has reached the channel begin recording to document the fluid behavior.

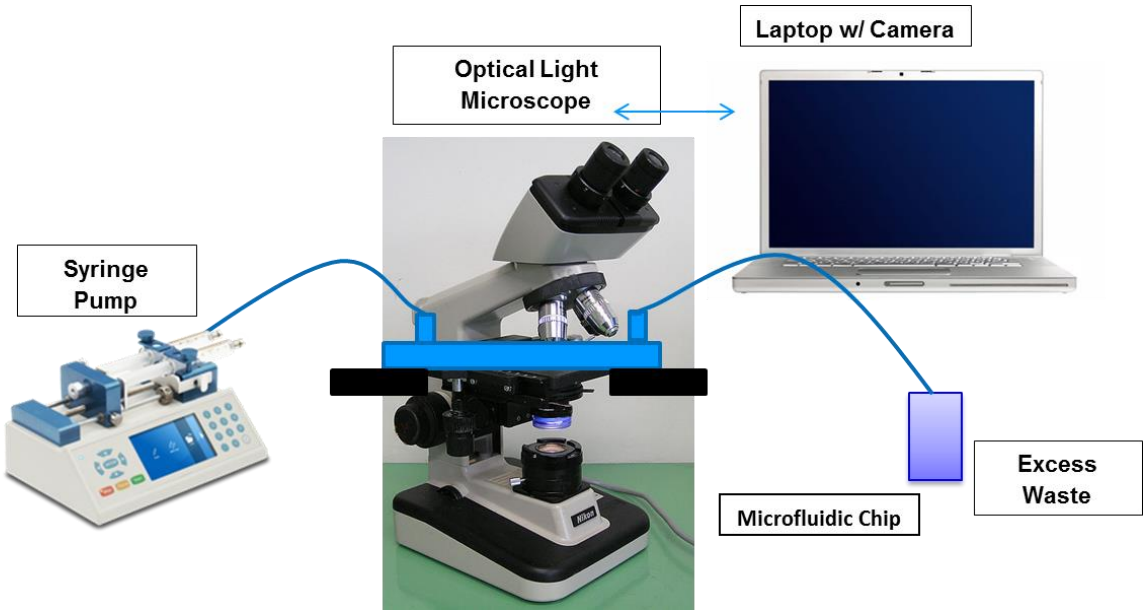

Figure 3.7 An example image of the experimental setup. The setup contains a syringe pump, an optical light microscope, a laptop with an attached camera, a waste container and the fabricated microfluidic device. The syringe pump injects fluid into the microfluidic device; the microscope is used to view the flow of the injected fluid into the device. The computer with attached camera records the fluid flow and the waste container collects spent fluid.

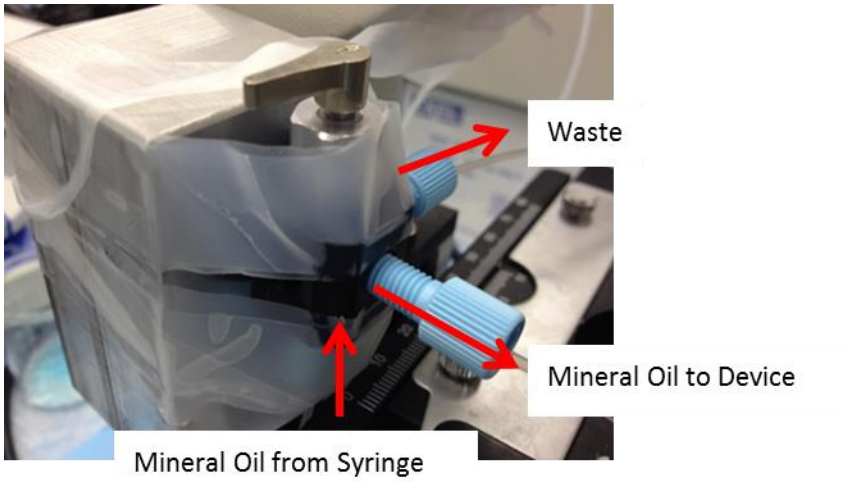

Figure 3.8 Image of the Hamilton HVD4-5 valve with attached tubing. The valve has one inlet port and 4 outlet ports. Oil and water flow into the inlet port (as shown with the red arrow and labeled "Mineral Oil from Syringe") and flow out to either the waste container (labeled "waste") or to the microfluidic device ("labeled "Mineral Oil to Device").

3.2.2.1 Fluid Flow Rate into Microfluidic Device

It was important to choose an appropriate flow rate when injecting fluid into the microfluidic device. The goal was to have a flow rate that would closely match the rate of a standard waterflood which is approximately 1 ft/day. The syringe pump only gave a volumetric reading of the fluid flow rate. Therefore the fluid rate must be determined by

$$u = 78720 * \frac{V}{A} \qquad \text{(Eqn. 3-1)}$$

where u is the fluid velocity is in ft/day and V is the fluid volumetric flow rate is in µl/hr. A is the microfluidic device cross-sectional area is in unit of um^2. The units of the coefficient are $\frac{hour*\mu m^2*feet}{day*\mu L}$.

While the goal was to create flow conditions that closely mimic field operations, sometimes this was not practical. On occasion the flow rate required was too low for the syringe pump to give an accurate reading and sometimes the desired condition does not give a valuable result. What "valuable result" means is that at certain flow conditions it may be difficult to consistently trap oil in the pore space. This was an important step in the research, before nanoparticle EOR can be tested, conditions where consistent and repeatable oil trapping was required. Therefore the flow rate that created these conditions may be higher or lower than what may be realistic.

3.3 GLASS MICROMODELS

After testing PDMS micromodels, glass micromodels were developed. Glass micromodels were fabricated because of their differing properties from polymer devices. Many of the property differences have been noted in the Chapter 2. Two of the major differences are that glass micromodels tend to have a surface that is much more hydrophilic than PDMS and injected oils will not leach from glass micromodels. The difference in wettability may have an impact on the recovery effects of the nanoparticles that have been used.

3.3.1 Glass Micromodel Fabrication

In this section, the methods used to fabricate and manufacture glass microfluidic devices are described. These fabricated devices were used to test the EOR potential of nanoparticles. Many experiments were run using glass devices and the procedure describing how to flow fluid through the device is described below.

The methods used to fabricate glass micromodels are not as standardized as PDMS micromodels. Grosse et al. (2001), Chen et al. (2007) and Kolari et al. (2008) are good resources for glass micromodel fabrication. These sources describe the two different etching techniques, dry etching and wet etching. The micromodels described in this thesis were wet etched.

3.3.1.1 Materials

Glass micromodels were created using Erias Home Designs™ mirrors purchased from the Home Depot. Mirrors were ideal for glass micromodel fabrication because they have a protective metallic layer and therefore one did not need to be deposited on the surface. This metallic layer both protected the glass that did not need to be etched and provided a better bonding surface for photoresist deposition.

3.3.1.2 Steps to Produce Glass Micromodels

1. Created artwork

A pattern was required to create a mask for development of the glass model. This is similar to the PDMS artwork that was needed. CAD software was used to create a pattern. The pattern was sent to CAD/Art Services, Inc. (Bandon, Oregon) to be printed. Figure 3.9 shows and example of a positive mask.

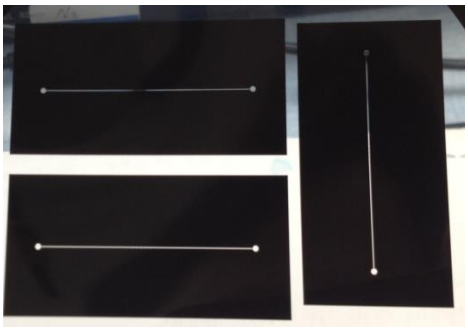

Figure 3.9 An example of a positive mask used in the development of a glass micromodel. Refer to Chapter 3 for details and images of negative mask, which are used to make PDMS microfluidic devices.

2. Mirror Modification

The mirrors have a protective hard paint layer on the back which needed to be removed, to expose the copper layer below. Methylene chloride was used to remove the backing from the mirror. The amount of time that the mirror needed to be left in the methylene chloride was dependent upon the paint backing. When removing the hard paint layer care should be taken, as the copper layer below can be easily scratched off. Figures 3.10 and 3.11 show the mirror back before and after methylene chloride treatment. It should be noted that mirrors bought from the Home Depot tend to have different backings from batch to batch. So far mirrors used have had silver or copper backings. The silver backed mirrors required only a few minutes to remove the hard backing, while the copper mirrors required longer soaking time. The rest of the described method will refer to the copper backed mirrors, but the procedure should be the same when working with silver backed mirrors.

Once the hard paint coating was removed, the plate was cleaned to remove any residual methylene chloride from the surface. The plate was then dried with compressed air.

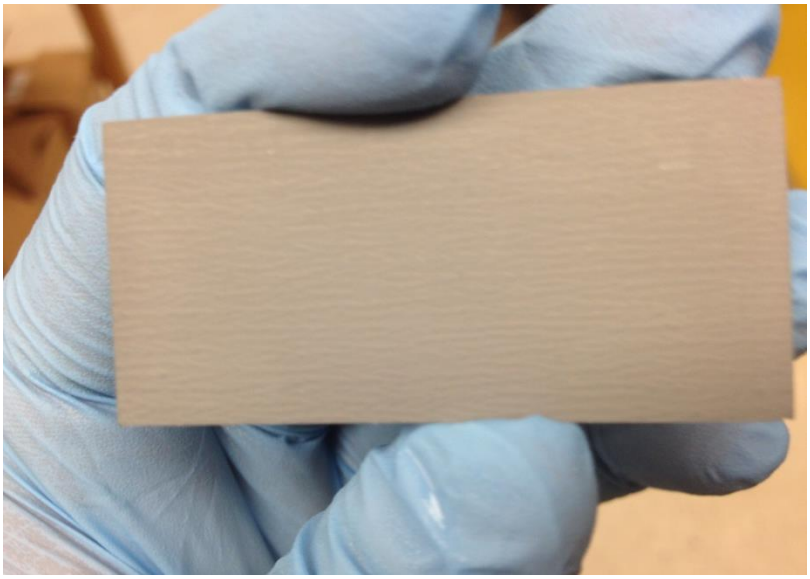

Figure 3.10 Mirror before treatment with methylene chloride

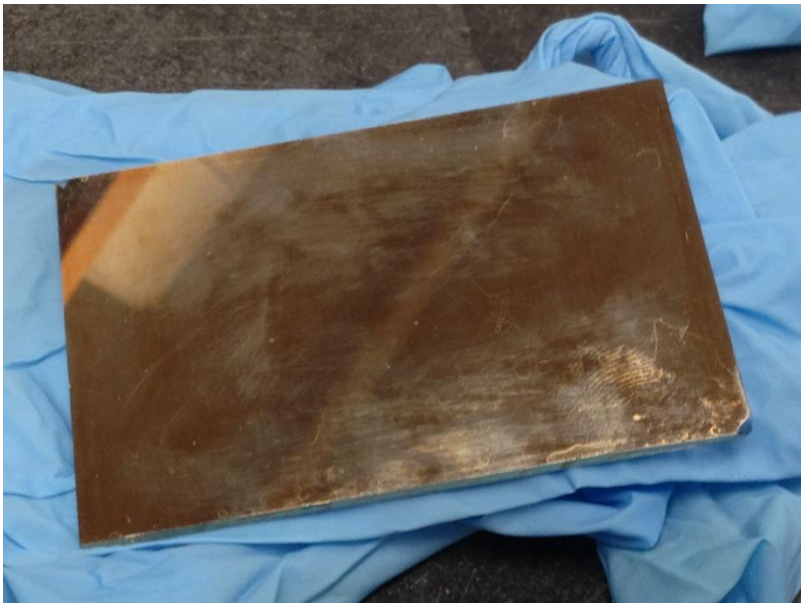

Figure 3.11 Copper backed mirror after treatment with methylene chloride

3. Cleanroom

After removing the hard paint backing from the mirror, it was brought to the cleanroom to imprint the pattern. First clean the copper side using acetone, isopropanol, and deionized water. Next, the copper side of the mirror was coated with a film of photoresist. S1818 was found to be the best photoresist to use. To create a thin uniform layer of photoresist, the Laurell Technologies spin coater was used. The spin coater procedure was to spin at 500 rpm for 5 seconds, then 3000 rpm for 5 seconds and finally 3000 rpm for 30 seconds.

After the photoresist layer has been spin coated onto the mirror, it must be baked for 2 minutes at 95°C. The layer should be fairly hard, so that when a finger was placed on the corner no imprint was left behind. Figure 3.12 shows an example of the S1818 coated mirror.

After the photoresist has hardened, the designed pattern was imprinted onto the mirror. To imprint, a Suss Mask Aligner was used to expose the mirror to UV light. This will bake the area on the mirror that was not covered by the mask. The exposure time was 17 seconds. After exposure, the mirror was developed for 1 minute in MF-319 developer solution. It is crucial to make sure that the developer solution has removed all of the photoresist from the exposed region as this was what would be etched. If the developer was not completely removed from the pattern, the final product would have an uneven and poorly etched surface. Once the mirror was developed using the developer solution, the pre-etching process can begin.

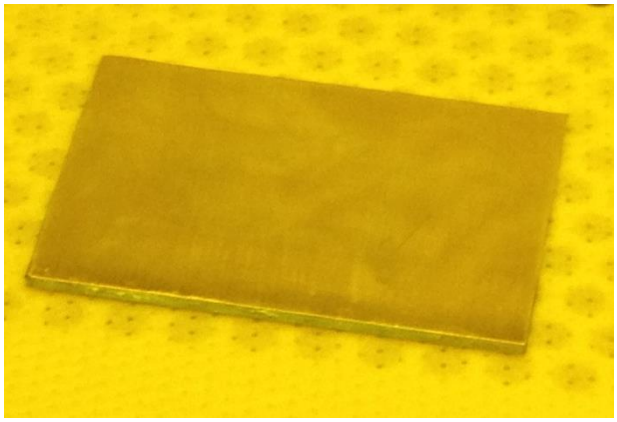

Figure 3.12 Copper backed mirror coated with S1818 photoresist

4. Pre-Acid Etching

The first step when etching the mirror was to remove the copper layer from the region of the mirror that was developed. This was initially done with nitric acid, but nitric acid may dissolve some of the photoresist. This would lead to unwanted etching and render the device unusable. Because of this finding, iron tri-chloride ($FeCl_3$) has been used as a replacement and the initial results have been positive. To remove the copper layer, a Q-tip soaked in the etchant was rubbed across the surface of the chip. The etchant was only used on the region where the copper was being removed. It was quickly washed from the mirror surface because it may react with the photoresist. Once the copper was removed, the mirror was checked under a microscope to make sure the pattern was clear of all residues.

Next, cover the back of the mirror with tape to prevent acid from unwanted etching. After covering the back of the mirror, the glass was etched using hydrofluoric acid (HF). Extreme caution was taken when working with hydrofluoric acid as it can do

extensive harm even at low concentrations. The HF used was a buffer solution, created by mixing ammonium fluoride with sulfuric acid.

To create the buffer solution, carefully mix ammonium fluoride with sulfuric acid. This was done in the glove box. The container needed to be stirred thoroughly to mix the contents. This was done using a stir plate and a stir bar inside the glove box. Once the hydrofluoric acid was completely mixed, etching can begin. Make sure not to store the hydrofluoric acid in a glass container as it will slowly dissolve it.

5. Safe Hydrofluoric Acid Etching Procedure

When working with hydrofluoric acid, all functions must be performed with extreme caution, as HF is extremely hazardous and harmful. Inform everyone in the lab that you will begin working with hydrofluoric acid. Do not allow anyone near the glove box without proper protective attire.

Before working with hydrofluoric acid ensure that the proper protective equipment is worn. Make sure all skin is covered, to ensure complete protection. Know the location of the Calcium Gluconate tube in case of emergency. In case of contact with HF, Calcium Gluconate should be applied to the affected region. Emergency personal must be called. If possible, there should be another person in the room to assist with the etching procedure and to make sure everything is done properly and safely.

6. Copper Etching

Once the etched mirror has been sufficiently washed, the tape and the remaining copper layer must be removed. Before the copper layer was removed, the leftover

photoresist layer must be cleaned off using acetone. The copper layer was removed using either nitric acid or iron chloride. After the copper layer has been removed, the etched glass was all that remained.

7. Glass Fabrication

Once the copper layer was removed the next step was to cut and drill holes into the device. The glass shop in the Chemistry Department at UT-Austin was used to cut and drill holes. The plates needed to be cut so they will fit comfortably on the microscope. The glass shop drilled 0.5" diameter holes into the glass at the inlet and outlet ports. The holes were drilled from both sides of the glass plate to avoid a "pop out" of the glass. These "pop outs" can cause problems when trying to flow fluid into the chip as it is more difficult to create a seal between the tubing and the surface of the device. Once the glass plate has been cut and drilled, etch depth was measured using the profilometer in the UT Nanocenter.

8. Glass Bonding

Another mirror plate must be stripped, first using the methylene chloride and then with nitric acid to remove the copper layer. This piece of glass was bonded to the etched glass plate. The glass plates were fused together using the kiln that is in the Core Lab in the PGE basement. The procedure for fusing the glass plates is shown below.

Table 3.1 Procedure for fusing glass plates

Step Number	Temperature	Time
1	200°C	60 minutes
2	400 °C	60 minutes
3	545 °C	60 minutes (Annealing Temperature)
4	690 °C	60 minutes (Fusion Temperature)
5	545 °C	60 minutes (Annealing Temperature)
6	400 °C	60 minutes
7	200 °C	Until it reaches 25°C

To fuse the plates together, place them on a piece of borosilicate. The glass plates will not fuse with the borosilicate because there is over a 100°C difference in the fusing point of borosilicate and the soda-lime glass mirrors used to make the microfluidic device. This is because the kiln temperature will never get close to the fusion point of borosilicate. However, the surface of the borosilicate may become sticky and that may make pulling the device and the borosilicate apart difficult. Therefore, a layer of Bull's Eye® Thin Fire shelf paper was placed in between the device and the borosilicate to provide an extra layer of protection.

9. Inspection

After the plates were fused and cooled to room temperature they were removed from the kiln. The micromodel was visually inspected to make sure that bonding was complete and there are no unbonded regions. Figure 3.13 shows an example of a

successfully bonded dead-end pore space that was created. If the bonding was not perfect, the device was put back into the kiln and fused using the written procedure. If the bonding looked good, no further fusing was required. The tubing was attached to flow fluid in and out of the device. Figure 3.14 shows an example of a glass micromodel attached to tubing. Unlike the PDMS devices the tubing was not irreversibly attached to the glass micromodel. It was screwed into the holder creating a tight seal with the glass micromodel.

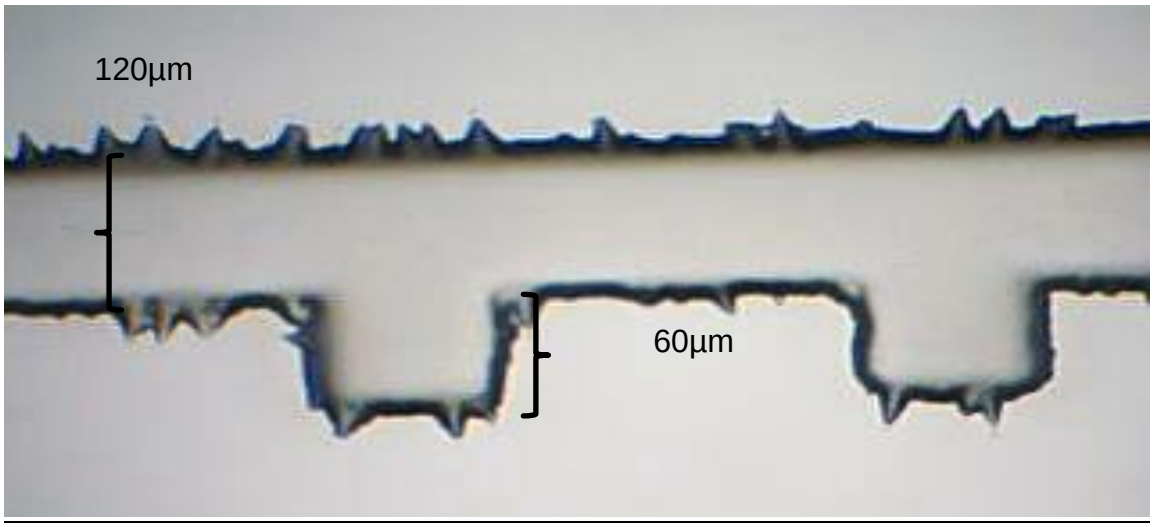

Figure 3.13 Example of a glass microfluidic device viewed under a microscope. This device is similar to the PDMS microfluidic devices as it has five dead-end pores. These pores are shallow rectangles.

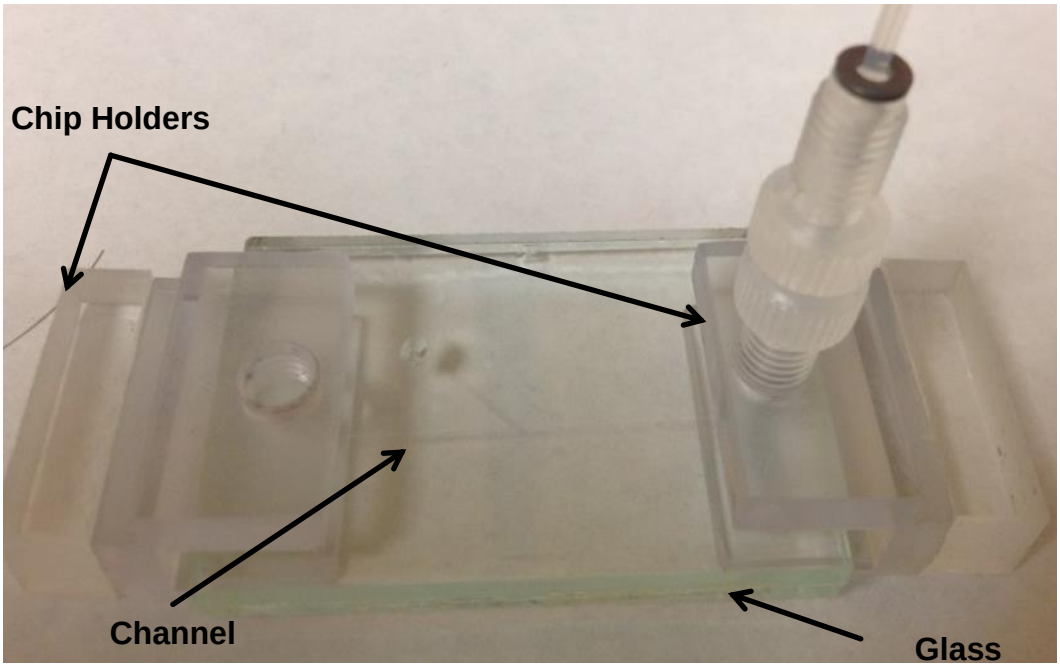

Figure 3.14 Example microfluidic device, shown in the image are the chip holders, the tubing and valve screw, and the microfluidic device. The chip holder aligns directly over the inlet port of the microfluidic device. The screw is then twisted into the chip holder

When reviewing Figure 3.13, the pore space does not look extremely uniform. There are lots of points and hard edges around the channel. These points likely result from scratching the hard paint layer that was initially on the back of the mirror. The metallic layer was so thin that no matter how carefully the paint layer was removed there will be abrasions on the surface. To reduce the likelihood of abrasions, new methods to create microfluidic devices were tested.

3.3.2 New Method of Fabrication

When trying different techniques to create microfluidic devices there were a couple of factors that were found to be important. The device must have clean etched

edges, and the procedure should not be too complex or costly. To create surfaces that do not have scratches or abrasions it was found that the metal layer was unnecessary. Instead an uncoated piece of glass would be best, but to ensure that the photoresist bonded to the glass surface different treatments were required.

The only differences between the new method and the previous one are the removal of the metal layer before etching and the cleanroom procedure. The uncoated glass mirrors were first left in a SURPASS 4000 priming solution for 30 seconds. After, priming, they were dried and coated with S1818. To create an even coat the same procedure that is written above was used. Then the glass plate was soft baked for 2 minutes at 95°C. The Suss Mask Aligner was used to crosslink the photoresist around the same conditions that are described in the above section. The device was then placed in the developer solution for 2 minutes. After developing the plate it was placed in the oven at 120°C for 30 minutes to hard bake the photoresist. After hard baking the same etching procedure that was used above was used again. Figure 3.15 shows the etched profile of a converging-diverging pore space. The edges are much more uniform and there are no scratches or abrasions on the surface.

Figure 3.15 Etched profile of a converging-diverging pore space. The profile is more uniform than the procedure used to create dead-end pore channels.

3.4 Flow in Glass Micromodels

The materials required for experiments to see the enhanced oil recovery potential of nanoparticles were a nanoparticle dispersion, oil, and deionized water. As stated, in Chapter 2, glass is a much more robust material than PDMS and most fluids do not diffuse into it. Decane and mineral oil were the two oils used and they should not permeate through glass easily.

3.4.1 Materials Used

Pumps

Two pumps were required for the system that has been setup. A Fusion 200 and a Fusion 400 syringe pump (Chemyx) were used. One pump was used to inject oil, and the other pump injects water, and nanoparticle dispersion into the microfluidic device. The low flow rates that the syringe pumps can reach made it extremely appealing for these experiments where low flow rates were required.

Microscope and Camera

An OMAX light microscope with an attached camera was used for these experiments. The microscope was required to view the small channel, and the video camera records what happens when fluid flows through the pore space.

Nanoparticle Dispersion

The nanoparticle dispersion used in these experiments was created through mixing synthetic brine with Nissan Chemical IPA-ST nanoparticles. These nanoparticles were initially at a weight concentration of 30.7% and the average size of the particles is 10 to 15 nm. They have a hydrophilic coating and they were initially in an isopropanol solution. The synthetic brine that was used to create the nanoparticle dispersion was 3wt.% sodium chloride (NaCl). The brine was mixed with the IPA-ST nanoparticles to create a dispersion that was 2wt.% nanoparticles. To create the dispersion, first dissolve NaCl in deionized water and then mix with IPA-ST nanoparticles. After mixing, the dispersion was put onto a stir plate for 3-5 minutes to ensure good distribution of the nanoparticles. Figure 3.16 shows what the IPA-ST nanoparticle dispersion looks like once it was fully mixed.

Figure 3.16 IPA-ST nanoparticle dispersion. The nanoparticle dispersion is 2 wt.% IPA-ST nanoparticles and 3 wt.% NaCl.

3.4.2 Glass Micromodel Flow Procedure

First, the pore space was filled with oil and then waterflooded. A tertiary nanoparticle flood followed. Decane has been the primary choice for oil phase in the micromodels. This was partly due to its low volatility and it was easy to obtain.

One item to note was that during experimental testing air pockets found their way into the pore space. These air pockets were found to initiate in the reservoir that was created when drilling flow ports. After oil fills the pore space and as water begins to flow into the microfluidic device the air pocket pushes into the channel. Air pockets created inconsistencies in the amount of oil that was displaced from the dead-end pores. To combat the problem of trapped air in the pore space; it was determined that flowing oil into one end of the device and then flowing water from the other side would reduce the possibility of air pockets disrupting the waterflood. Figure 3.17 shows the experimental

setup used to flow fluid into the glass microfluidic devices. As it shows in the figure there are 2 syringe pumps and 2 valves used to regulate flow into the device.

1. Attach the decane filled syringe to the Hamilton HVD4-5 valve (Figure 3.18)
2. Attach waste line to the Hamilton HVD4-5 valve
3. Attach microfluidic device to the chip holders
4. Attach microfluidic device to the Hamilton HVD4-5 valve
5. Place the microfluidic device under the microscope and find the geometry
6. Once the geometry is found turn on the syringe pump and begin flowing the decane, if there are pockets of air in the tubing make sure the valve is turned to flow towards the waste to remove the pockets
7. Once the pockets of air are removed from the flow line, begin flowing fluid into the channel
8. Once the channel is filled with decane, make sure that there is no air trapped in the tubing that the water will flow through; if there is air in this line then there will be problems with air in the pore space
9. After removing all of the trapped air setup the flow for deionized water/nanoparticle dispersion.; the deionized water flows into the other side of the device
10. Attach the deionized water syringe to the other Hamilton valve; flow the deionized water through the waste line to remove any air pockets (Figure 3.19)

11. Once the air is removed, begin flowing the deionized water into the microfluidic device

12. Once the fluid has reached the channel begin recording to document the fluid behavior.

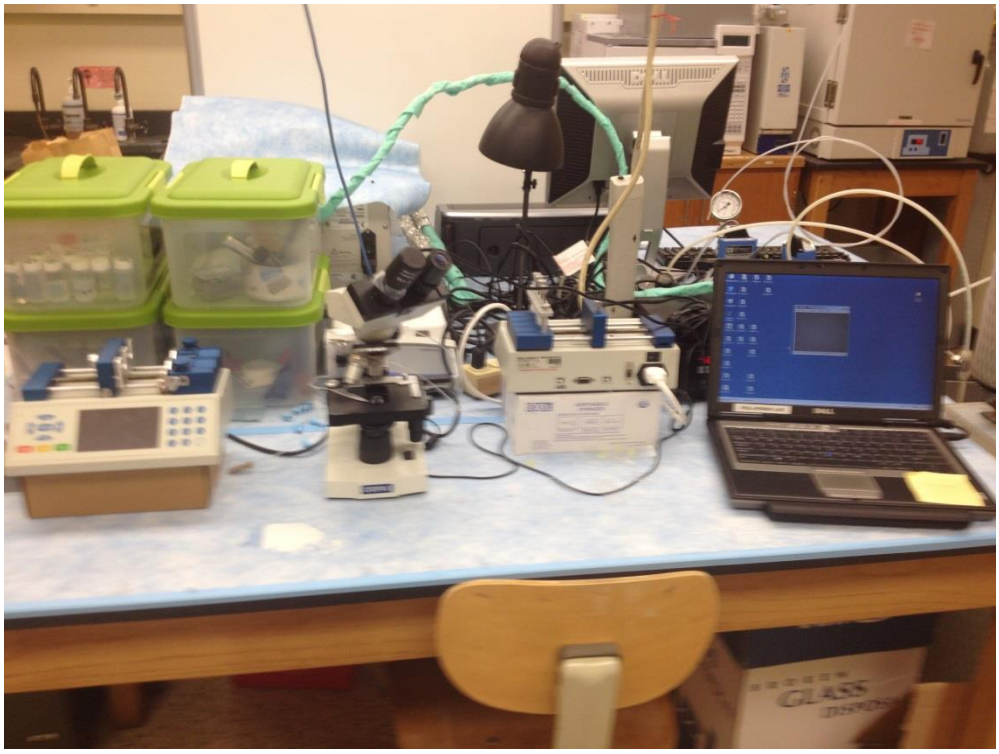

Figure 3.17 Example of the experimental setup which contains both syringe pumps, the laptop and the microscope with attached camera

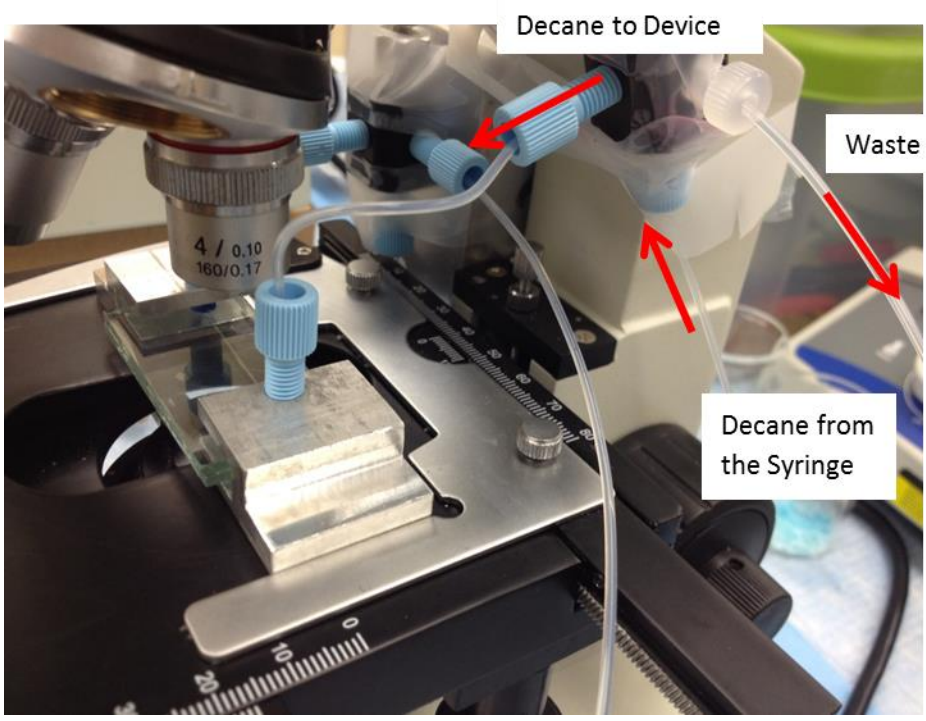

Figure 3.18 Side view of the microscope platform. This view shows how decane is injected into the microfluidic device. The red arrows show the direction of flow that the decane will follow.

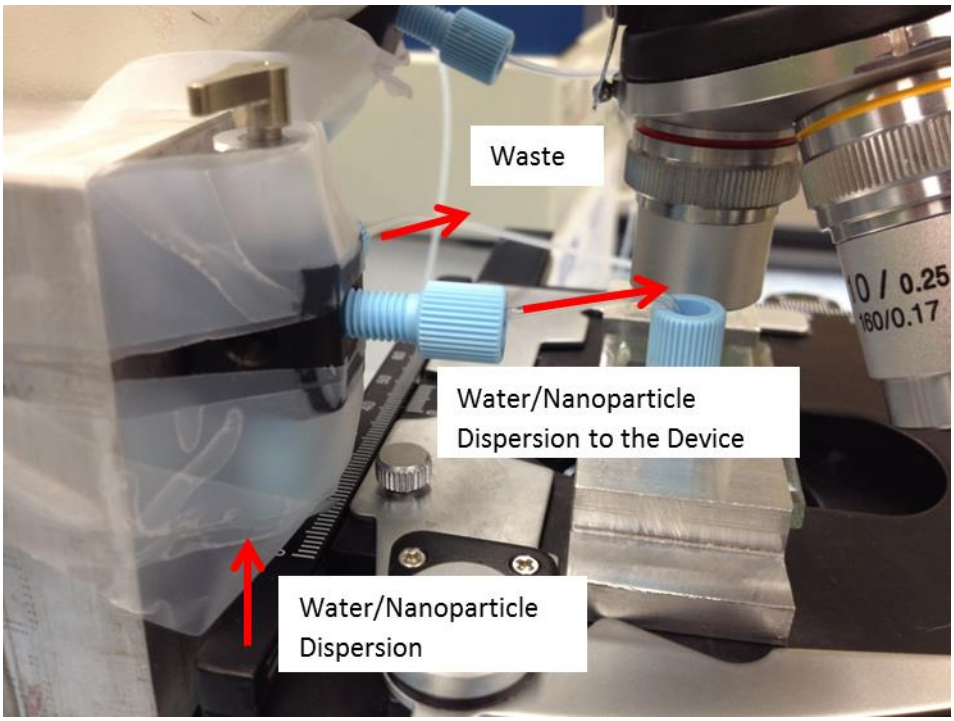

Figure 3.19 Side view of the other side of the microscope platform. The flow of the water/nanoparticle dispersion is shown using red arrows.

CHAPTER 4: EXPERIMENTAL RESULTS AND DISCUSSION

4.1 PDMS MICROMODELS

This section describes the results obtained using PDMS microfluidic devices to research nanoparticle use for EOR. Two different oils were tested to determine which is suitable to use in PDMS microfluidic devices.

4.1.1 Oil Injection into PDMS Microfluidic Devices

The first goal when using PDMS microfluidic devices was to inject oil and ensure that it did not quickly permeate through the PDMS device. The first oil tested was mineral oil, which had a viscosity of 19 cp. Shown in Figure 3.10 are the results of injecting mineral oil into the PDMS device.

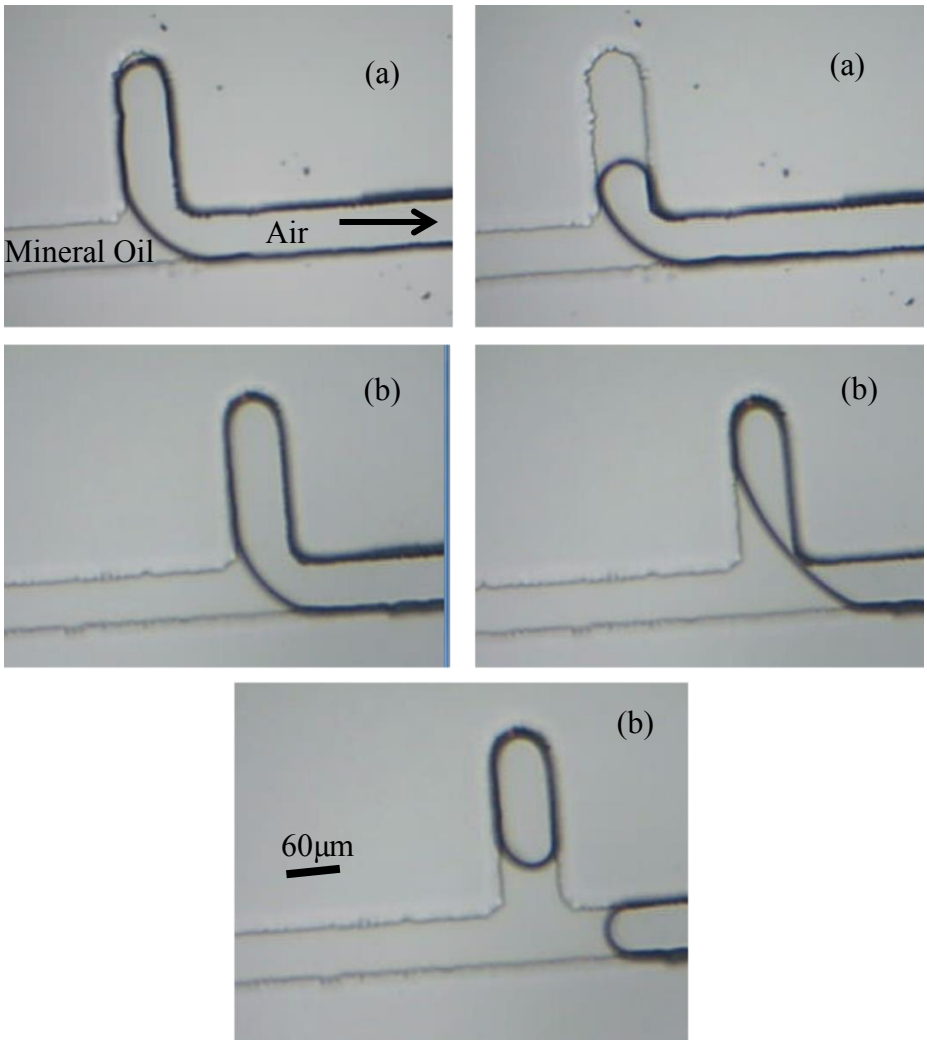

Figure 4.1 Images from the injection of mineral oil into a pore space that is initially filled with air. The top images (a) show air being pulled out of one of the dead-end pores. The middle images and the image at the bottom (b) show mineral oil snapping-off air.

In Figure 4.1 above, there are labels on the upper left hand corner image to help differentiate the fluids. In this trial, air that was initially in the channel was displaced by mineral oil. The mineral oil did not quickly permeate through the pore walls. The air that was initially in the pore space seemed to be displaced by two different mechanisms.

Either (a) the dead-end pore was completely wetted by the oil and the air was pulled out of the pore or (b) snap-off occurs. The upper left and upper right images of Figure 4.1 show the first of five dead-end pores. In this pore, the air was pulled out of the dead-end. The middle images and the bottom image show snap-off occurring in the second of the five pores. Snap-off was not unexpected, as simulation results by Reddy et al. (2005) had shown this was possible. Reddy et al. (2005) used GOMA to simulate fluid flow into empty "T-shaped" pores. Their results showed that if the fluid interface moved through the "T-shape" and caught the far corner of the "T", snap-off would occur and air would be trapped in the pore. Snap-off, was most likely to occur if the aspect ratio was high, or the pore was narrow. If the inflowing fluid does not contact the far side of the "T" before filling then snap-off will not occur. They were able to find a region that if certain conditions were met, complete pore filling would occur.

After snap-off occurred, the air pocket in the dead-end would slowly decrease in size until it was completely gone. PDMS has high gas permeability (Eddings and Gale, 2006) and air will diffuse from the dead-end pores. Complete pull out of mineral oil from the dead-end pore was not expected. It may be due to defects found in certain dead-end pores. Throughout the trials that were completed, there was no distinct pattern as to whether the air would be pulled from the pore or snap-off would occur.

4.1.2 Waterflood into PDMS

Once oil was successfully trapped in the pore space, the next step was to perform a waterflood and attempt to reach residual oil saturation and trap mineral oil in the dead-

end pores. The ultimate goal was to follow up the waterflood with the nanoparticle dispersion and determine if there was any change in the original residual oil saturation. Figure 4.2 displays images taken from a video recording that shows water flowing into the pore space and displacing mineral oil. The water entering the channel was dyed blue and the mineral oil was clear. This color difference is slight, but it helps to differentiate between the fluids.

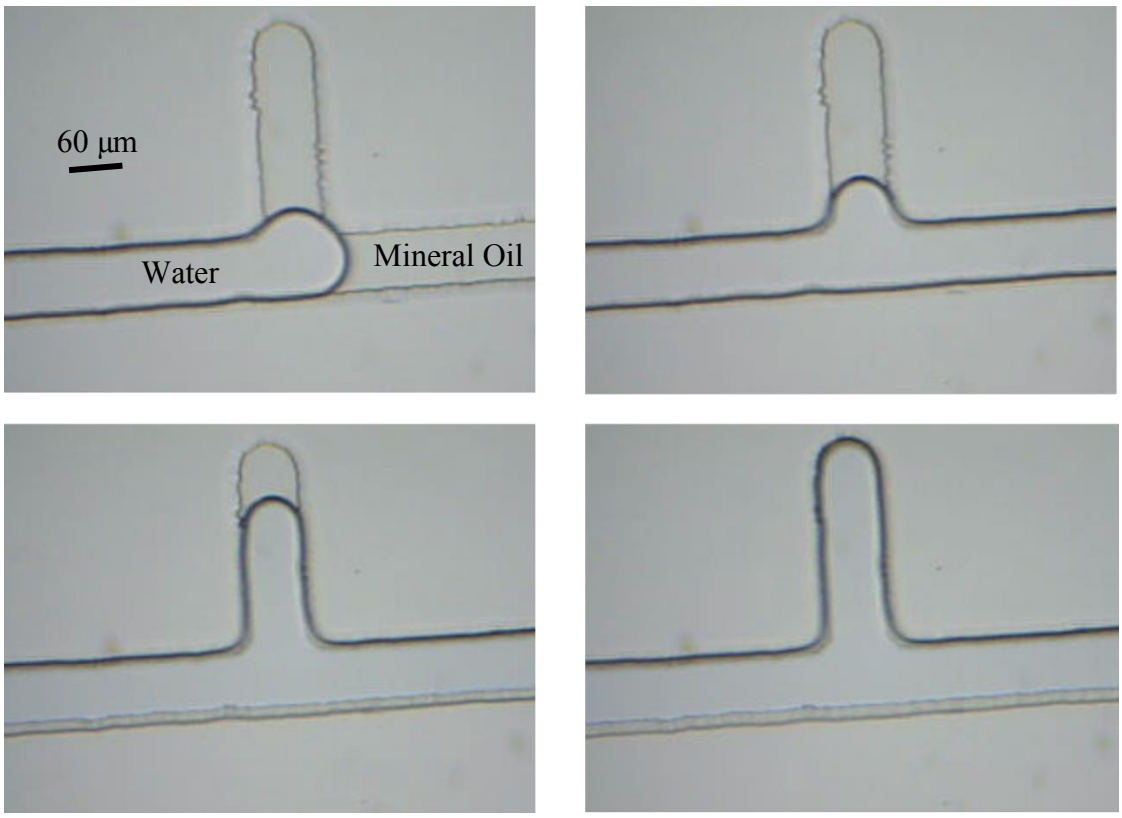

Figure 4.2 An example of water displacing mineral oil. The water (colored blue) easily displaces all of the mineral oil from the pore space.

From the above images it is obvious that water completely displaces the mineral oil from the pore space. This experiment was attempted many times, at different flow

rates, and the same result occurred. It is unrealistic and does not help to reach the ultimate goal, which is to reduce the remaining oil saturation using nanoparticles. The next step taken was to try different surface modifications and attempt to make the PDMS more water-wet.

Before attempting any surface modifications, it was decided that it would be interesting to see if mineral oil could displace water in a similar manner to Figure 4.2. The results of this experiment are shown in Figure 4.3. Reviewing the images below, it can be seen that mineral oil does not squeeze water out of the dead-end pore that same way that water squeezes mineral oil out.

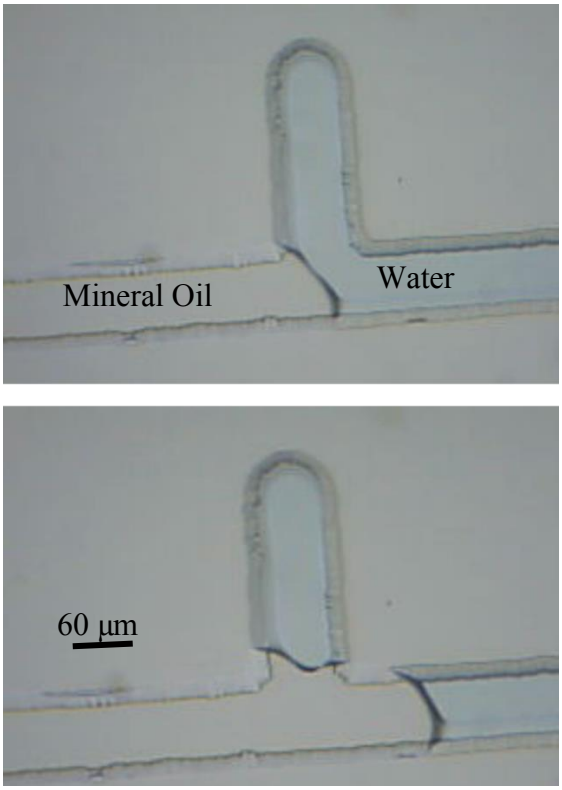

Figure 4.3 Images showing that mineral oil does not displace water in the same manner as water displaces mineral oil.

As previously stated, the next step was to try different surface coatings an attempt to alter the surface wettability of the microfluidic device. Oxygen plasma was one of the techniques used. In addition to bonding PDMS surfaces together, oxygen-plasma will also make PDMS devices more water-wet. While it can be used for bonding, here it was only used to modify the surface wettability. In the clean room the device was placed into the March Plasma etching system. Oxygen plasma treatment was attempted both before and after sealing the device to determine if either method would be more effective. Initially, the surface of the device would be water-wet, but quickly it would revert back to

being oil-wet and the same issue that was seen in Figure 4.2 happened. The problem with oxygen plasma was that the effects only last for a short period of time; before any fluid could flow into the channel the effects had worn off.

4.1.3 Fluorinated Oil

Fluorinated oil was tested because Duboin (2013) was able to trap it in dead-end pores. Duboin's work involved using micromodels to determine the effectiveness of polymer and surfactant tertiary floods. Using mineral oil in dead-end PDMS microfluidic devices he saw similar results. The mineral oil would leak from the pore space. Figure 4.4 shows the experimental results that Duboin (2013) obtained when using distilled water to displace mineral oil. Initially the mineral oil traps in the pore space. Over time the amount of oil decreases. Duboin (2013) noted that the mineral oil likely diffused into the PDMS. The results that he encountered are similar to the findings in this thesis.

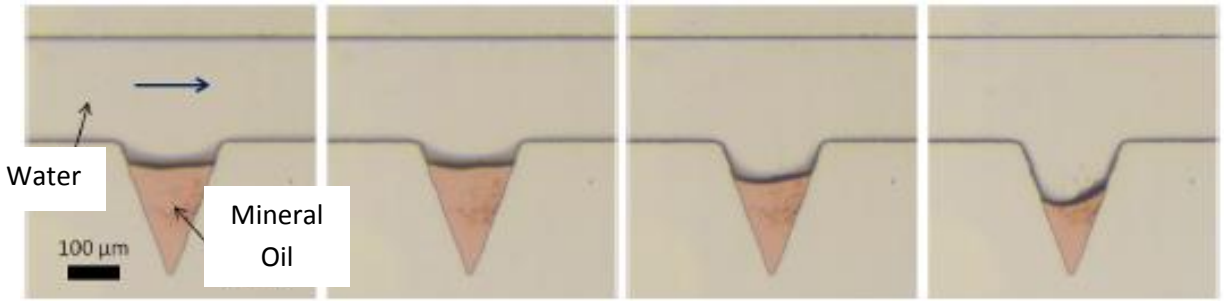

Figure 4.4 Waterflood from Duboin (2013), mineral oil leaches from the PDMS pore space over time. The results are similar to the results that were gathered here at the University of Texas at Austin.

As previously stated, Duboin (2013) tested fluorinated oil to determine if it would trap in the pore space. Duboin (2013) tested two types of fluorinated oil FC40 and FC70.

FC40 and FC70 are clear colorless liquids. From Sigma-Aldrich, FC40 has a density range of 1.845-1.895g/ml and a viscosity between 1.6-2.6cSt. FC70 has a density between 1.91-1.95g/ml and a viscosity range of 11-17 (Sigma-Aldrich). Both of these oils do not easily mix with oil dyes (Duboin 2013).

Figure 4.5 shows the results using fluorinated oil obtained by Duboin (2013). He stated that over time the amount of oil trapped in the dead-end pore did not change. The yellow fluid is distilled water and the clear fluid is fluorinated oil. Because oil stayed trapped in the dead-end pores, tertiary floods such as polymers, surfactants, or nanoparticles were tested. The fact that trapping occurs is good news as it may allow nanoparticle EOR effectiveness to be determined.

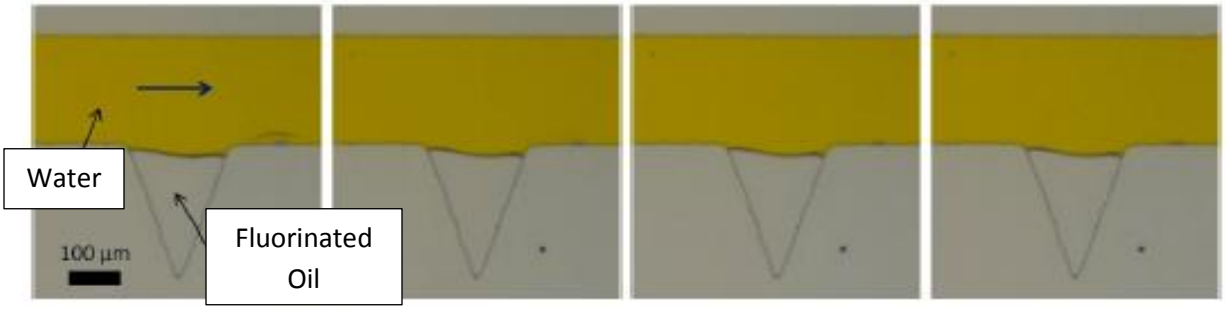

Figure 4.5 The pore space was initially filled with fluorinated oil. The oil is then displaced by distilled water. The fluorinated oil stays trapped in the pore space over time. This is important because tertiary floods can be tested (Duboin 2013).

The positive results seen by Duboin (2013) precipitated the testing of fluorinated oil. Figure 4.6 shows a PDMS microfluidic device that is being filled with FC40. Reviewing the images it can be that the micromodel filling is similar to mineral oil filling

the pore space. The pore filling either caused the initially trapped air to be pulled out of the dead-end or to snap-off.

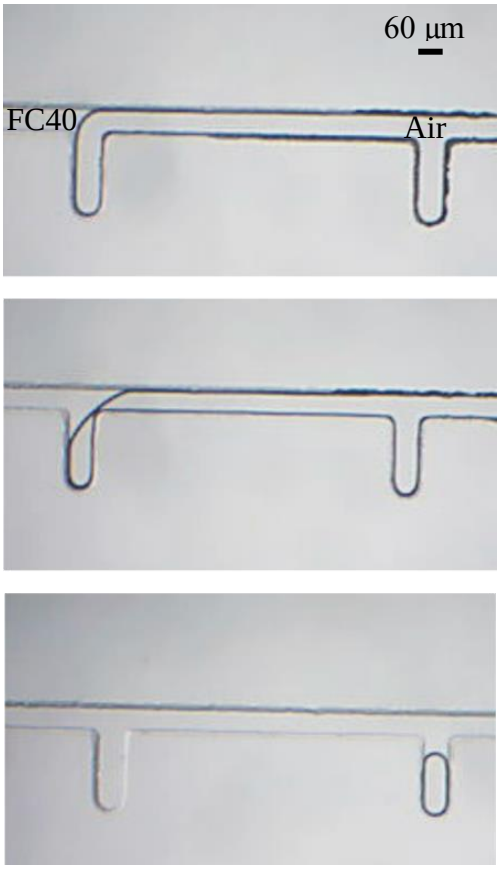

Figure 4.6 Filling up a PDMS microfluidic with FC-40. The filing was similar to mineral oil filling the pore space.

After successfully filling the pore space with FC40, a waterflood was attempted. During the waterflood, there was a noticeable difference in the amount of FC40 that trapped in the pore space compared to the mineral oil. Although over time the amount of FC40 in the first dead-end pore began to decrease. The rest of the pores stayed at the same amount of FC40 trapped in the pore space. While this result was better than what

was seen with mineral oil, there were still problems. The waterflood rate was low initially 2 μl/hr and about 1/3 of the FC-40 in each dead-end pore was displaced. As the flow rate was increased to 25 μl/hr, oil in the first pore was further displaced. Increasing the water flow rate to 200 μl/hr saw the amount of fluorinated oil in the first pore decrease further. The fact that water began to fill the first dead-end pore was a disappointing result. Another test was run flowing water initially at 5 μl/hr; the rate was quickly decreased to 0.5 μl/hr. The results of this experiment are shown below in Figure 4.7. Both fluids are labeled in the figure. The images from the video recording show that water flows in and pushes FC40 from the pore space. This result was unexpected and is different from Duboin (2013). There are a number of potential reasons for the opposite results that were seen. The different results may be due to the geometry used; Duboin used both triangle and rectangular dead-end pores. The dead-end pores in these experiments are more rounded. Based upon this result, it seems that using PDMS devices to test nanoparticle EOR potential may be difficult.

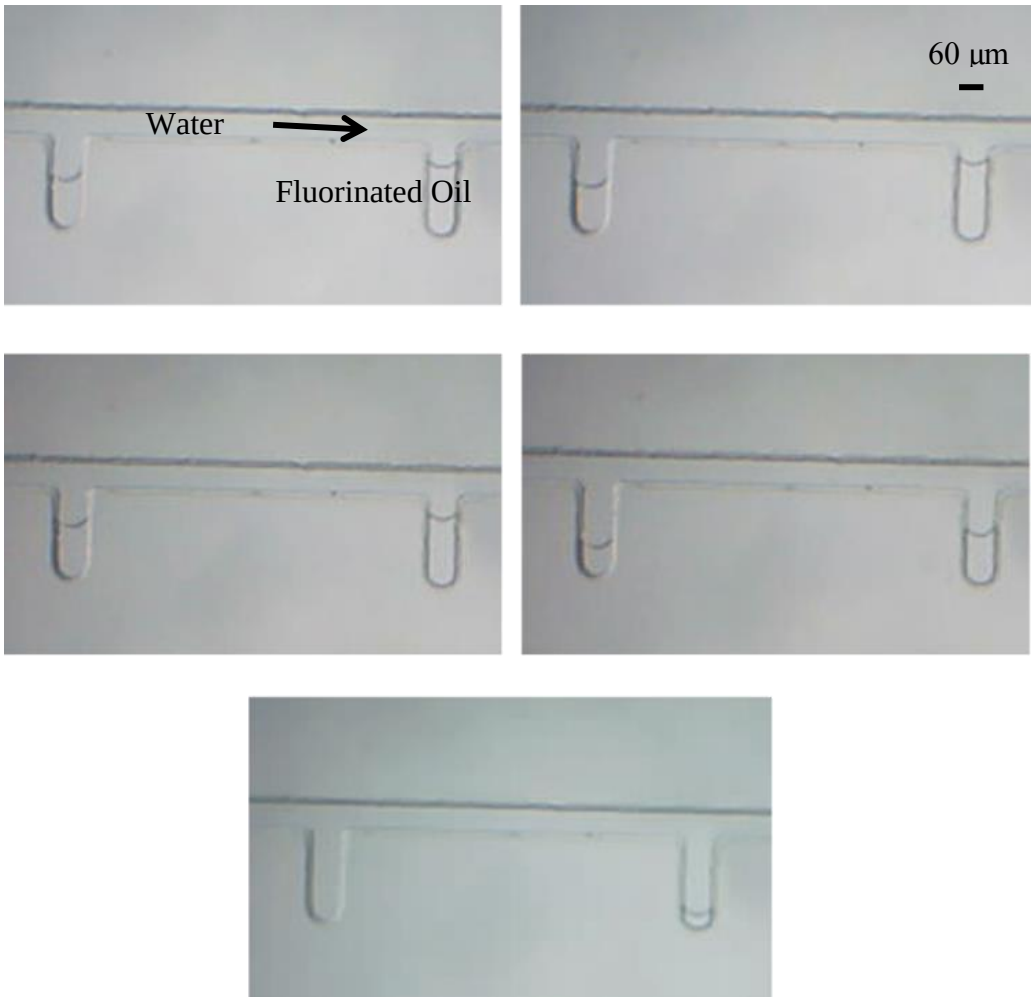

Figure 4.7 Images from a video recording of water displacing fluorinated oil. In this experiment water completely displace the fluorinated oil from the dead-end pores.

4.2 GLASS MICROMODEL RESULTS AND DISCUSSION

Glass micromodel fabrication was much more time consuming, complex and dangerous to produce than PDMS micromodels. Once it was determined that PDMS would not effectively trap oil, glass was the next best option. This section will describe the results that have been obtained using glass micromodels.

4.2.1 Filling Microfluidic Device with Oil

The first step was to inject oil into the glass micromodel. For the first trial decane was used as it was believed it would be easier to displace the air that was initially in the channel with decane.

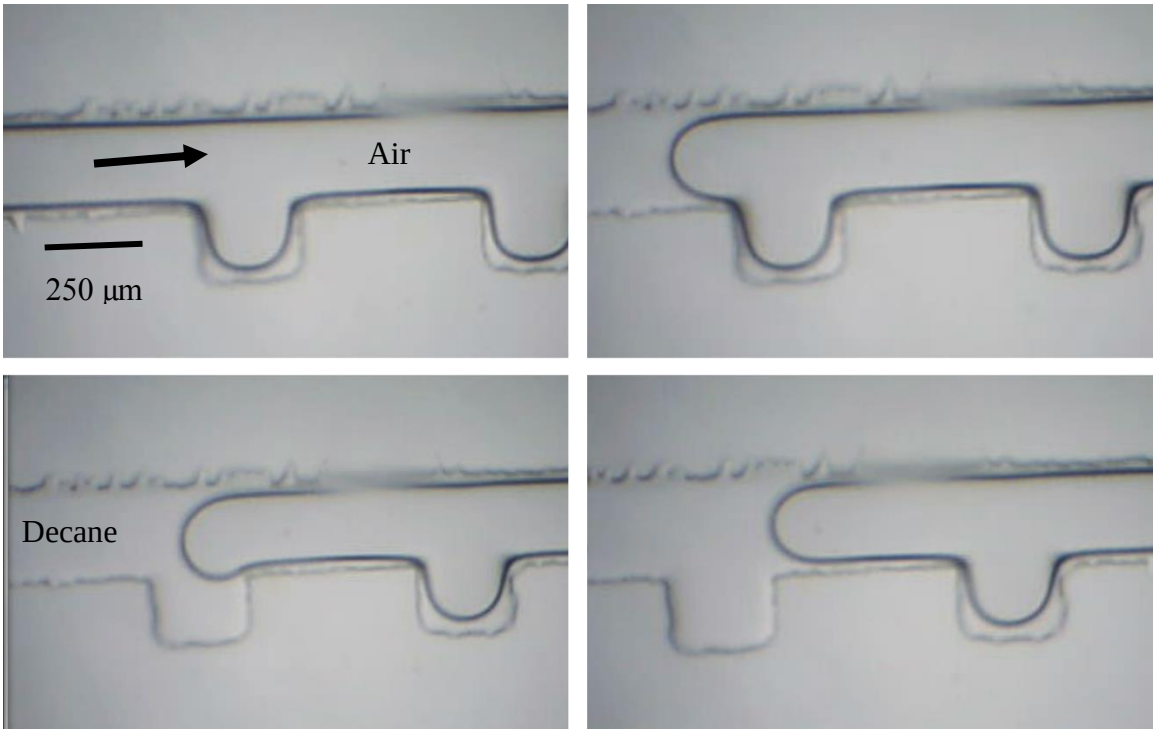

Figure 4.8 Decane displacing air from the dead-end pores.

The results shown in Figure 4.8 were common with the initial glass micromodel that was created. The oil tended to pull the air out of the dead-end. This was likely due to the fact that the dead-end is more of a square. Before testing the glass micromodels there was a worry that air would get trapped in the dead-end pores and there would be no way to get it out. This was experimentally proven to not be an issue as any oil that was used removed air from the dead-end pores.

4.2.2 Trapping Oil in Dead-End Geometry

After oil was successfully trapped in the glass micromodels, waterfloods were tested at different rates to the best method for consistently tapping oil in dead-end pores. Aside from developing quality micromodels, consistently trapping oil proved to be the most difficult part of the research.

4.2.2.1 Low Aspect Ratio Dead-End Pores

Dead-end pores that were more square-like and had lower aspect ratios were first tested. What was found was initially the first waterflood for each micromodel had an extremely water-wet surface. This highly water-wet nature caused all of the decane to be pulled right out of each dead-end. Figure 4.9 shows a waterflood (blue fluid) attempted in a glass micromodel. Traditionally, and shown below in Figure 4.9 some oil was trapped in the square dead-end.

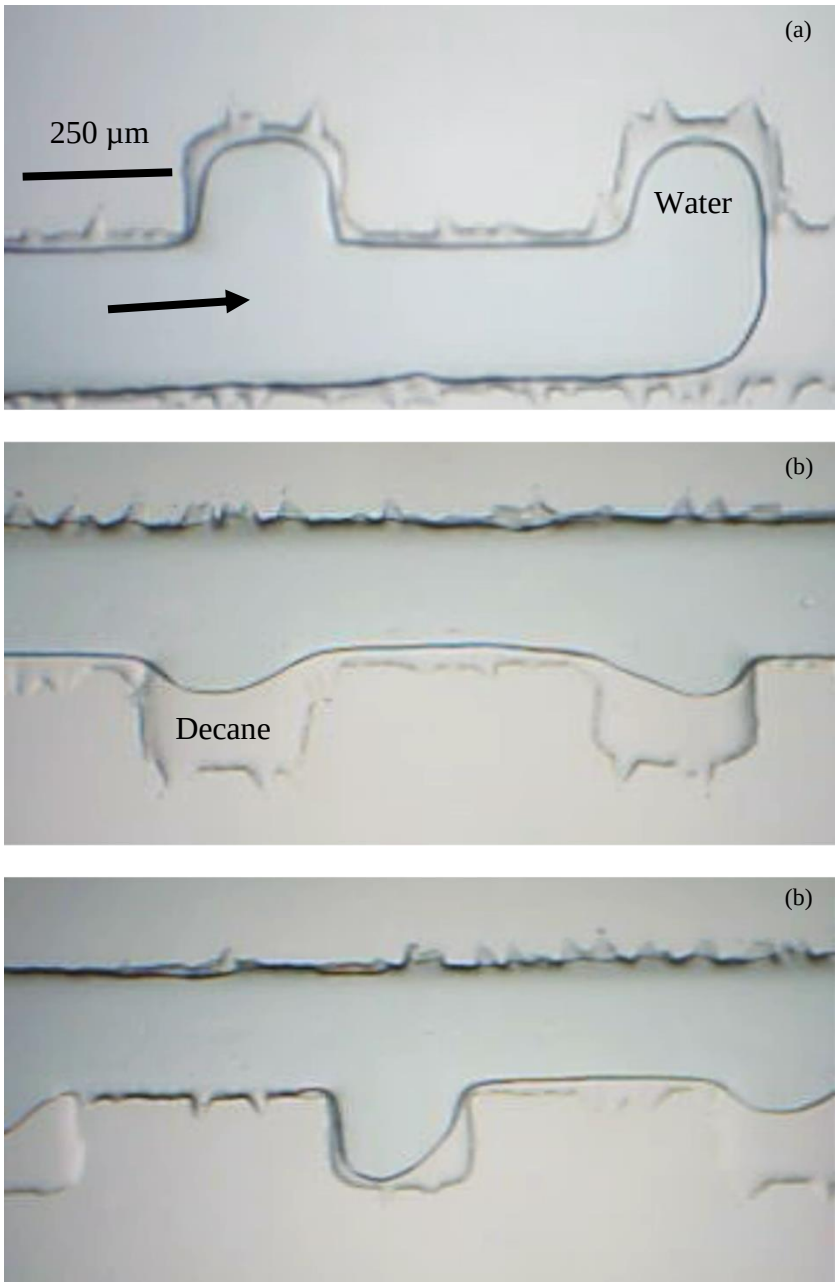

Figure 4.9 Waterflood showing blue-dyed water displacing decane. Some of the dead-end pores trapped decane and in other pores much of the decane was displaced by water. The top image (a) is from an experiment that was run at 10µl/hr. The middle and bottom image (b) are from a waterflood that was run at 25µl/hr. Changing the waterfllod flow rate will impact the amount of oil that is trapped in the dead-end pores.

The top image of Figure 4.9 is from a waterflood that was at a flow rate of 10 μl/hr. In all five of the dead-end pores, water displaced oil with relative ease. After every experiment micromodels were cleaned with isopropanol, acetone and deionized water. This removed all of the colored water and decane. The model was then refilled with decane and another waterflood was then attempted. This time the water flow rate was 25μl/hr. The middle and bottom images of Figure 4.9 show this trial was slightly more successful, as a few of the dead-end pores contain trapped decane. This was an interesting result, as the flowing water had less time to contact and displace the decane. The same experiment was run again, this time the waterflood rate was 50μl/hr. Figure 4.10 shows the results of flowing water at a higher rate.

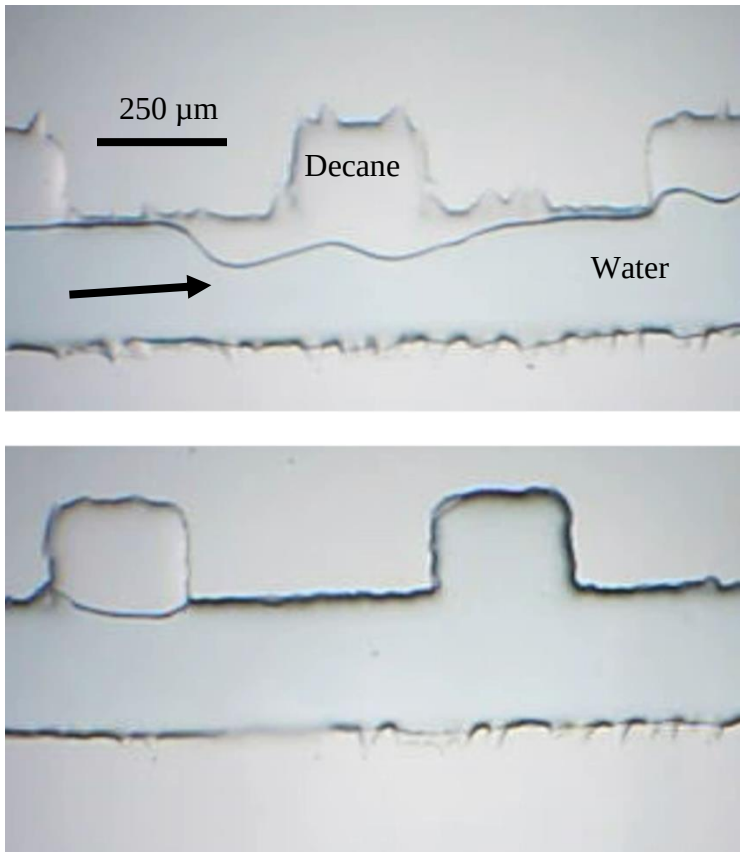

Figure 4.10 Images taken from a waterflood that was at a rate of 50µl/hr. This shows better trapping than the lower waterflood rates

The upper image of Figure 4.10 shows three of the five dead-ends and the lower image shows the other 2 of the five dead-ends. This result follows what was previously seen, that less oil was displaced when the displacing water was at a higher flow rate. Although decane trapping occurred, it was inconsistent from pore to pore and trial to trial. Because of these inconsistencies with decane it was decided that using higher viscosity oil may help to improve oil trapping. This idea was tested using mineral oil, which has a higher viscosity than decane. The results using mineral oil are shown below in Figure 4.11. In the experiment, the water flow rate was 50µl/hr; which was the same as the

highest flow rate tested using decane. It can be seen in the images below that the oil trapping is similar from the decane tests. The mineral oil results show trapping in four out of the five dead-end, similar to the decane experiment results. These results showed that a small change in viscosity did not greatly change the trapping seen in the dead-end pores.

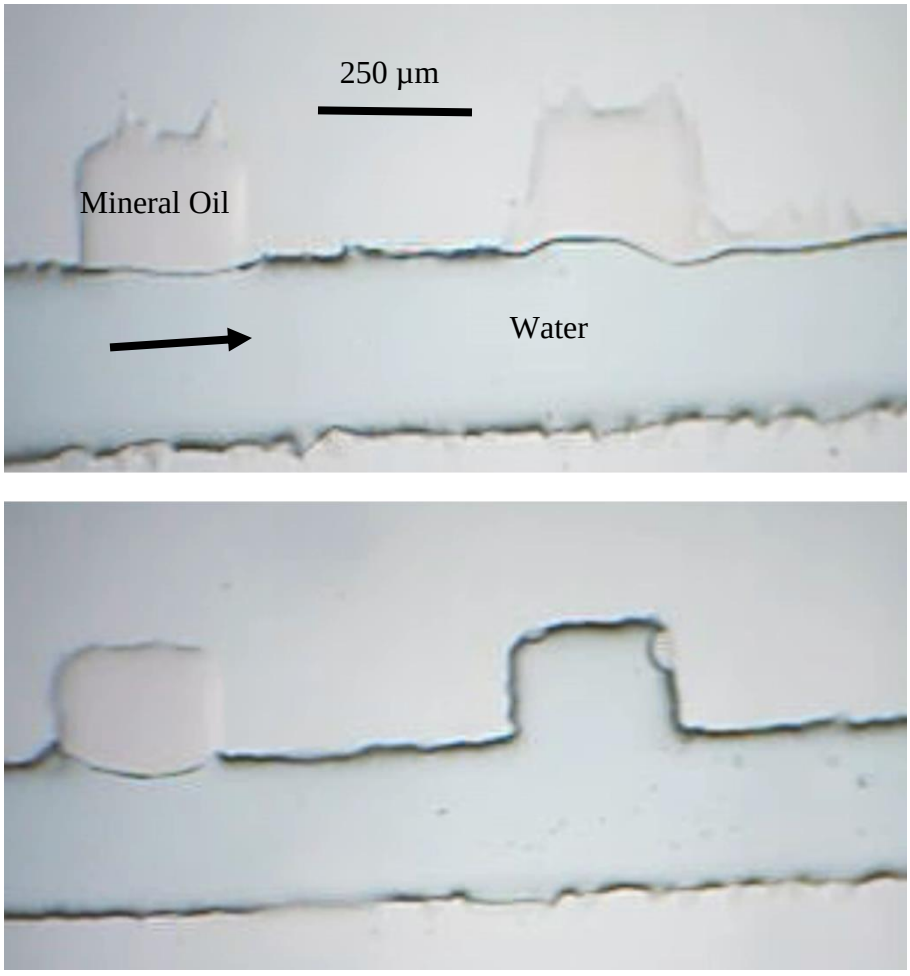

Figure 4.11 Images taken from a waterflood which is displacing mineral oil. The flow rate of the waterflood is 50µl/hr. The mineral oil shows similar promising, but inconsistent results as the decane filled pore space

Another experiment that was run was to fill the pore space with water and then flood the channel with decane. This was tested to see any potential differences in

wettability that may occur when decane displaces water. The top image of Figure 4.12 shows that the initially flooded water wets the surface of the channel. After decane has filled the pore space, water was then flooded again. The hope was that the some of the decane will stay trapped in the dead-end pores as the water flows past. The bottom image in Figure 4.12 shows that decane did not stay trapped in the dead-end pores. Instead it was pulled right out of the dead-end pores in a similar manner to earlier results.

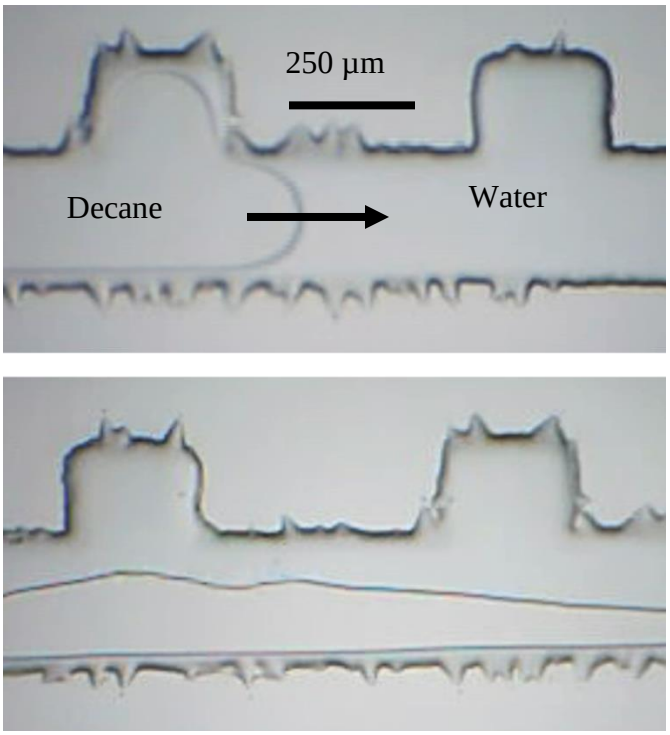

Figure 4.12 Decane is flowed into the pore space after it is initially filled with water. The bottom images shows what happens when water is then flowed into the pore space. The decane is completely displaced.

Figure 4.13 shows an outcome that is similar to what was seen in Figure 4.12. The only difference was that the flow rate was lower in Figure 4.13. The result was not

necessarily an unexpected outcome. If an extremely water-wet surface removed all of the oil from the dead-end pores, then it is not surprising that a pore that was initially filled with water would be able to push all of the decane out of the dead-end pores. The results compiled using the lower aspect ratio square-like dead-end show that it likely will be difficult if not impossible, to consistently trap oil in the dead-end pores. This may be due to a number of factors such as the irregular nature of the dead-end pores created or the wettability alterations after each test. The dead-end pores shown in the figures above are not mirror images of one another and this lack of congruency may be the cause of the inconsistent oil trapping. Wettability alterations were likely due to difficulties related to cleaning the device after testing. The lack of completely flat surfaces made cleaning the device challenging. While these issues may be overcome through the use of new methods of fabrication, another factor was considered. The aspect ratio of the dead-end pore length to its width was modified. Reddy et al. (2005), state that larger features that have lower aspect ratios are easier to fill than narrower dead-end pores. Because consistent trapping did not seem possible with the lower aspect ratio dead-end geometry, it was decided that the best course of action would be to test a new, more rectangular (higher aspect ratio) geometry. The belief was that a more rectangular geometry (higher aspect ratio) would help to consistently trap oil in the dead-end pores. Narrower, higher aspect ratio geometry may also help to overcome some of issues that were encountered during etching.

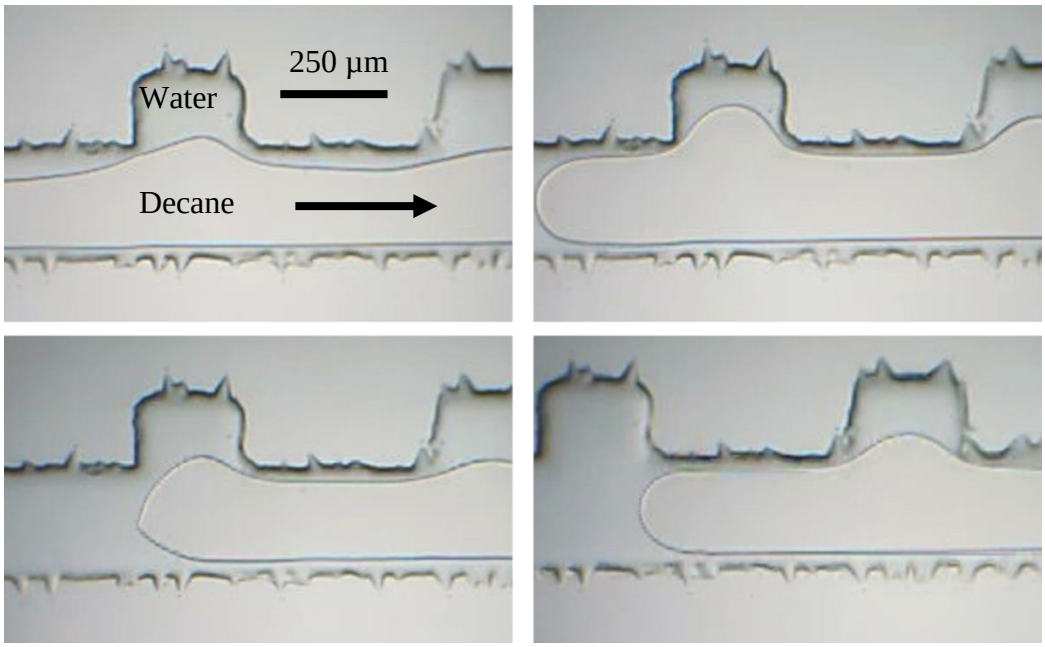

Figure 4.13 The pore space is initially filled with water and then displaced with decane. Then water flows back into the pore space and displaces all of the decane

. As stated above, the square dead-end pores did not allow for consistently trapped oil. Higher aspect ratio dead-end pores were used to attempt to remedy the consistency issue. An example of this new geometry, with dimensions, is shown in Figure 4.14. The expectation is that length to width ratio of the rectangle will make it difficult for water to enter the dead-end pore.

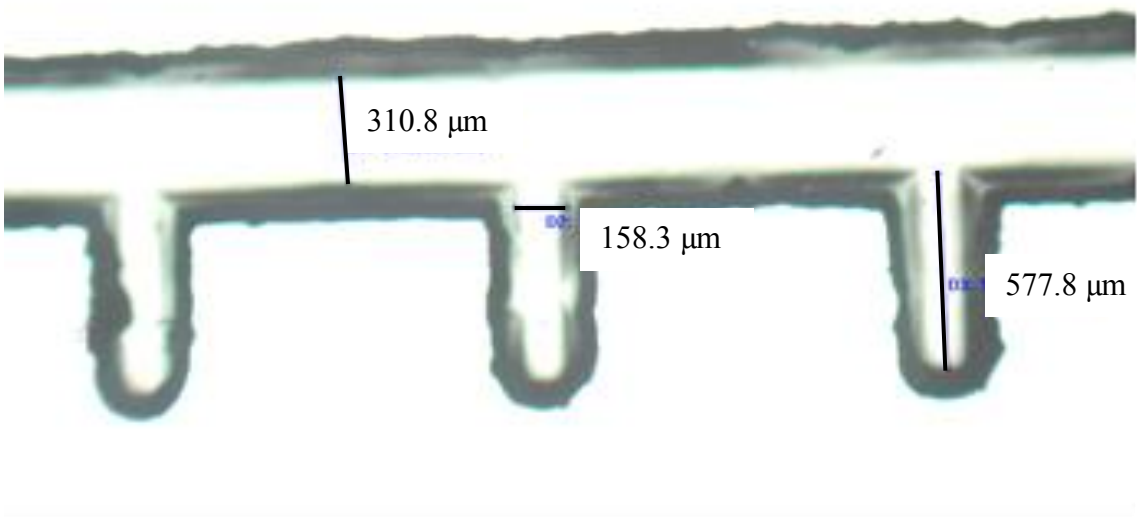

Figure 4.14 Higher aspect ratio dead-end pore that was created to improve the consistency of dead-end oil trapping.

4.2.2.2 High Aspect Ratio Dead-End Pores

Figure 4.15 shows the first successful results of oil trapping in all five dead-end pores. The flow rate of this trial was 20 µl/hr, which would be a much higher rate than would be expected for a traditional waterflood at reservoir scale. Nonetheless, this was a positive result, which showed that oil trapping in dead-end pores was possible. The next step was to prove that oil could consistently trap in each dead-end pore. This proved to be difficult because air began flowing into the pore space. Air would flow in right before the waterflood, and many times the inflowing water and air would contact. This created a three phase displacement, which was not the goal and it made determining the effectiveness of flooding nanofluids extremely difficult. Determining the air source and

how to ensure that it did not enter the channel became a priority. After some trial and error, the source was determined to be the reservoir that was created when drilling flow ports into the device. When oil flowed into the reservoir it would snap-off some of the air that already occupied the reservoir. This snapped off air would stay in the reservoir until it was pushed into the channel by inflowing water. Adding air to the channel disrupted the point of the test; which was to trap oil in the dead-end pores. This problem was solved by flowing oil into one end of the device and then flowing water into the opposite end. This was determined to be the best solution because it allowed the trapped air to be bypassed. Instead of pushing the trapped air into the channel, the waterflood would push the air away from the device and towards the waste container. Once this solution was found, the next step was to show repeatability when trapping oil in the dead-end pores.

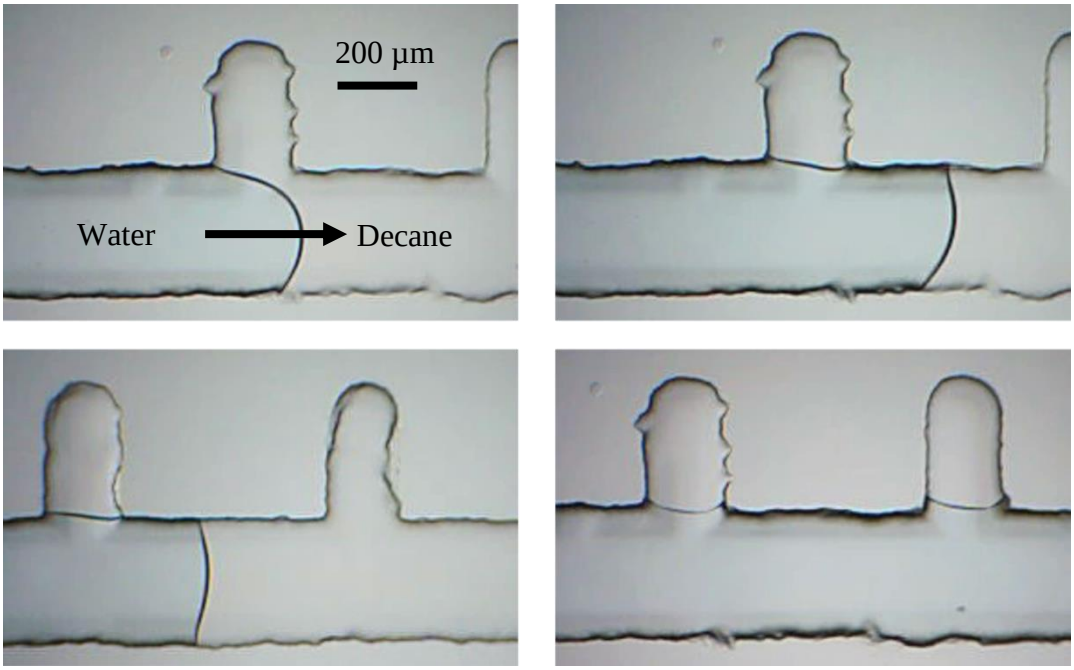

Figure 4.15 One of the first trials with the new higher aspect ratio rectangular dead-ends. Oil trapping after waterflooding kept decane in all five of the dead-end pores.

Figure 4.16 is an example of the results obtained using the new flow procedure. During this trial the flow rate was 2µl/hr (approximately 5ft/day), which is much closer to a typical field-scale waterflood. The result was that each dead-end pore had similar levels of trapped decane. Once decane was consistently trapped in the dead-end pores, the next step was to determine if the amount of decane in each pore would be altered if water flow rate was increased after trapping.

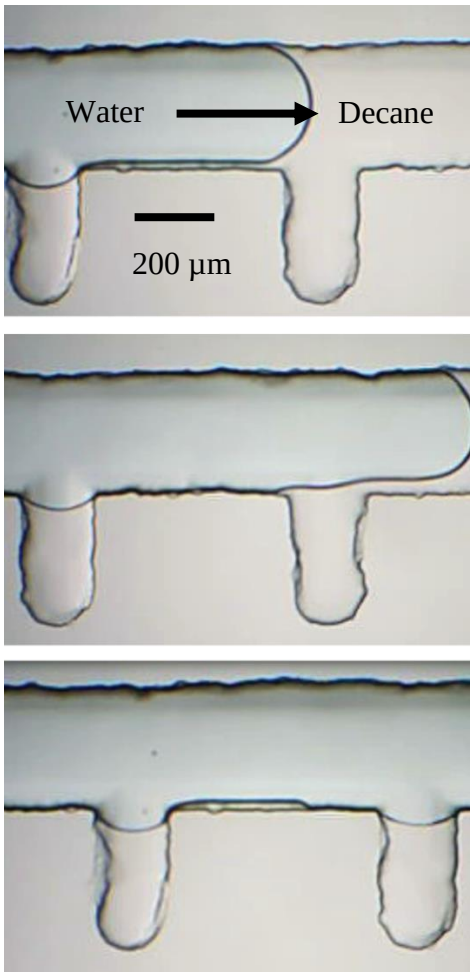

Figure 4.16 An experimental test of water displacing decane at a waterflood rate of 2µl/hr. In this trial all of the dead-end pores had decane remaining in them.

Determining whether the flow rate changed the amount of trapped oil was important because it would tell whether or not the flow rate could be increased to a higher rate when bringing the nanoparticle dispersion from the syringe to the device. The ability to increase this rate would lower trial time and increase efficiency. Figure 4.17 shows the results when the flow rate was initially at 20µl/hr and then increased, first to 200µl/hr and

then to 500µl/hr. In the images below the flow rate has no impact on the amount of decane trapped in the dead-end pores.

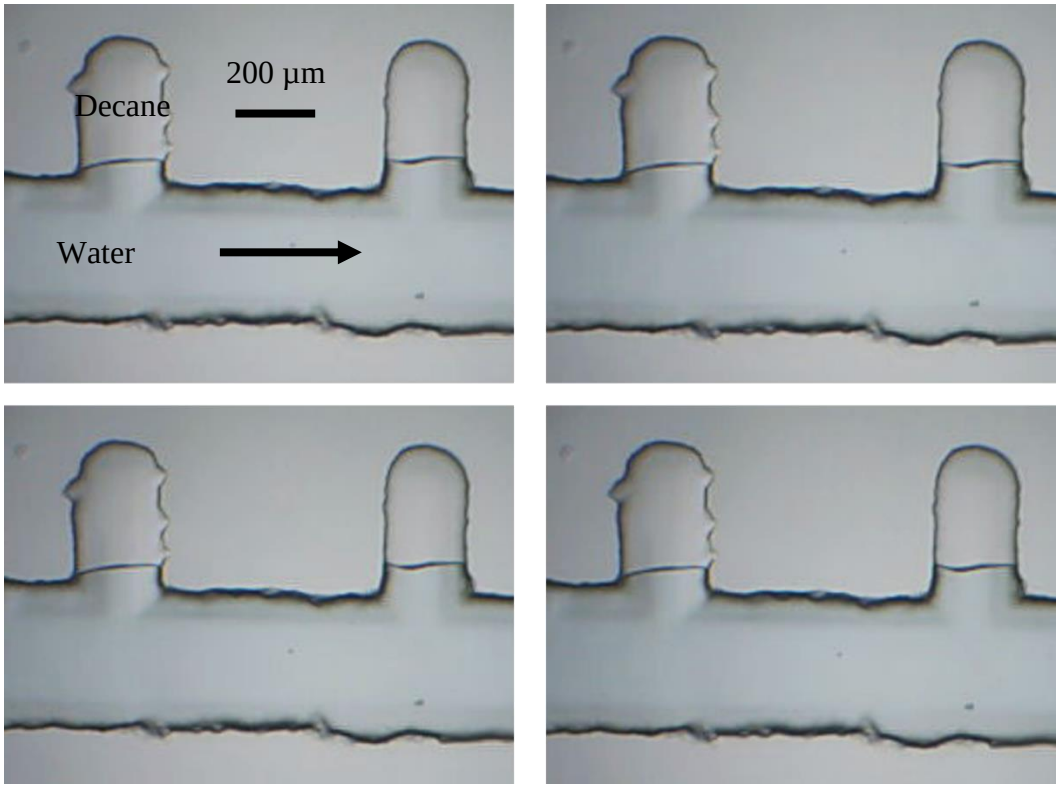

Figure 4.17 Testing whether the amount of decane trapped in the dead-end pores changes as the waterflood rate is increased. From the images it can be seen that the amount of decane trapped in the dead-end pores does not change when the waterflood rate is increased

Through experimental work, the results show that decane consistently trapped in a dead-end structure under certain waterflooding conditions. After waterflooding, nanoparticles were tested to determine their EOR potential.

4.2.3 Nanoparticle Flooding Glass Micromodels

4.2.3.1 Nanoparticle Tertiary Flooding

After successfully trapping decane in the dead-end pores, and ensuring that no more of the trapped oil would be removed from the pores; a nanoparticle solution was used to attempt to remove some of the remaining oil. Many of the figures below show images captured after the above waterflood videos and images. As such, some of the figures show the lower aspect ratio dead-end pores that do not trap oil with any consistency. While this geometry was not perfect for trapping oil; it was tested with nanoparticles because it was useful to test the EOR potential of the larger geometry. There were many different flow rates and methods tested to determine if nanoparticles reduce residual oil saturation and the results of these experiments are shown below.

Figure 4.18 shows experimental results using Nissan Chemical EOR-12 nanoparticles. The EOR-12 nanoparticles are a proprietary dispersion. Some information that is known about the particles is that they have a hydrophilic surface coating and that the average particle size is 12 nm. Initially, the pore space was filled with decane and then flooded with water. The waterflood rate was 50μl/hr and showed reasonable decane trapping. The remaining decane was assumed to be the residual saturation after a waterflood. After waterflooding, the EOR-12 nanoparticles were used to as a tertiary flood. For this experiment the nanoparticle solution was not diluted to create a standard dispersion. The nanoparticle solution flow rate was 2 μl/hr. It was decided that it would be best to start at a low flow rate, as it would be easier to watch what would happen. The

video was kept positioned over the same portion of the channel for the entire length of filming. This was done because, while there are five dead-end pores, only two can be viewed concurrently. Another reason to use this method was that it will allow for accurate understanding of the changes that may or may not occur during a nanoparticle flood.

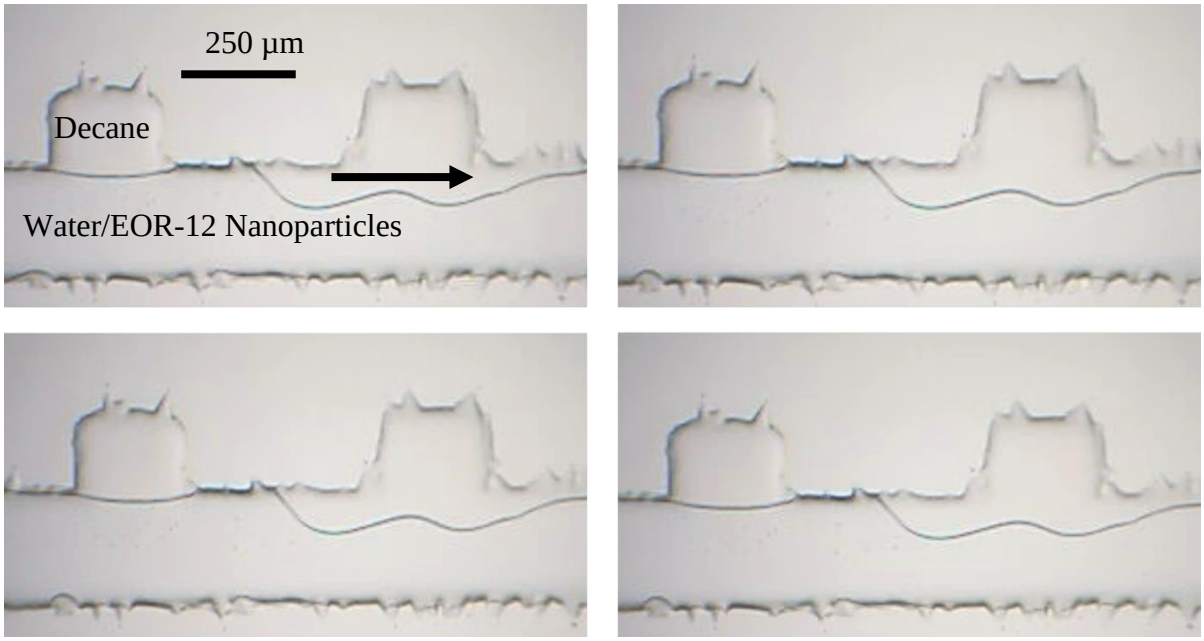

Figure 4.18 An EOR-12 nanoparticle flood at 2µl/hr. The nanoparticle solution was flowed for about 80 minutes. After the 80 minutes, there was no noticeable change in the amount of decane trapped in the dead-end pores.

Figure 4.18 shows images taken from a video that was about 1 hour and 20 minutes long. The images show that there was no noticeable change in the decane that was trapped in the pore space. Because there was no noticeable change in the oil that was

recovered, the nanoparticles used, and the nanoparticle solution flow rate were altered in an attempt to alter the residual oil saturation.

The parameter changes made were similar to the changes that were made when attempting to consistently trap oil in the dead-end pores. One parameter that was changed was the oil that was used in testing. The above experiment used decane which was displaced by water, in Figure 4.19 mineral oil was displaced by water. Once the mineral oil saturation was no longer changing, the displacing solution was changed from water to EOR-12 nanoparticles. The images below show the results of a 2µl/hr nanoparticle flood. Again, the video was kept in the same position for the entire experiment.

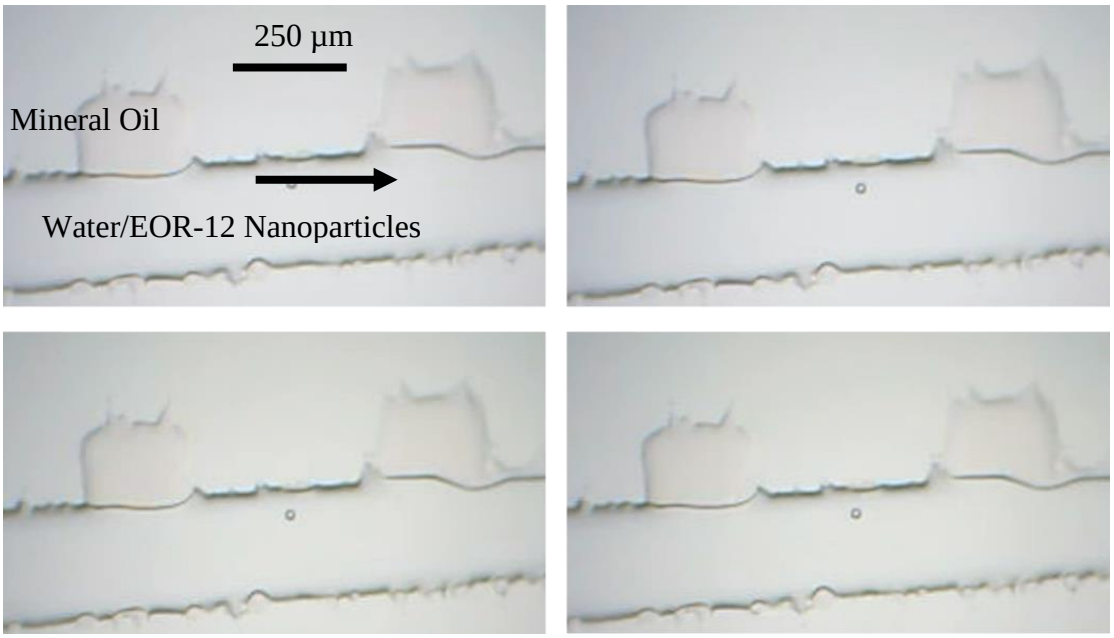

Figure 4.19 Mineral oil was used to initially fill the channel with oil. The pore space was then waterflooded until no more mineral oil was displaced. The images above show snap shots of the results of an EOR-12 nanoparticle flood. The nanoparticle flow rate is 2µl/hr and the flood time was about 80 minutes. There is no noticeable change in the amount of oil trapped in the dead-end pores.

The experiment was run for about 1 hour and 20 minutes. When reviewing the images, it can be seen that there was no noticeable change in the oil trapped in the dead-end pores. Experiments in the lower aspect ratio dead-end, using decane and mineral oil with a 2 μl/hr nanoparticle solution have not shown an increase in oil recovery. The next experiment changed the flow rate at which the nanoparticles enter the pore space. The flow rate was increased in one experiment and in another experiment, once the particles entered the channel the rate was set to zero. The idea was that if the nanoparticles contact oil for longer periods (lower flow rates) that would help to increase recovery. Higher nanoparticle flow rates would increase the shearing force on the oil and help to peel in out of the dead-end pores. Figure 4.20 shows the same experiment as Figure 4.19, the only difference is the flow rate. In Figure 4.20 the nanoparticle flow rate was increased to 20 μl/hr to determine the effect of increased nanoparticle flow rate on the oil recovery. Looking at the figure below, there was no noticeable change in the oil saturation in the dead-end pores. Even at the higher flow rate there was no change in the amount of oil that remained in the pore. The next step was to determine if a lower flow rate or zero flow rates will help to recover more oil.

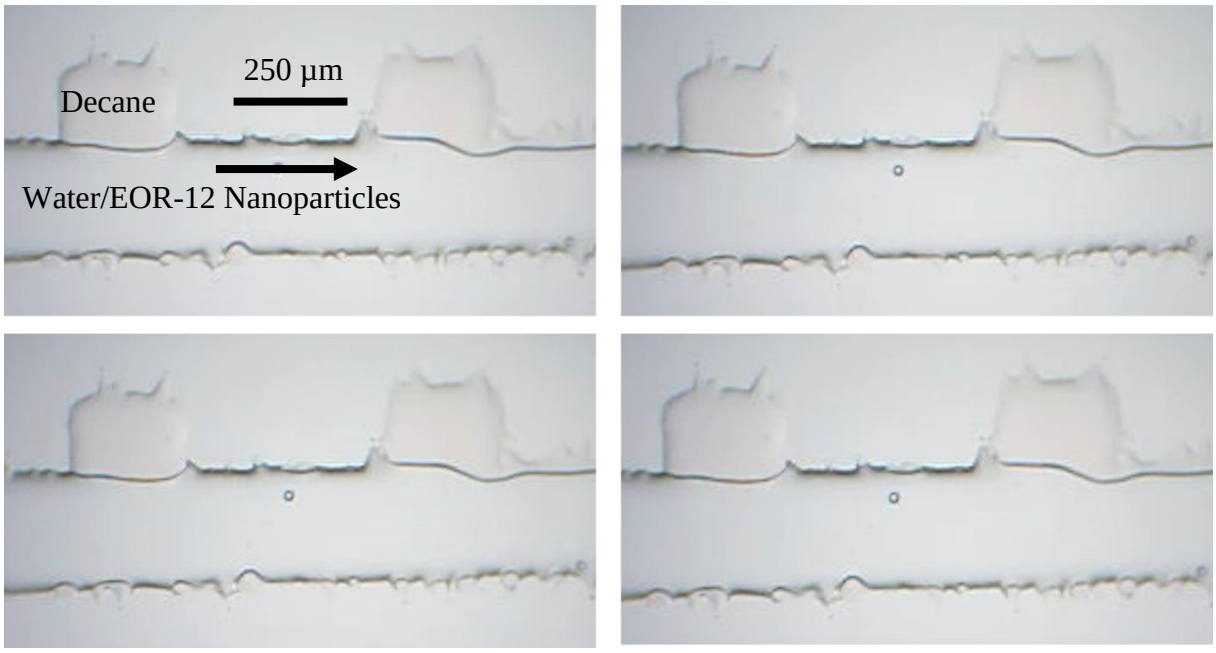

Figure 4.20 An example of a nanoparticle flood. EOR-12 particles were used in this experiment. The result shows that over 80 minutes at 20µl/hr there is no noticeable change in the decane trapped in the dead-end pores.

Figure 4.21 shows images from a waterflood and then a tertiary nanoparticle flood. The top image (a) is the final result of a waterflood. After the waterflood, EOR-12 nanoparticles were injected into the pore space. The middle and bottom image (b) show images from a video that was taken of the nanoparticle flood. Initially, the nanoparticles were flowed in at 20µl/hr. This flow rate was before the video recording started. As the video recording began, the flow rate of the nanoparticles was turned off and there was no flow into the channel. The bottom image shows what the section of the pore space looks like after 1 hour of no flow. As can be seen from the images below, there was no noticeable change in the amount of mineral oil that saturates the pore space.

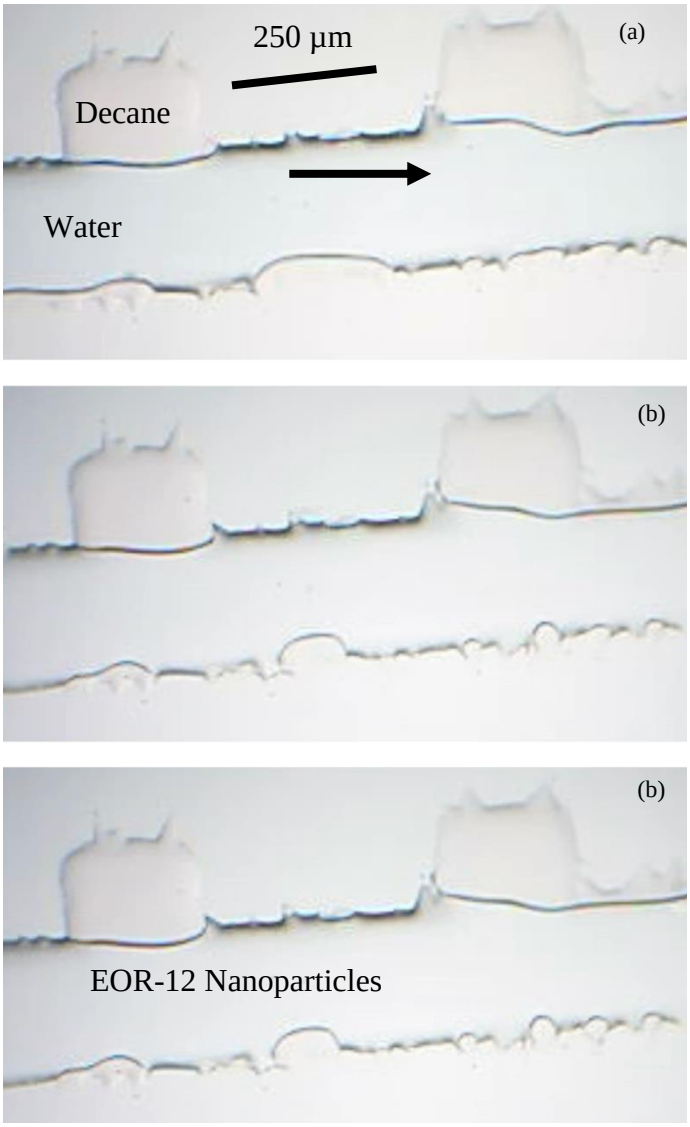

Figure 4.21 EOR-12 nanoparticles tested at a flow rate of 0µl/hr. There is no noticeable change in the amount of decane trapped in the dead-end pores.

After attempting to reduce the remaining oil saturation in the square shaped dead-end pores, the rectangular dead-end pores were tested. While it was expected that the higher aspect ratio rectangular dead-end pores would consistently trap oil. It was unknown whether they would be preferable for reducing residual oil saturation. This was

because there was less contact area between the trapped oil and the displacing nanoparticle solution. Besides the geometric difference between the more square dead-end pores and the higher aspect ratio rectangular dead-end pore experiments was the type of nanoparticles used. In the rectangular dead-end pores IPA-ST nanoparticles (Nissan Chemical) were used. They are hydrophilic particles with an average diameter of 10 to 15 nm. These particles are originally in an isopropyl alcohol (IPA) solution. In the trials with IPA-ST nanoparticles, a dispersion was made, using the method described in Chapter 4.1.

Figure 4.22 shows an experimental trial using the IPA-ST nanoparticle dispersion. The flow rate of the inflowing nanoparticle dispersion was 2 μl/hr. The nanoparticle dispersion flowed through the pore space for about 90 minutes. The top image in Figure 4.22 shows the initial decane saturation when the dispersion was entering the pore space. The bottom image shows the pore space after the nanoparticle dispersion had been flowing for 90 minutes. It can be seen in the images that there is no noticeable change in the trapped decane. Because the nanoparticles did not increase the oil recovery at a low flow rate, a higher flow rate was tested.

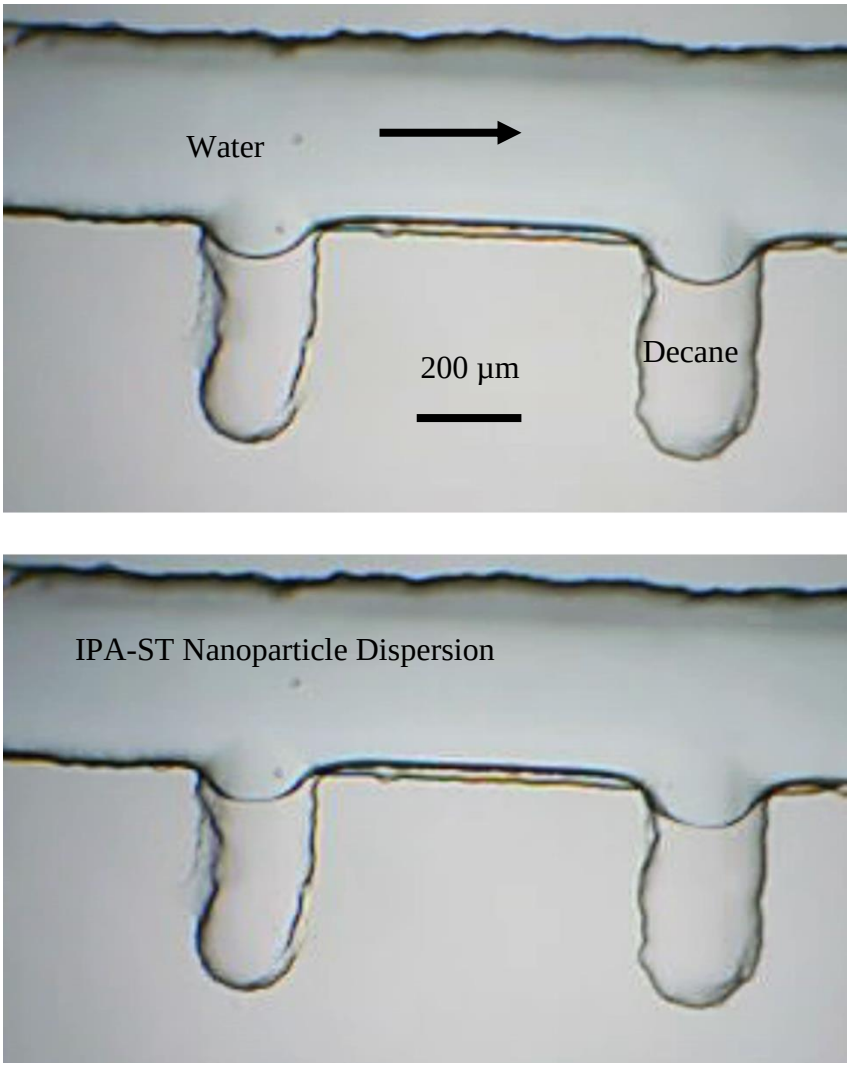

Figure 4.22 Results of flowing an IPA-ST nanoparticle dispersion into an already waterflooded pore space. The nanoparticle flow rate was 2µl/hr and it was flowed in for 90 minutes. The nanoparticle dispersion did not change the amount of decane that was trapped in the pore space.

Figure 4.23 shows the results of increasing the IPA-ST dispersion flow rate from 2 µl/hr to 5 µl/hr. The same pores as above were recorded for the entire length of the video. In this experiment, the pore space was first filled with decane, and then waterflooded. Once there was no change in the amount of decane in the dead-end pores,

the displacing fluid was switched to the IPA-ST nanoparticle dispersion. In this experiment, the nanoparticle dispersion flood lasted three hours. The top image in Figure 4.23 shows the initial pore space, just as the nanoparticle flood commenced. The bottom image shows the dead-end pores after three hours of flooding the nanoparticle dispersion. Reviewing the images below, there was no noticeable change in the amount of trapped decane. After testing the effect of increasing the flow rate on the decane concentration, it was decided that attempting to further increase the flow rate may lead to positive results due to the higher shear rates.

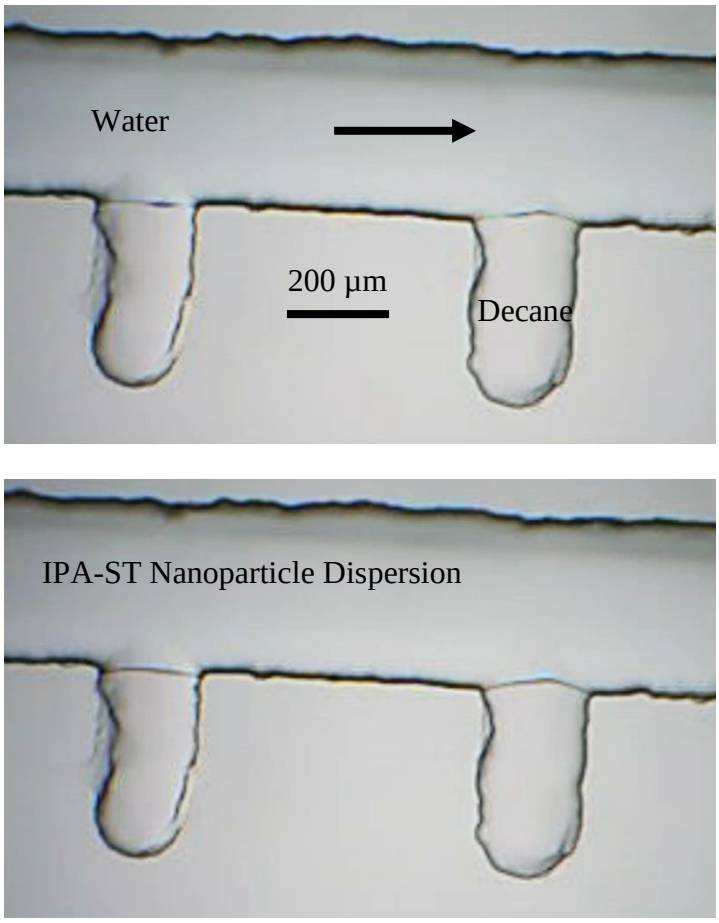

Figure 4.23 Results of flowing an IPA-ST nanoparticle dispersion, at a higher flow rate (5 µl/hr), into an already waterflooded pore space. Over 3 hours the nanoparticle dispersion did not change the amount of decane that was trapped in the pore space.

Figure 4.24 shows the results of steadily increasing the flow rate over the experiment. The process was the same as seen above, the channel was filled with decane and then a waterflood was done until the oil reached a point where there was no more reduction in the amount of decane. Next a nanoparticle dispersion was injected into the pore space. The IPA-ST nanoparticle dispersion was used again. Initially, the dispersion flow rate was 5 µl/hr. The top image in Figure 4.24 shows the pore space at the initial

flow rate. After one minute of recording, the flow rate was increased to 500µl/hr. The middle image in Figure 4.24 shows the pore space at the one minute mark of the video. The flow rate was then increase gradually from 1000µl/hr, to 2000µl/hr, then 4000µl/hr, 8000µl/hr and finally 16000µl/hr. The bottom image shows the pore space after 14 minutes and 30 seconds. This was about a minute after the flow rate was increased to 16000µl/hr. When reviewing the the image, the only noticeable difference was that the color of the displacing fluid was clear. There was no change noticeable change in the decane that was trapped in the dead-end pores. This seems to show that even at high flow rates, oil would not be removed from the dead-end pores. One issue with the trial was that at the high flow rates there was some leaking that occurred at the valves. While there was leaking towards the end of the trial, the flow rates were 250 to 8000 times higher than the flow rates that were run in previous trials.

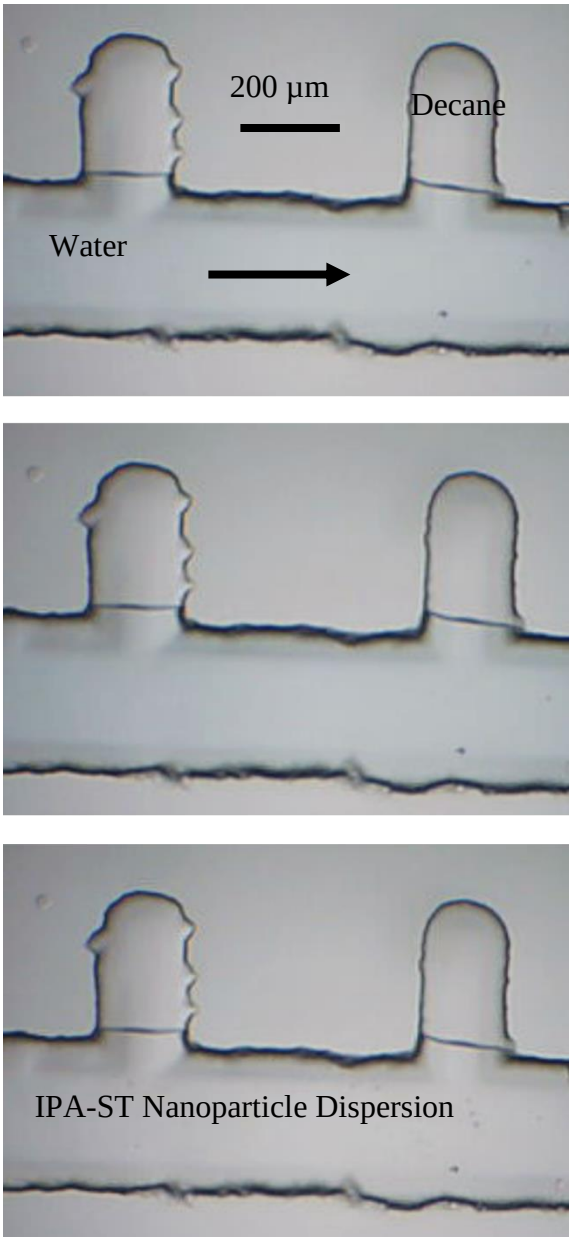

Figure 4.24 Flowing the nanoparticle dispersion at increasing rates up to 16000 µl/hr did not change the amount of decane that is trapped in the pore space.

4.2.3.2 Nanoparticle Particle Dispersion as a Secondary Flood

Another experiment that was run was to test if more oil was recovered when using the nanoparticle dispersion as the primary displacement mechanism. In this experiment there was no waterflood, only the nanoparticle dispersion was used to displace oil. The IPA-ST nanoparticle dispersion was used in this experiment. The flow rate of the nanoparticle dispersion was 2 µl/hr. Figure 4.25 shows images from the video recording that was taken. The nanoparticle flood was extremely similar to the standard waterflood, and there was no noticeable difference between the two different methods of oil displacement.

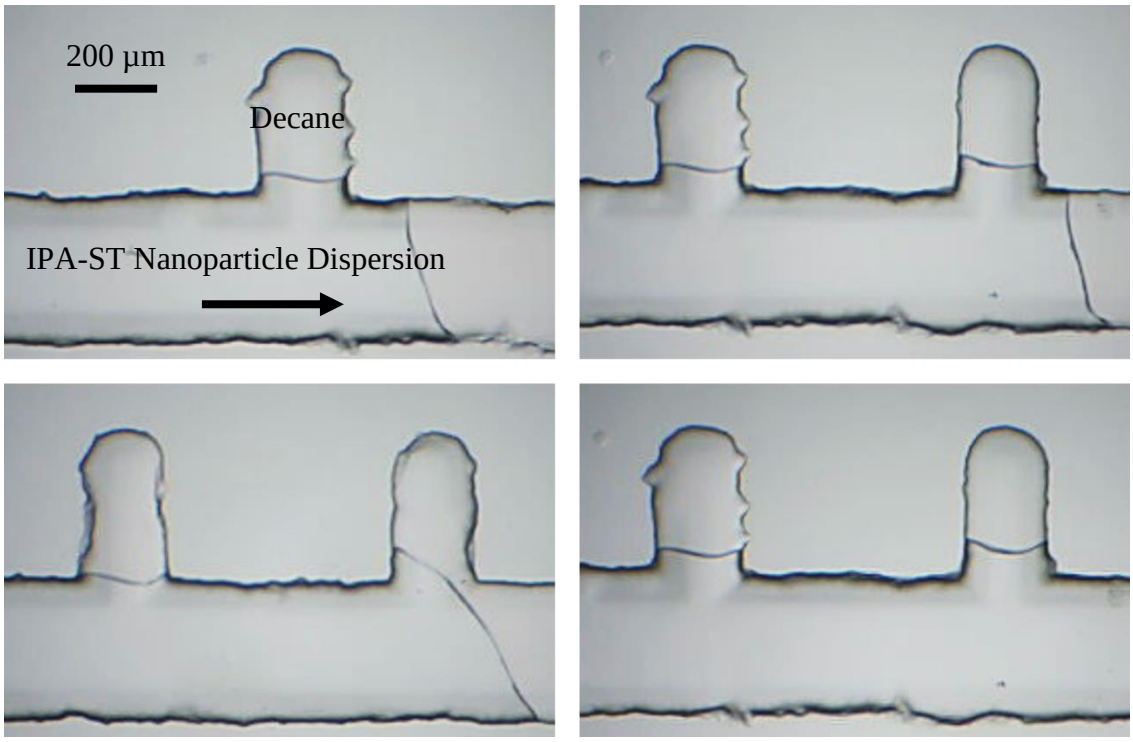

Figure 4.25 Compared to a waterflood, a secondary nanoparticle dispersion flood shows no difference in the amount decane trapped in the dead-end pores.

4.2.3.3 HPAM Tertiary Flood

A tertiary hydrolyzed poly-acrylamide (HPAM) flood was tested to see if it would increase oil recovery from the dead-end pores. If the HPAM flood does not increase oil recovery that may point to the geometrical constraints of the dead-end pore as a barrier to additional recovery. Figure 4.26 shows the results of an HPAM flood. The top picture is the pore space after waterflooding but before the HPAM flood begins. The bottom images show the pore space after 4.5 hours of polymer flooding. This image shows that there is no noticeable oil recovered due the HPAM flood.

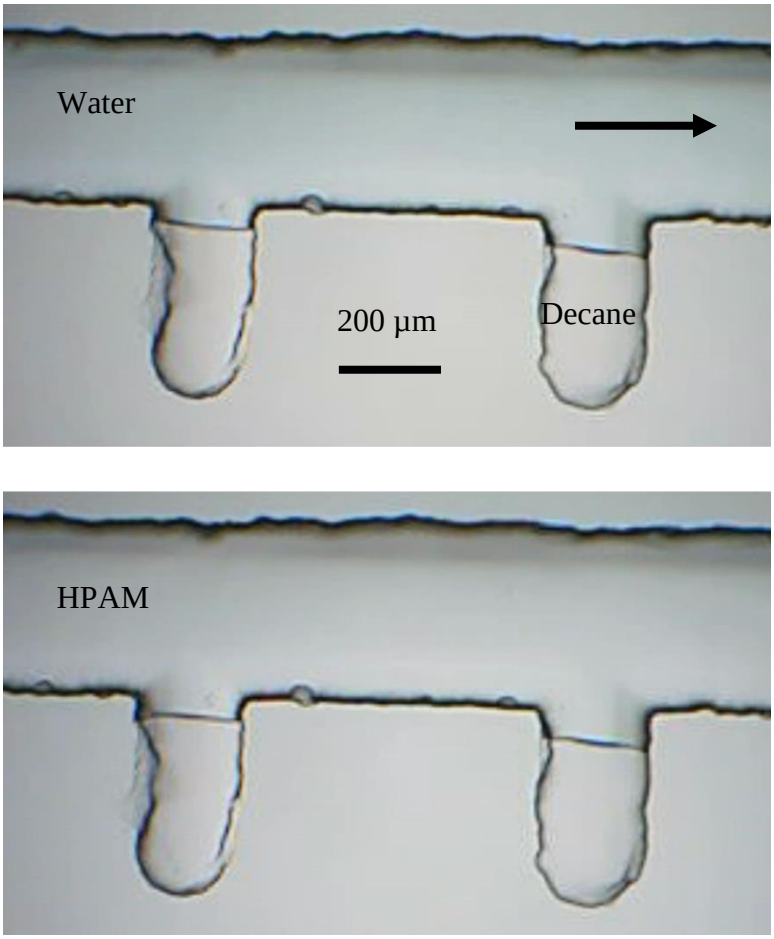

Figure 4.26 There is no difference in the amount of decane that is recovered when using HPAM as a tertiary flood compared to IPA-ST nanoparticles

Through trial and error, consistent and repeatable trapping of oil in dead-end pores was accomplished. After trapping the oil in the dead-end pores no additional oil recovery was noticed when using nanoparticle dispersions. HPAM was also tested once and there was no discernable oil recovery. The fact that there was no change in the amount of oil in the dead-end pores may be associated to dead-end pore geometry and not the nanoparticle dispersion. As stated in the Chapter 2, Gabel (2014) tested the oil recovery potential of an IPA-ST nanoparticle dispersion in a Berea sandstone coreflood.

Gabel (2014) found that at higher flow rates (12 mL/min and 24 mL/min) a stable emulsion forms and oil recovery increased. At these flow rates the shear rate through the core was $1784s^{-1}$ and $3568s^{-1}$ respectively. Gabel (2014) noted that at these flow rates the capillary number must have been high enough to increase oil mobility and improve recovery. The flow rates at which the microfluidic devices reached this shear rate were calculated using a shear rate through a pipe equation.

$$\dot{\gamma} = \frac{8v}{d} \quad \text{(Eqn. 4-1)}$$

$$v = \frac{Q}{A} \quad \text{(Eqn. 4-2)}$$

where $\dot{\gamma}$is the shear rate measured in inverse seconds, v is the fluid velocity and d is the inner diameter of the pipe. Q is the flow rate of the fluid through the pipe and A is the cross-sectional area of the pipe. Using these equations the minimum waterflood rate was calculated to be about 400 µl/hr. Values above this rate was tested using an IPA-ST nanoparticle dispersion and there was no change in the amount of decane in the dead-end pore.

This result differs from the coreflood results presented in Gabel (2014). In his coreflood results he saw an increase in the amount of oil recovered using an IPA-ST nanoparticle dispersion over a brine flood. There are many potential reasons for this result. As stated above it could be due to the constraints of the dead-end geometry, which makes it too difficult to remove oil from the dead-end. Much of the trapped oil in sandstones is not found in dead-end pores. This may be why Gabel (2014) saw an

increase in oil recovery at higher flow rates. The medium through which the fluid flow may have an impact on the amount of oil recovered.

CHAPTER 5. CONCLUSIONS AND RECOMMENDATIONS

5.1 CONCLUSIONS

5.1.1 PDMS Micromodels

- Being polymer based, PDMS micromodels were easy to fabricate and the mold used to create devices could be used repeatedly. Another benefit of PDMS micromodels was that it was easier to create finer and more detailed features than with glass.
- The PDMS micromodels, whose surface was hydrophobic, did not trap mineral oil in dead-end pores. A range of waterflood rates were tested, none of which showed any potential for trapping mineral oil in dead-end pores. Mineral oil likely diffused through the pore walls during a simulated waterflood, as was also observed by Duboin (2013).
- Fluorinated oil (FC40) was tested to determine its effectiveness for trapping in PDMS dead-end pores.
    - During a waterflood, FC40 stayed in the pore space for longer periods than mineral oil; but it always was expelled. The manner of expulsion from the dead-end pores was similar to mineral oil tests.
    - A limited numbers of trials using fluorinated oil were completed. Although none of the trials trapped fluorinated oil in the dead-end pores, there is still potential for success. Duboin (2013) saw success using

fluorinated oil (FC 40 and FC70). Other fluorinated oils (FC70) may still have potential use for EOR experimental work.

5.1.2 Glass Micromodels

- The use of microfluidic devices with detailed pore geometry was a novel approach to observe and quantify the effects of nanoparticle dispersions for EOR. The novelty of them makes glass fabrication difficult.
- Improved glass micromodel fabrication techniques were developed to create a more uniform etching which involved:
    - Decreasing the hydrofluoric acid concentration
    - Increasing the etching time
    - Modifying the photolithography procedure so that it did not require a metal layer.
- Waterflooding glass micromodels proved to be much more successful for trapping oil than PDMS models; decane and mineral oil consistently stayed trapped in dead-end pores.
- When testing nanoparticle dispersions as a tertiary flood in the dead-end pores geometry there was no noticeable increase the oil recovery.
    - Many coreflood experiments (Hendraningrat, Mcelfresh) have seen improved recovery when testing nanoparticle potential for EOR.
    - Observed recovery in core floods may not have come from trapped oil in dead-end pores, but instead from other mechanisms of trapping such as

bypassed oil due to local heterogeneities, or ganglia trapping at pore throats due to capillary force.

5.2 Recommendations for Future Work

5.2.1 PDMS Micromodels

- Different polymer materials such as PMMA or polycarbonate may help to trap oil and prove more successful.
- It is recommended to find a dye to definitively determine whether mineral oil diffuses into the bulk PDMS
- Testing different surface coating on PDMS devices or other polymer materials may assist with oil trapping. Norland Optical adhesive (NOA) treatment may be useful as it allows for manipulation of PDMS surface wettability (Levaché, 2012). NOA treatment modifies PDMS wettability (hydrophobic to hydrophilic).

5.2.2 Glass Micromodels

- Continue to improve fabrication and etching method.
    - Work to reach greater etched depths (100 μm) without destroying photoresist. This may be possible by priming the glass substrate and etching in a higher concentration hydrofluoric acid bath for longer periods of time.
    - Continue to improve etching consistency. Test adding hydrochloric acid to the buffer hydrofluoric acid; this make improve etch quality.

    - Work to create an etched surface with multiple etched depths. This can be accomplished by covering etched regions with wax and leaving the areas to be etched deeper uncovered.
- Test EOR potential for different channel geometries.
    - A snap-off micromodel and pore doublet model are currently in development.
    - Future geometries that could be tested are pore network or geometries with more dimensionality.

REFERENCES

Anderson, J. R., Chiu, D. T., Wu, H., Schueller, O. J., & Whitesides, G. M. (2000). Fabrication of microfluidic systems in poly (dimethylsiloxane). *Electrophoresis*, *21*, 27-40.

Baram, A., & Naftali, M. (2006). Dry etching of deep cavities in Pyrex for MEMS applications using standard lithography. *Journal of Micromechanics and Microengineering*, *16*(11), 2287.

BP Statistical Review of World Energy June 2014. (2014, June). Retrieved from www.bp.com/en/global/corporate/about-bp/energy-economics/statistical-review-of-world-energy.html

Caldelas, F. M., Murphy, M., Huh, C., & Bryant, S. L. (2011, January). Factors governing distance of nanoparticle propagation in porous media. In *SPE Production and Operations Symposium*. Society of Petroleum Engineers.

Chatzis, I., Morrow, N. R., & Lim, H. T. (1983). Magnitude and detailed structure of residual oil saturation. *Society of Petroleum Engineers Journal*, *23*(02), 311-326.

Chemical Methods | netl.doe.gov. (n.d.). Retrieved from http://www.netl.doe.gov/research/oil-and-gas/enhanced-oil-recovery/chemical_methods

Chen, Q., Li, G., Jin, Q. H., Zhao, J. L., Ren, Q. S., & Xu, Y. S. (2007). A rapid and low-cost procedure for fabrication of glass microfluidic devices. *Microelectromechanical Systems, Journal of*, *16*(5), 1193-1200.

Chengara, A., Nikolov, A. D., Wasan, D. T., Trokhymchuk, A., & Henderson, D. (2004). Spreading of nanofluids driven by the structural disjoining pressure gradient. *Journal of colloid and interface science*, *280*(1), 192-201.

De Gennes, P. G. (1985). Wetting: statics and dynamics. *Reviews of modern physics*, *57*(3), 827.

Duboin, A. (2013). *Écoulements de fluides complexes en présence d'interfaces dans des systèmes microfluidiques* (Doctoral dissertation, Université Pierre et Marie Curie-Paris VI).

Duffy, D. C., McDonald, J. C., Schueller, O. J., & Whitesides, G. M. (1998). Rapid prototyping of microfluidic systems in poly (dimethylsiloxane). *Analytical chemistry*, *70*(23), 4974-4984.

Eddings, M. A., & Gale, B. K. (2006). A PDMS-based gas permeation pump for on-chip fluid handling in microfluidic devices. *Journal of Micromechanics and Microengineering*, *16*(11), 2396.

Eddings, M. A., Johnson, M. A., & Gale, B. K. (2008). Determining the optimal PDMS–PDMS bonding technique for microfluidic devices. *Journal of Micromechanics and Microengineering*, *18*(6), 067001.

Fukasawa, T., & Horiike, Y. (2003). Deep dry etching of quartz plate over 100 μm in depth employing ultra-thick photoresist (SU-8). *Japanese journal of applied physics*, *42*(6R), 3702.

Gabel, S.T. (2014). *Generation, Stability, and Transport of Nanoparticle-Stabilized Oil-in-Water Emulsions in Porous Media*. (Master's thesis, The University of Texas at Austin).

Giraldo, J., Benjumea, P., Lopera, S., Cortés, F. B., & Ruiz, M. A. (2013). Wettability alteration of sandstone cores by alumina-based nanofluids. *Energy & Fuels*, *27*(7), 3659-3665.

Green, D. W., & Willhite, G. P. (1998). *Enhanced oil recovery*. Richardson, Tex.: Henry L. Doherty Memorial Fund of AIME, Society of Petroleum Engineers.

Grosse, A., Grewe, M., & Fouckhardt, H. (2001). Deep wet etching of fused silica glass for hollow capillary optical leaky waveguides in microfluidic devices. *Journal of micromechanics and microengineering*, *11*(3), 257.

Hendraningrat, L., & Shidong, L. (2012, January). A glass micromodel experimental study of hydrophilic nanoparticles retention for EOR project. In *SPE Russian Oil and Gas Exploration and Production Technical Conference and Exhibition*. Society of Petroleum Engineers.

Hendraningrat, L., & Torsater, O. (2014, March). Unlocking the Potential of Metal Oxides Nanoparticles to Enhance the Oil Recovery. In *Offshore Technology Conference-Asia*. Offshore Technology Conference.

Höök, M., Hirsch, R., & Aleklett, K. (2009). Giant oil field decline rates and their influence on world oil production. *Energy Policy*, *37*(6), 2262-2272.

Iliescu, C., Chen, B., & Miao, J. (2007, January). Deep wet etching-through 1mm pyrex glass wafer for microfluidic applications. In *Micro Electro Mechanical Systems, 2007. MEMS. IEEE 20th International Conference on* (pp. 393-396). IEEE.

International Energy Outlook 2013 - Energy Information Administration. (2013, July). Retrieved from http://www.eia.gov/forecasts/ieo/

Javadpour, F., & Fisher, D. (2008). Nanotechnology-based micromodels and new image analysis to study transport in porous media. *Journal of Canadian Petroleum Technology*, *47*(2), 30-37.

Jia, Z. J., Fang, Q., & Fang, Z. L. (2004). Bonding of glass microfluidic chips at room temperatures. *Analytical chemistry*, *76*(18), 5597-5602.

Kapusta, S., Balzano, L., & Te Riele, P. M. (2011, January). Nanotechnology Applications in Oil and Gas Exploration and Production. In *International Petroleum Technology Conference*. International Petroleum Technology Conference.

Karimi, A., Fakhroueian, Z., Bahramian, A., Pour Khiabani, N., Darabad, J. B., Azin, R., & Arya, S. (2012). Wettability alteration in carbonates using zirconium oxide nanofluids: EOR implications. *Energy & Fuels*, *26*(2), 1028-1036.

Koh, K. S., Chin, J., Chia, J., & Chiang, C. L. (2012). Quantitative studies on PDMS-PDMS interface bonding with Piranha solution and its swelling effect. *Micromachines*, *3*(2), 427-441.

Kolari, K., Saarela, V., & Franssila, S. (2008). Deep plasma etching of glass for fluidic devices with different mask materials. *Journal of Micromechanics and Microengineering*, *18*(6), 064010.

Kondiparty, K., Nikolov, A., Wu, S., & Wasan, D. (2011). Wetting and spreading of nanofluids on solid surfaces driven by the structural disjoining pressure: statics analysis and experiments. *Langmuir*, *27*(7), 3324-3335.

Lake, L. W. (1989). *Enhanced oil recovery*. Englewood Cliffs, N.J: Prentice Hall. Li, X., Abe, T., & Esashi, M. (2001). Deep reactive ion etching of Pyrex glass using SF $_6$ plasma. *Sensors and actuators A: Physical*, *87*(3), 139-145.

Levaché, B., Azioune, A., Bourrel, M., Studer, V., & Bartolo, D. (2012). Engineering the surface properties of microfluidic stickers. *Lab on a Chip*, *12*(17), 3028-3031.

Li, X., Abe, T., & Esashi, M. (2001). Deep reactive ion etching of Pyrex glass using SF_6 plasma. *Sensors and actuators A: Physical*, *87*(3), 139-145.

Li, S., Hendraningrat, L., & Torsaeter, O. (2013, March). Improved Oil Recovery by Hydrophilic Silica Nanoparticles Suspension: 2 Phase Flow Experimental Studies. In *IPTC 2013: International Petroleum Technology Conference*.

Liu, K. L., Kondiparty, K., Nikolov, A. D., & Wasan, D. (2012). Dynamic spreading of nanofluids on solids Part II: Modeling. *Langmuir*, *28*(47), 16274-16284.

Mcelfresh, P. M., Olguin, C., & Ector, D. (2012, January). The Application of Nanoparticle Dispersions To Remove Paraffin and Polymer Filter Cake Damage. In *SPE International Symposium and Exhibition on Formation Damage Control*. Society of Petroleum Engineers.

Mcelfresh, P. M., Holcomb, D. L., & Ector, D. (2012, January). Application of nanofluid technology to improve recovery in oil and gas wells. In *SPE International Oilfield Nanotechnology Conference and Exhibition*. Society of Petroleum Engineers.

Miranda, C. R., Lara, L. S. D., & Tonetto, B. C. (2012, January). Stability and Mobility of Functionalized Silica Nanoparticles for Enhanced Oil Recovery Applications. In *SPE International Oilfield Nanotechnology Conference and Exhibition*. Society of Petroleum Engineers.

Ogolo, N. A., Olafuyi, O. A., & Onyekonwu, M. O. (2012, January). Enhanced oil recovery using nanoparticles. In *SPE Saudi Arabia Section Technical Symposium and Exhibition*. Society of Petroleum Engineers.

Park, J. H., Lee, N. E., Lee, J., Park, J. S., & Park, H. D. (2005). Deep dry etching of borosilicate glass using SF_6 and SF_6/Ar inductively coupled plasmas. *Microelectronic engineering*, *82*(2), 119-128.

Reddy, S., Schunk, P. R., & Bonnecaze, R. T. (2005). Dynamics of low capillary number interfaces moving through sharp features. *Physics of Fluids (1994-present)*, *17*(12), 122104.

Robelius, F. (2007). Giant oil fields-the highway to oil: GIant oil fields and their importance for future oil production.

Roof, J. G. (1970). Snap-off of oil droplets in water-wet pores. *Society of Petroleum Engineers Journal*, *10*(01), 85-90.

Samel, B., Chowdhury, M. K., & Stemme, G. (2007). The fabrication of microfluidic structures by means of full-wafer adhesive bonding using a poly (dimethylsiloxane) catalyst. *Journal of Micromechanics and Microengineering*, *17*(8), 1710.

Satyanarayana, S., Karnik, R. N., & Majumdar, A. (2005). Stamp-and-stick room-temperature bonding technique for microdevices. *Microelectromechanical Systems, Journal of*, *14*(2), 392-399.

Shell. (2012). *Enhanced Oil Recovery*. Retrieved from http://s05.static-shell.com/content/dam/shell/static/future-energy/downloads/eor/eor-brochure-2012.pdf

Sigma-Aldrich: Analytical, Biology, Chemistry & Materials Science products and services. | Sigma-Aldrich. (n.d.). Retrieved July 24, 2014, from http://www.sigmaaldrich.com Stosur, G. J. (2003, January). EOR: Past Present and What the Next 25 Years May Bring. In *SPE International Improved Oil Recovery Conference in Asia Pacific*. Society of Petroleum Engineers.

Tan, S. H., Nguyen, N. T., Chua, Y. C., & Kang, T. G. (2010). Oxygen plasma treatment for reducing hydrophobicity of a sealed polydimethylsiloxane microchannel. *Biomicrofluidics*, *4*(3), 032204.

Tata, B. V. R., Boda, D., Henderson, D., Nikolov, A., & Wasan, D. T. (2000). Structure of charged colloids under a wedge confinement. *Physical Review E*, *62*(3), 3875.

Tiab, D., & Donaldson, E. C. (2011). *Petrophysics: theory and practice of measuring reservoir rock and fluid transport properties*. Gulf professional publishing.

Torsater, O., Engeset, B., Hendraningrat, L., & Suwarno, S. (2012, January). Improved Oil Recovery by Nanofluids Flooding: An Experimental Study. In *SPE Kuwait International Petroleum Conference and Exhibition*. Society of Petroleum Engineers.

Torsater, O., Li, S., & Hendraningrat, L. (2013, April). A coreflood investigation of nanofluid enhanced oil recovery in low-medium permeability Berea sandstone. In *SPE International Symposium on Oilfield Chemistry*. Society of Petroleum Engineers.

Waldbaur, A., Rapp, H., Länge, K., & Rapp, B. E. (2011). Let there be chip—towards rapid prototyping of microfluidic devices: one-step manufacturing processes. *Analytical Methods*, *3*(12), 2681-2716.

Wang, Q., Lee, J. H., Jeong, S. W., Jang, A., Lee, S., & Choi, H. (2011). Mobilization and deposition of iron nano and sub-micrometer particles in porous media: A glass micromodel study. *Journal of hazardous materials*, *192*(3), 1466-1475.

Wasan, D. T., & Nikolov, A. D. (2003). Spreading of nanofluids on solids. *Nature*, *423*(6936), 156-159.

Whitesides, G. M. (2006). The origins and the future of microfluidics. *Nature*, *442*(7101), 368-373.

Xia, H., Wang, D., Wang, G., Ma, W. G., Deng, H. W., & Liu, J. (2008, January). Mechanism of the effect of micro-forces on residual oil in chemical flooding. In *SPE Symposium on Improved Oil Recovery*. Society of Petroleum Engineers.

Yu, J., An, C., Mo, D., Liu, N., & Lee, R. L. (2012, January). Study of adsorption and transportation behavior of nanoparticles in three different porous media. In *SPE Improved Oil Recovery Symposium*. Society of Petroleum Engineers.

Zhang, T., Espinosa, D., Yoon, K. Y., Rahmani, A. R., Yu, H., Caldelas, F. M., ... & Huh, C. (2011, January). Engineered nanoparticles as harsh-condition emulsion and foam stabilizers and as novel sensors. In *Offshore Technology Conference*. Offshore Technology Conference.